

**VIBRATION ANALYSIS AND OPTIMIZATION OF FULLY  
AND PARTIALLY MR-FLUID TREATED MULTI-LAYER  
BEAMS**

**Vasudevan Rajamohan**

**A thesis**

**In the Department of  
Mechanical and Industrial Engineering**

**Presented in Partial Fulfillment of the Requirements  
for the Degree of Doctor of Philosophy at  
Concordia University  
Montreal, Quebec, Canada**

**August 2010**

**© Vasudevan Rajamohan, 2010**



Library and Archives  
Canada

Published Heritage  
Branch

395 Wellington Street  
Ottawa ON K1A 0N4  
Canada

Bibliothèque et  
Archives Canada

Direction du  
Patrimoine de l'édition

395, rue Wellington  
Ottawa ON K1A 0N4  
Canada

*Your file* *Votre référence*  
ISBN: 978-0-494-71158-3  
*Our file* *Notre référence*  
ISBN: 978-0-494-71158-3

**NOTICE:**

The author has granted a non-exclusive license allowing Library and Archives Canada to reproduce, publish, archive, preserve, conserve, communicate to the public by telecommunication or on the Internet, loan, distribute and sell theses worldwide, for commercial or non-commercial purposes, in microform, paper, electronic and/or any other formats.

The author retains copyright ownership and moral rights in this thesis. Neither the thesis nor substantial extracts from it may be printed or otherwise reproduced without the author's permission.

---

In compliance with the Canadian Privacy Act some supporting forms may have been removed from this thesis.

While these forms may be included in the document page count, their removal does not represent any loss of content from the thesis.

**AVIS:**

L'auteur a accordé une licence non exclusive permettant à la Bibliothèque et Archives Canada de reproduire, publier, archiver, sauvegarder, conserver, transmettre au public par télécommunication ou par l'Internet, prêter, distribuer et vendre des thèses partout dans le monde, à des fins commerciales ou autres, sur support microforme, papier, électronique et/ou autres formats.

L'auteur conserve la propriété du droit d'auteur et des droits moraux qui protègent cette thèse. Ni la thèse ni des extraits substantiels de celle-ci ne doivent être imprimés ou autrement reproduits sans son autorisation.

---

Conformément à la loi canadienne sur la protection de la vie privée, quelques formulaires secondaires ont été enlevés de cette thèse.

Bien que ces formulaires aient inclus dans la pagination, il n'y aura aucun contenu manquant.

  
**Canada**

## **ABSTRACT**

### **Vibration Analysis and Optimization of Fully and Partially MR-Fluid Treated Multi-Layer Beams**

Vasudevan Rajamohan, Ph.D.  
Concordia University, 2010.

Magnetorheological (MR) fluid is known to exhibit rapid variations in their rheological properties when subjected to varying magnetic field and thus offers superior potential for applications in smart structures requiring high bandwidth. MR sandwich structures can apply distributed control force to yield variations in stiffness and damping properties of the structure, and thus provide enhanced vibration suppression over a broad range of external excitation frequencies. In this study, the governing equations of a three-layer beam structure employing MR-fluid layer as the mid-layer are presented in the finite element form and Ritz formulation. The validity of the finite element formulations is demonstrated by comparing the results with those obtained from the Ritz formulation and laboratory measurements performed on a prototype sandwich beam. Furthermore, the relationships between the magnetic field and the complex shear modulus of the MR material in the pre-yield regime is estimated through the free vibration experiment of the prototype MR sandwich beam. Simulations are performed to derive the essential properties (natural frequencies and loss factors), and the dynamic response of the multi-layered structure as functions of the applied magnetic field and thickness of the MR-fluid layer under different boundary conditions.

A concept of a partially-treated multi-layer MR fluid beam is proposed to achieve a compact and cost effective design. Laboratory experiments are performed on a partially

treated beam and the data are used to demonstrate the validity of both the finite element and Ritz formulations. The properties of partially treated MR-fluid beams are evaluated to investigate the influences of the location and length of the treatment for different boundary conditions, and compared with those of the fully-treated beams. The damping performance of the partially treated MR multilayer beam is studied in terms of the modal damping factors corresponding to different modes that are evaluated using the principle of modal strain energy in the finite element model. The results showed enhanced stiffness and damping properties of the MR-treated beams with increasing magnetic field intensity. A design optimization problem is then formulated to achieve maximum modal damping factors by combining the finite element analysis with the genetic algorithm and sequential quadratic programming optimization algorithms. Optimal configurations of partially treated beams are identified for realizing maximum damping factors corresponding to the first five modes, individually or simultaneously.

An optimal control strategy based on the linear quadratic regulator (LQR) is subsequently formulated to achieve enhanced vibration suppression for the fully- and partially treated beams. A state estimator based on the flexural mode shapes (FMS) is introduced and implemented to synthesize a full-state feedback controller design. The validity of the proposed FMS-based LQR controller is demonstrated by comparing the results with those obtained with observer-based LQR controller. The effectiveness of both the control strategies is demonstrated by investigating the tip displacement response to an impulse and a white noise disturbance for different boundary conditions. The results show that the settling time, peak displacement and FFT amplitude corresponding to each mode of the system have significantly been reduced in the controlled structure. The

closed loop power spectral density of the tip displacement response due to the white noise disturbance confirms the controllable capability of the LQR controller in semi-active control to attenuate the vibration of the MR sandwich beam under high band frequencies.

**This work is dedicated with all my heart to  
my beloved parents, C. Rajamohan and V. Sambooranam whose  
continuous support made this achievement possible.**

## ACKNOWLEDGEMENTS

I would like to take this opportunity to express my deep sense of gratitude and profound feeling of admiration to my thesis supervisors, Dr. Subhash Rakheja and Dr. Ramin Sedaghati. Advices I received from my supervisors concerning the scope and direction of this dissertation have been invaluable.

I would also like to thank the faculty members of Mechanical and Industrial Engineering Department at Concordia University, in particular, my committee members.

The technical assistance provided by the Department's technical staff specially Dan Juras and Henry Szczawinski is also appreciated.

My eternal thanks and gratitude to my parents for continuous support and encouragement throughout my educational career. Without their support I would not have been able to complete my studies. I am also thankful to my brothers and sisters for their constant care and prayers. I would also like to express my deepest gratitude to my wife, T. Mahalakshmi, for her limitless patience, understanding and encouragement during the period of my thesis preparation. Last but not least, I would like to express my warmest thanks to my friends Alfin, Bala, Lakshmish, Krishna and Anand for their support and help.

## TABLE OF CONTENTS

NOMENCLATURE	xii
LIST OF FIGURES	xv
LIST OF TABLES	xix

### CHAPTER 1

#### INTRODUCTION AND LITERATURE SURVEY

1.1 GENERAL	1
1.2 LITERATURE REVIEW	3
1.2.1 MR fluids	4
1.2.2 Modes of operation of MR fluids	6
1.2.3 Modeling of MR fluids	7
1.2.4. MR dampers for vibration reduction	11
1.2.5. Application of ER/MR fluids in vibration reduction of sandwich construction	17
1.3 MOTIVATION AND OBJECTIVES	23
1.4 ORGANISATION OF THE DISSERTATION	25

### CHAPTER 2

#### VIBRATION ANALYSIS OF A MULTI-LAYER BEAM WITH MAGNETORHEOLOGICAL FLUID

2.1 INTRODUCTION	30
2.2 MATHEMATICAL MODELING OF THE MULTI-LAYER BEAMS	31
2.2.1 Formulation of energy equation	35
2.2.2 Finite element formulation	37
2.2.3 Ritz formulation	39
2.3 EXPERIMENTAL METHOD AND DATA ANALYSIS	40
2.3.1. Estimation of complex shear modulus and model validations	42
2.4. RESULTS AND DISCUSSION	47
2.4.1. Influences of magnetic field intensity	48

2.4.2. Influences of MR layer thickness	52
2.4.3. Effect of magnetic field intensity on the transverse response of the beam	55
2.5 CONCLUSIONS	57

### **CHAPTER 3**

#### **VIBRATION ANALYSIS OF A PARTIALLY TREATED MULTI-LAYER BEAM WITH MAGNETORHEOLOGICAL FLUID**

3.1 INTRODUCTION	59
3.2 DYNAMIC MODEL OF A PARTIALLY TREATED MULTI-LAYER BEAM	61
3.2.1 Formulation of energy equations	65
3.2.2 Finite element formulation	69
3.2.3 Ritz formulation	71
3.3 EXPERIMENTAL STUDY AND VALIDATION OF THE DEVELOPED FINITE ELEMENT FORMULATION	72
3.4 PARAMETRIC STUDIES	77
3.4.1. Influence of magnetic field intensity on natural frequencies	79
3.4.2. Influence of magnetic field intensity on loss factor	82
3.4.3. Influences of location of MR fluid	85
3.4.4. Influence of the length of MR fluid layer	90
3.4.5. Transverse response of the partially treated MR sandwich beam	91
3.5 CONCLUSIONS	95

### **CHAPTER 4**

#### **OPTIMUM DESIGN OF A MULTI-LAYER BEAM PARTIALLY TREATED WITH MAGNETORHEOLOGICAL FLUID**

4.1 INTRODUCTION	96
4.2 FINITE ELEMENT MODELING OF A PARTIALLY TREATED MULTI-LAYER BEAM	97
4.2.1 Formulation of finite element matrices	101

4.3 MODAL DAMPING FACTOR	103
4.3.1. Influence of location of MR fluid segments on the modal damping factor and natural frequency	104
4.4 FORMULATION OF THE OPTIMIZATION PROBLEM	110
4.4.1. Optimization methods and validation	112
4.5. RESULTS AND DISCUSSION	
4.5.1. Optimal locations based on individual modes (Case 1)	115
4.5.2. Optimal locations based on linear combination of the modal damping factors (Case 2)	121
4.5.3. Optimal locations based on logarithmic combination of the modal damping factors (Case 3)	122
4.5.4. Transverse vibration response	124
4.6 CONCLUSIONS	126

## **CHAPTER 5**

### **OPTIMAL VIBRATION CONTROL OF BEAMS WITH TOTAL AND PARTIAL MR-FLUID TREATMENTS**

5.1 INTRODUCTION	128
5.2. FINITE ELEMENT FORMULATION OF MR SANDWICH BEAM	129
5.3 DESIGN OF AN OPTIMAL CONTROLLER	133
5.3.1. Observer based optimal controller	135
5.3.2. Flexural mode shape (FMS) based optimal controller	137
5.4 RESULTS AND DISCUSSION	138
5.4.1. Full-state observer based LQR control	
5.4.1.1. Response to impulse disturbance	140
5.4.1.2 Response to white noise disturbance	148
5.4.2 Flexural mode shape (FMS) based LQR control	151
5.5. CONCLUSIONS	156

## **CHAPTER 6**

### **CONCLUSIONS AND RECOMMENDATIONS**

6.1 MAJOR CONTRIBUTIONS AND HIGHLIGHTS OF THE STUDY	158
6.2 MAJOR CONCLUSIONS	159
6.3 RECOMMENDATION FOR THE FUTURE WORKS	162

APPENDIX A	164
------------	-----

APPENDIX B	167
------------	-----

REFERENCES	170
------------	-----

## NOMENCLATURE

Symbols	Nomenclature
$A$	Cross sectional areas of layer
$B$	Intensity of magnetic field in Gauss
$E$	Young's moduli of layer
$\{F\}$	System force vector
$F_1$ and $F_3$	Longitudinal forces in the elastic layers 1 and 3, respectively
$\bar{G}$	Equivalent shear modulus of the homogeneous layer
$G^*$	Complex shear modulus of the MR fluid.
$G_r$	Shear modulus of the rubber
$G'$	Storage modulus of the MR fluid
$G''$	Loss modulus of the MR fluid
$I$	Second moment of inertia about the centroidal axis of the layer
$[K]$	System stiffness matrix
$[M]$	System mass matrix
$L$	Length of the MR sandwich beam
$[L]$	Observer gain
$Q$	Generalized force
$[Q]$	Symmetric semi-definite weighting matrix
$[R]$	Symmetric positive-definite weighting matrix
$T$	Kinetic energy of the layer
$[U]$	Control input matrix
$V$	Strain energy of the layer
$b$	Widths of the rubber
$b_r$	Widths of the entire sandwich beam

$\{d_e(x, t)\}$	Estimated displacement vector of the beam
$\{f\}$	Generalized excitation force vector
$\{f^e\}$	Element force vector
$h_1$ and $h_3$	Thicknesses of the elastic layers 1 and 3, respectively
$[k^e]$	Element stiffness matrix
$[m^e]$	Element mass matrix
$m$	Total mass of the beam
$n$	Number of MR fluid elements
$m_{eff}$	Effective mass of the beam
$u$	Longitudinal displacement component of any point in the MR fluid
$u_1$ and $u_3$	Longitudinal displacements of the mid-planes of the elastic layers
$w$	Transverse displacement of the beam
$\{\hat{x}_s\}$	Estimated state vector
$\{y_s\}$	Output matrix of state variables
$\gamma$	Shear strain in the MR layer
$\{\gamma\}$	Control input vector
$\tau_y$	Magnetic field induced dynamic yield stress
$\eta$	Plastic viscosity
$\dot{\gamma}$	Shear strain rate
$\rho$	Mass density of the layer
$\theta$	Rotational displacements of the beam
$\Pi$	Total potential of the system
$\omega_n$	Natural frequency
$\delta$	Logarithmic decrement
$\eta_r$	modal damping factor
$\phi^{(r)}$	$r^{\text{th}}$ mode shape vector

$\eta_d$

Loss factor of MR fluid

$\xi$

Modal damping ratio

$\varepsilon$

Observer error

### **Math symbols**

### **Nomenclature**

[ ]

Matrix

{ }

Vector

### **Acronym**

### **Nomenclature**

CCB

Clamped-clamped beam

CFB

Clamped-free beam

MR fluid

Magnetorheological fluid

SSB

Simply supported beam

LQR

Linear Quadratic Regulator

## LIST OF FIGURES

		Page
Figure 1.1	Configurations of particles suspended in ER/MR fluid: (a) in the absence of electric or magnetic field applied; (b) under electric or magnetic field; and (c) formation of particle chain structure under applied field	6
Figure 1.2	Basic modes of operation of MR fluid devices; (a) flow mode; (b) shear mode; and (c) squeeze mode	7
Figure 1.3	Shear stress–shear strain relationship of MR materials under varying intensities of magnetic field	8
Figure 2.1	(a) The sandwich beam with a MR-fluid layer; (b) Deformed and undeformed beam cross sections; and (c) Plan view of mid-layer of the sandwich beam	32
Figure 2.2	Experimental set-up	41
Figure 2.3	Influence of variations in the magnetic field intensity on the loss factor corresponding to different modes: (a) simply supported beam; and (b) clamped - free beam	51
Figure 2.4	Effect of boundary conditions on loss factors corresponding to first five modes	52
Figure 2.5	Influence of the thickness ratio ( $h_2/h_1$ ) of the MR fluid layer on the natural frequencies at magnetic field of 500 Gauss under simply supported end conditions	53
Figure 2.6	Influence of the thickness ratio ( $h_2/h_1$ ) of the MR fluid layer on the loss factor at magnetic field of 500 Gauss under simply supported end conditions	54
Figure 2.7	Influence of magnetic field on the transverse response: a) simply supported beam b) Clamped free beam	56
Figure 3.1	(a) Fully treated MR sandwich beam. (b) Partially treated MR sandwich beam(c) Deformed and undeformed beam cross section	62
Figure 3.2	The test specimen of a partially treated MR fluid sandwich beam	73

Figure 3.3	Experimental set-up. (a) Block diagram of the experimental setup (b) Photograph of the partially treated MR sandwich beam experimental set up	75
Figure 3.4	Various configurations of partially treated MR fluid sandwich beam	78
Figure 3.5	Different arrangements of configuration A of a partially treated MR sandwich beam	86
Figure 3.6	First four mode shapes of the fully and partially treated MR sandwich beam without applying magnetic field: (a) Mode 1 (b). Mode 2 (c) Mode 3 (d) Mode 4	89
Figure 3.7	Influence of MR fluid layer length on the natural frequencies of a simply supported partially treated MR sandwich beam (Configuration A) under the magnetic field of 500 Gauss	91
Figure 3.8	Influence of magnetic field on the transverse response of configuration D of a simply supported partially treated MR fluid sandwich beam	92
Figure 3.9	Transverse displacement of fully and partially treated MR sandwich beam at a magnetic field of 250 Gauss under simply supported end conditions	94
Figure 4.1	(a) Partially treated MR sandwich beam with multiple MR fluid segments. (b) Partially treated MR sandwich beam with single MR fluid segment (c) Plan view of mid-layer of the sandwich beam	98
Figure 4.2	Two different configurations of a partially treated MR fluid sandwich beam. a) Configuration A b) Configuration B	105
Figure 4.3	Photograph of the experimental set-up of the fully treated MR sandwich beam to evaluate the complex shear modulus of the MR fluid	106
Figure 4.4	Influence of the location of a single MR fluid (80 mm long) segment on the modal damping factors of a partially treated MR sandwich beam with different end conditions subject to a magnetic field of 250 Gauss: (a) Mode 1; and (b) Mode 4	108
Figure 4.5	Influence of the location of a single MR fluid (80 mm long) segment on the natural frequencies of a partially treated MR sandwich beam with different end conditions subject to a	109

magnetic field of 250 Gauss: (a) Mode 1; and (b) Mode 4

Figure 4.6	Comparison of the transverse response of the clamped-free untreated beam and partially treated MR sandwich beams with optimum configurations of cases 2 and 3	125
Figure. 5.1	(a) Fully treated MR sandwich beam. (b) Partially treated MR sandwich beam	130
Figure 5.2	Selected configurations of partially treated MR sandwich beams with maximum modal damping factors corresponding to first five modes under a constant magnetic field: (a) configuration A; and (b) configuration B	139
Figure 5.3	The tip deflection responses of the fully-treated MR sandwich beam with and without the LQR control and subject to a unit load impulse: (a) time-history: without control; (b) time-history: with observer based control; (c) amplitude spectrum; (d) time-history of control magnetic field	143
Figure 5.4	The tip deflection responses of the partially-treated MR sandwich beam (configuration A) with and without the observer based LQR control and subject to a unit load impulse: (a) time-history; (b) amplitude spectrum	145
Figure 5.5	The tip deflection responses of the partially-treated MR sandwich beam (configuration B) with and without the observer based LQR control and subject to a unit load impulse: (a) time-history; (b) amplitude spectrum	147
Figure 5.6	Comparisons of the transfer functions of the tip displacement responses of beams with and without observer based LQR control: (a) Fully treated beam; (b) configuration A; and (c) configuration B	151
Figure 5.7	Comparisons of deflection responses of the fully treated passive beam estimated using FMS and the finite element model: (a) $x = 100$ mm; and (b) $x = 200$ mm	153
Figure 5.8	Comparisons of deflection responses of the fully treated beam estimated using FMS based and observer based LQR controllers : (a) $x = 100$ mm; and (b) $x = 200$ mm	154
Figure 5.9	Open and closed loops responses at the tip of the fully treated MR sandwich beam under the impulse disturbance at the tip of the beam using FMS based controller	154

Figure 5.10 Comparisons of the transfer functions of the tip displacement responses of the fully treated beam with and without FMS based LQR control

156

## LIST OF TABLES

		Page
Table 2.1	Comparisons of measured natural frequencies of the cantilever MR sandwich beam with those derived from the finite-element formulation employing estimated and refined complex shear moduli of the MR fluid	44
Table 2.2	Comparisons of natural frequencies of a cantilever MR-sandwich beam derived from the finite-element and Ritz formulations with the measured frequencies	46
Table 2.3	Influence of variations in the magnetic field intensity on the natural frequencies of the MR sandwich beam for different boundary conditions	49
Table 3.1	Comparison of natural frequencies of a partially treated cantilever MR- sandwich beam derived from the finite-element and Ritz formulations with the measured frequencies	76
Table 3.2	Comparison of natural frequencies of a partially treated simply supported MR- sandwich beam derived from the finite-element with Ritz formulations at the magnetic field of 0 Gauss	78
Table 3.3	Influence of variations in the magnetic field intensity on the natural frequencies of different configurations of a partially treated simply supported MR sandwich beam	80
Table 3.4	Influence of variations in the end conditions on the natural frequencies of the fully and partially treated MR sandwich beams at the magnetic field of 500 Gauss	80
Table 3.5	Influence of variations in the magnetic field intensity on the loss factor for the various configurations of a partially treated MR sandwich beam under different end conditions	83
Table 3.6	Influence of variations in the location of MR fluid on the natural frequency of configuration A of the partially treated MR sandwich beam at the magnetic field of 500 Gauss	87
Table 3.7	Influence of variations in the location of MR fluid on the loss factor of configuration A of the partially treated MR sandwich beam at the magnetic field of 500 Gauss	87
Table 3.8	Location and magnitude of the maximum displacement of	94

transverse displacement at magnetic field of 500 Gauss for simply supported end conditions

Table 4.1	Comparisons of optimum locations of the MR fluid segments and modal damping factors of configuration A of a partially treated MR sandwich beam with clamped-free end conditions computed using GA and SQP with those identified from figure 4.4	114
Table 4.2	Optimum location of MR fluid segments of the partially treated (configuration B) simply-supported beam, and the modal damping factors and deflection modes corresponding to the first five modes (Magnetic field = 250 Gauss; ——— With MR fluid treatment; - - - - - without MR fluid treatment)	118
Table 4.3	Optimum location of MR fluid segments of the partially treated (configuration B) clamped-free beam, and the modal damping factors and deflection modes corresponding to the first five modes (Magnetic field = 250 Gauss; ——— with MR fluid treatment; - - - - -without MR fluid treatment)	119
Table 4.4	Optimum location of MR fluid segments of the partially treated (configuration B) clamped-clamped beam, and the modal damping factors and deflection modes corresponding to the first five modes (Magnetic field = 250 Gauss; ——— with MR fluid treatment; - - - - - without MR fluid treatment)	120
Table 4.5	Optimum locations of the MR fluid segments of the partially treated MR sandwich beams identified through the linear combination of the first five modes (Case 2)	122
Table 4.6	Optimum locations of the MR fluid segments of the partially treated MR sandwich beams identified through the logarithmic combination of the first five modes (Case 3)	123
Table 5.1.	The lower and upper bounds of $[R]$ and $[Q]$ and the optimal values, $[R^*]$ and $[Q^*]$ - Impulse disturbance	141
Table 5.2.	The lower and upper bounds of $[R]$ and $[Q]$ and the optimal values, $[R^*]$ and $[Q^*]$ - White noise disturbance	148

# CHAPTER 1

## INTRODUCTION AND LITERATURE SURVEY

### 1.1 GENERAL

Damping augmentation of dynamic structures exposed to uncertain excitations is of key interest to aerospace, mechanical and civil engineers. Noise and vibration reduction is a major challenge pertaining to these fields; especially in aerospace applications and such a reduction must be achieved with a minimal increase in weight. The existing techniques primarily use passive and active devices for attenuating the vibration. Although passive devices featuring elastomeric materials, hydraulic and frictional dampers provide design simplicity at a low cost, the performance limitations are inevitable due to their constant stiffness and damping properties over the entire ranges of external excitations. On the other hand, active control systems are easily adaptable to changes in excitation and structural properties. However, the applications of such systems cannot always be justified in situations where high cost and large power requirements outweigh the performance gains. Alternatively, a wide range of semi-active devices have evolved to achieve a compromise between the simplicity of the passive approach and performance benefits of the active devices while maintaining the versatility and adaptability of the fully active systems. A range of semi-active damping control concepts have evolved for various structural vibration control applications, which could offer performance gains comparable to those of the active control devices with only minimal power requirements [e.g., Spencer and Nagarajaiah, 2003; Xu, *et al.*, 2000 ].

Electrorheological (ER) and Magnetorheological (MR) fluids are increasingly being used as the working hydraulic fluid in semi-active vibration devices in various applications such as automotive suspensions and structures [Peel *et al.*, 1996; Choi, *et al.*, 2001; Pranoto *et al.*, 2002]. Such fluids can provide significant and rapid changes in the damping and stiffness properties with application of an electric or magnetic field [Weiss *et al.*, 1994], respectively. Although these fluids have been widely presented as smart controllable fluids, ER fluids exhibit a number of shortcomings compared to MR fluids such as low yield strength, requirement of high voltage and greater sensitivity to common impurities [Carlson, 1994]. MR fluids, with their rapid response time, have been considered promising for various semi-active damping control applications in the low to moderate frequency ranges (50-100 KHz).

Surface damping treatments are often used to solve a variety of resonant noise and vibration problems, especially those associated with sheet metal structure vibration [Nashif *et al.*, 1985, Baz and Ro, 1995]. Such treatments can easily be applied to existing structures and provide high damping capability over wide temperature and frequency ranges. They are usually classified in two categories: (a) unconstrained or free layer damping, where the damping material is subjected to axial deformation; and (b) constrained-layer damping treatment, where the damping material is subjected to shear deformation. A constrained-layer damping system is usually recommended for structural systems because the energy is dissipated as a result of shear deformation of the damping layer with the face layers [Liu and Chattopadhyay, 2000; Stanway *et al.*, 2003]. Alternatively, MR and ER fluids could be applied in structures using multiple layers or sandwich configurations to achieve enhanced stiffness and damping properties [Gandhi *et*

*al.* 1989; Yalcintas and Dai, 1999; Qiu and Khajika, 1999]. The multiple layer structures, in general, are known to yield improved performance due to their high flexural stiffness to weight ratio, reduced lateral deformation, higher buckling resistance and higher natural frequencies [Zenkert, 1995; Rao, 2003].

The MR or ER fluid treated sandwich structures offer attractive potential for realizing constrained layer damping treatment and semi-active vibration control. This forms the primary motivation for this dissertation research. Owing to the rapid response time and higher yield strength of MR fluids, this dissertation research presents a detailed study of a sandwich beam with integrated MR-fluid layer. The dynamic properties of the sandwich structure with both full- and partial- treatments of MR fluid are evaluated through development and analysis of analytical models for various boundary conditions. The laboratory experiments are also performed to explore the properties of a MR fluid-treated cantilever beam subject to constant levels of magnetic fields. The design optimization methods are also applied to identify localized fluid treatments for enhanced vibration control. Furthermore, an optimal closed loop control strategy based on a full order observer and flexural mode shape (FMS) based Linear Quadratic regulator (LQR) for suppression of vibration of the fully and partially treated MR sandwich beams under impulsive and random excitations is formulated.

## **1.2. LITERATURE REVIEW**

The design and analysis of multiple layer sandwich beams with semi-active vibration control encompasses several technical challenges associated with analyses of multi-layer structures, characterization of MR-fluid properties, design and fabrication,

identifications of localized fluid treatment locations, analysis of sandwich structures with localized MR-fluid treatments, controller design, etc. The reported relevant studies are thus thoroughly reviewed to build essential background, to seek knowledge on analytical and experimental methods, and to formulate the scope of the dissertation research. The reported studies, grouped under relevant topics, are briefly discussed in the following subsections.

### **1.2.1 MR fluids**

Controllable fluids such as Electrorheological (ER) and Magnetorheological (MR) fluids have been used in various semi-active vibration control applications [See, 2004; Carlson, 1994]. Such fluids exhibit rapid change in their rheological properties and thus in the damping and stiffness properties with application of an electric or magnetic field [Carlson, 1994]. Unlike the active control systems that generally require a significant amount of energy be injected into the system, the semi-active control devices involve modifications of mechanical properties of the system in the desired manner with only modest external energy [Dogruer et al., 2008]. Consequently, a vast number of studies in the past few decades have focused on developments in semi-active devices, including those based on the controllable ER and MR fluids, for wide ranges of engineering application. The most fundamental property of interest for the controllable ER and MR fluids is that they exhibit an electric or magnetic field-dependent yield stress which is associated with the formation of chains of polarizable particles in the direction of the applied electric or magnetic field (Fig. 1.1). The formation of chains yields force of attraction among the particles due to the induced field and consequently, manifest the

resistance to shear deformation in the fluid. The yield force and viscosity of such fluids can be continuously varied under the application of varying electric or magnetic fields.

The primary difference between ER and MR fluids lies in the magnitude of their characteristic yield stresses. MR fluids are known to exhibit considerably higher dynamic yield strength, nearly twice that of ER fluids [Phule, 1999]. Furthermore, MR fluids offer greater insensitivity to temperature variations and contaminants compared to ER fluids [Weiss *et al.*, 1994; Wang and Meng, 2001]. The yield stress of the MR fluid, MRF-100, lies in the order of 2-3 kPa in the absence of a magnetic field and it rapidly exceeds 80kPa under the application of a magnetic field in the order of 3000 Oe [Carlson, 1994]. The degree of change is related to the strength of the applied magnetic field, while the change can occur in less than 1 millisecond (Carlson *et al.*, 1995). MR fluids can operate in environments with wide variations in temperature, namely  $-40^{\circ}\text{C}$  to  $150^{\circ}\text{C}$  [Weiss *et al.*, 1997], while their viscosity can vary between 0.20–0.30 Pa-s at  $25^{\circ}\text{C}$  in the absence of magnetic field [Goncalves *et al.*, 2006; Carlson *et al.*, 1995].

MR fluids are also considered to yield high bandwidth control through rapid variations in the rheological properties under a varying magnetic field. Factors such as the size and volume fraction of the iron particles, and nature of the carrier fluids and the additives used will affect these properties. Among these properties, the off state viscosity and the field dependent yield stress are major parameters, which are considered in the design of MR devices [Ashour *et al.*, 1996]. MR fluids have been considered promising for various semi-active damping control applications involving low to moderate frequency ranges, including automotive suspension [Han *et al.*, 2006], structures [Yao *et al.*, 2002; Oh and Onoda, 2002; Pranoto *et al.*, 2002], optical polishing (Kordonski and

Golini, 1999), telerobotic systems ( Farzhad, 2008), fluid clutches (Lee *et al.* 2000), vibration isolation systems (Yoshoka *et al.* 2002; Stelzer *et al.* 2003; Choi *et al.* 2005; Hiemenz *et al.*, 2008), valves (Yoo and Wereley, 2002) and a variety of aerospace (Kamath *et al.*, 1999; Wereley *et al.*, 1999; Marathe *et al.*, 1998; Choi and Wereley, 2003; Zhao *et al.* 2004; Hu and Wereley, 2008), civil (Sodeyamma *et al.*, 2001; Ribakov and Gluck, 2002) and automotive (Lam and Liao, 2003; Linder *et al.*, 2003, Breese, D.G. and Gordaninejad, F., 2003) damping applications.

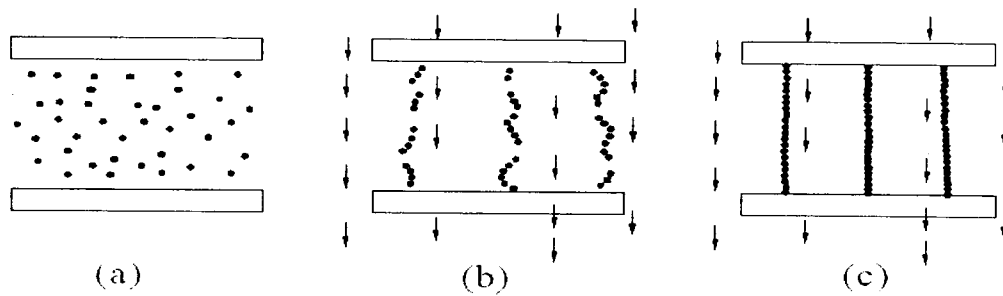


Figure 1.1: Configurations of particles suspended in an idealized ER/MR fluid: (a) in the absence of electric or magnetic field applied; (b) under electric or magnetic field; and (c) formation of particle chain structure under applied field.

### 1.2.2 Modes of operation of MR fluids

For vibration control applications, MR fluid could be employed in one of three primary modes, namely the flow mode, the shear mode and the squeeze-flow mode (Figure 1.2) [Wereley and Pang, 1998; Wang and Meng, 2001]. These modes involve, respectively, fluid flowing as a result of pressure gradient between two stationary plates; fluid between two plates moving relative to one another; and fluid between two plates moving in a direction perpendicular to the plane of the plates. In all cases the magnetic field is applied in a direction perpendicular to the plane of the plates, so as to restrict fluid

flow in the direction parallel to the plates. The applications of these various modes are numerous. Flow mode can be used in dampers [Xu *et al.*, 2000; Yao *et al.*, 2002] and shock absorbers [Wang and Li, 2006; Ericksen and Gordaninejad, 2003; Nguyen and Choi, 2009] by using the movement to be controlled to force the fluid through channels across which a magnetic field is applied. Shear mode is particularly useful in clutches and brakes [Jansen and Dyke, 2000; Li and Du, 2003] where a resistance to rotational motions is required. Squeeze-flow mode on the other hand, is most suitable for applications involving the control of small magnitude movements, in the order of millimeters, but large forces [Mazland *et al.* 2007; Wang *et al.*, 2005; See, 2003].

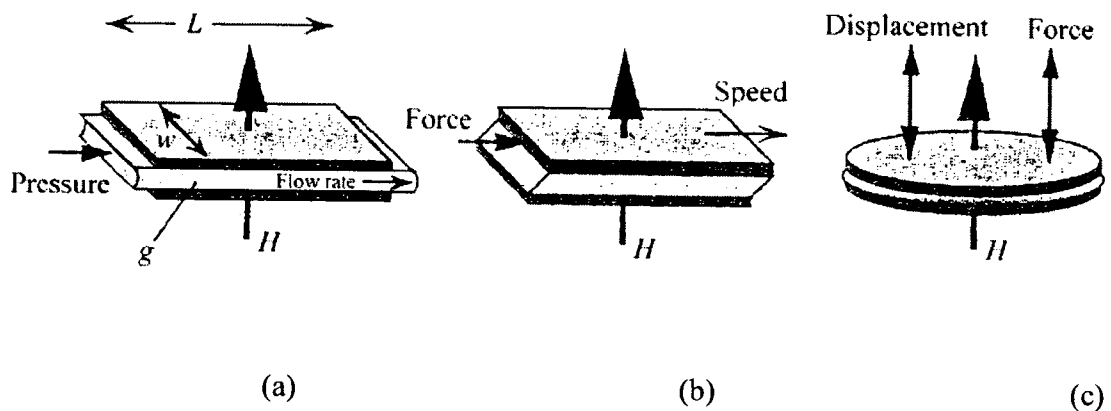


Figure 1.2: Basic modes of operation of MR fluid devices; (a) flow mode; (b) shear mode; and (c) squeeze mode. [Wang and Meng, 2001]

### 1.2.3 Modeling of MR fluids

The rheological properties of the MR fluid have been widely characterized [Weiss *et al.*, 1994; Jolly *et al.*, 1998; Genç and Phulé; 2002]. The shear modulus of the MR fluid has been described in a number of studies on the basis of measured shear stress-shear strain properties [Weiss *et al.*, 1994; Choi *et al.*, 1995, Li *et al.*, 1999; Nakano and Yamamoto, 1999; Wang and Kamath, 2006]. These studies have characterized the shear

stress-strain properties in two distinguished regions, referred to as ‘pre-yield’ and ‘post-yield’ regions, as shown in Figure 1.3. Although the shear stress-strain properties of the MR material strongly depend upon the applied magnetic field, the measured properties generally exhibit quite comparable patterns. In the pre-yield regime, the MR material demonstrates viscoelastic behavior, which has been described by the complex modulus  $G^*$ , given by [Li *et al.*, 1999; Li *et al.*, 2002]:

$$G^* = G' + iG'' \quad (1)$$

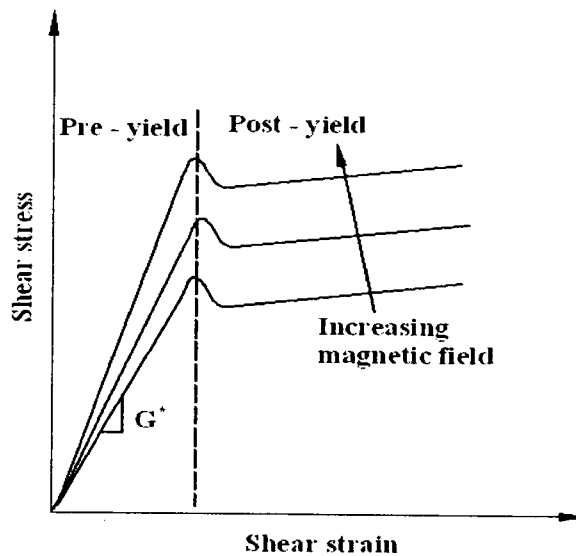


Figure 1.3. Shear stress–shear strain relationship of MR materials under varying intensities of magnetic field [Li *et al.*, 1995]

where  $G'$  is the storage modulus of the MR fluid, which is related to the average energy stored per unit volume of the material during a deformation cycle, and  $G''$  is the loss modulus, a measure of the energy dissipated per unit volume of the material over a loading and unloading cycle. The shear stress can thus be expressed as,  $\tau = G^* \gamma$ , where  $\gamma$  is the shear strain [Jolly *et al.*, 1998].

The post-yield regime is the dominant mode of operation, in most devices such as dampers, valves, and clutches. When the fluid undergoes a shear thinning or thickening, its post-yield behavior is non-linear and this effect requires a fluid model to account for the non-Newtonian behavior of MR fluids. The post-yield behavior of the MR materials has been approximately characterized by three phenomenological models, namely, the Bingham plastic model, the Herschel-Bulkley model and the biviscous model [Choi *et al.*, 2001]. According to Bingham and Herschel-Bulkley models, the MR fluid behaves as a Newtonian fluid in the absence of the magnetic field. The fluid, however, is characterized by a non-Newtonian fluid, when exposed to a magnetic field. Mathematically, these models describing the shear stress-strain behavior are expressed as:

Bingham plastic model:

$$\tau = \begin{cases} \tau_y + \eta\dot{\gamma}; & \tau > \tau_y \\ 0; & \tau \leq \tau_y \end{cases}$$

Herschel-Bulkley model:

$$\tau = \begin{cases} (\tau_y + K|\dot{\gamma}|^{1/m})\text{sgn}(\dot{\gamma}); & \tau > \tau_y \\ 0; & \tau \leq \tau_y \end{cases}$$

Biviscous model:

$$\tau = \begin{cases} (\tau_{yd} + \eta_{po}\dot{\gamma}); & \tau > \tau_{ys} \\ \eta_{pr}\dot{\gamma}; & \tau \leq \tau_{ys} \end{cases} \quad (2)$$

where  $\tau$  is the shear stress,  $\tau_y$  is the yield stress,  $\eta$  is the plastic viscosity,  $\dot{\gamma}$  is the shear strain rate,  $m$  is the flow index and  $K$  is a consistency parameter. The constants  $\eta_{pr}$  and  $\eta_{po}$  are the viscosity in the pre-yield and post yield regions, respectively. For  $K = \eta$  and  $m=1$ , the Herschel-Bulkley model reduces to the Bingham plastic model.

The Bingham plastic model is often used to describe the post yield phenomenon (Stanway *et al.*, 1996, Weiss *et al.*, 1994; Li *et al.*, 1999; Choi *et al.*, 1995) of the MR fluid. In the Bingham plastic model, MR fluids are typically assumed to be Newtonian fluids in post-yield regime, with a constant plastic viscosity assumption. However, for cases where the fluid experiences post-yield shear thinning or shear thickening, the assumption of constant plastic viscosity may not be valid. The shear thinning effect of ER fluid was shown through experimental investigation on ER grease damper by Marksmieir *et al.* (1998). The study concluded that the Herschel-Bulkley model would be more appropriate than the Bingham plastic model for ER/MR fluids in the post yield region. Wang and Gordaninejad (1999) extended the work by Marksmieir *et al.* (1998) and demonstrated experimentally and theoretically that Herschel-Bulkley fluid model could be successfully employed for MR fluids characterizing the non-Newtonian post yield behavior.

Numerous models based on the iron particle size have also been proposed to describe the characteristics of MR materials with applied magnetic field. Jolly *et al.* (1996) presented a model that examines shear stress of the chain caused by inter-particle magnetic force. Furthermore, the model was experimentally verified for MR fluids containing three different iron volume concentrations and concluded that the yield stress could be increased by increasing the iron concentration in the fluid. Two - and three -

dimensional models have also been developed for characterizing the variations in the yield stress of the MR fluid with the applied magnetic field and total volume fraction of iron particles (Tang and Conrad, 2000). The proposed models were also validated using the measured properties. It was concluded that the saturation yield stress of MR fluids is proportional to the square of the saturation magnetization. Ciocanel (2006) proposed a micro structural model by considering the relative motion of a pair of particles within the MR fluid medium. It was concluded that the yield stress could be determined by the stress level required to separate any two particles in the fluid and exposed to certain shear stress rate and magnetic field strength.

The stress-strain properties of MR-fluids are known to vary significantly with the intensity of applied magnetic field [Weiss *et al.*, 1994; Jolly *et al.*, 1998; Li *et al.*, 1999]. The properties of MR-fluid damper have been widely characterized by current-dependent force-velocity properties via laboratory measurements [Choi *et al.*, 2001; Yang *et al.*, 2002;]. These clearly suggest nonlinear variations in the damping properties with applied magnetic field. Furthermore, these have shown considerable hysteresis. A vast number of studies have thus attempted to develop models for describing the damping force as a function of both the applied current and the damping velocity [Li *et al.*, 2002; Koo *et al.*, 2006].

#### **1.2.4. MR dampers for vibration reduction**

With advancements in vibration control strategies and developments in controllable actuators, the MR-fluid dampers are increasingly being applied as vibration isolators, particularly in vehicle suspension systems. This is attributed to the fact that they

can offer large range of damping force capacity and robust operation in a reliable fail-safe manner with low power requirements to provide improved ride comfort and road handling performances. A comparison among the passive, active and semi-active vibration isolation systems was presented by Margolis (1983) which concluded that semi-active system provide much better performance which could be employed with the realistic feedback signals when controlling the vibration. Choi *et al.* (2000) proposed a semi-active suspension seat employing MR-fluid damper on the basis of Bingham model and the sky-hook control. Goncalves (2001) investigated experimentally the dynamic performance of a quarter car system incorporating an MR fluid suspension damper and compared the response characteristics of various semi-active control strategies including skyhook, ground hook, hybrid, displacement skyhook and relative displacement skyhook controls.

Lai and Liao (2002) investigated the performance of a MR damper integrated in a single-degree of-freedom (DOF) suspension system model subjected to a random excitation. The study proposed a control law based on sliding mode controller. Yao *et al.* (2002) presented a semi-active control strategy based on the sky-hook control and Bouc-Wen MR damper model for a quarter-car model to control the transmission of road vibration. Sammier *et al.* (2003), in a similar manner, investigated a semi-active control law based on  $H_\infty$  controller design for a single wheel MR-suspension model to improve vehicle ride comfort.

Guo *et al.* (2004) analyzed the effectiveness of a neural network controller based MR damper to suppress the road induced vibration in vehicles at low frequency range. The study presented a numerical and experimental investigation on a quarter vehicle

model and concluded that semi-active suspensions with MR damper could yield superior performance to passive suspensions. Du et al. (2005) conducted an experiment on a prototype MR damper subjected to cyclic excitation and proposed a semi-active  $H_\infty$  control law for a quarter car suspension model. Batterbee and Sims (2007) also developed a two degree of freedom quarter-car model with sky-hook damping control strategy and experimentally investigated the effectiveness of the MR damper control using hardware-in-the-loop simulation (HILS) method. The study demonstrated that the feedback linearization could provide better performance in terms of passenger comfort and road handling compared with other control strategies.

Dogrue *et al.* (2008) developed and tested a new MR damper design for high mobility and multi-purpose wheeled vehicle (HMMV) to achieve non-symmetrical force characteristics in rebound and compression. Yu *et al.* (2009) developed a dynamic model of a half car MR suspension system and a human simulated intelligent control (HSIC) scheme to attenuate the pitch vibrations. The effectiveness of the control scheme was also demonstrated using the actual passenger car test installed with four MR dampers. Choi *et al.* (2002) further investigated the performance characteristics of the MR-fluid suspension using a  $H_\infty$  controller for vibration suppression of a full vehicle system model comprising four independent MR damper suspensions. Choi and Han (2003) experimentally analyzed the control responses of the cylindrical MR suspension seat damper in terms of the acceleration at the driver's seat of a full-vehicle model under both bump and random road excitations. Liao and Wang (2003) investigated the feasibility of implementation of MR damper for improving the ride quality of railway vehicles using the LQG control law.

Giuclea *et al.* (2004) analyzed the effectiveness of a fuzzy controller for the semi-active MR-suspension system to reduce the chattering effect. Savaresi *et al.* (2005) developed a model based on black box non-linear model for MR damper in vehicle applications and concluded that for variable current settings, the black box model outperforms the semi-physical model developed by Spencer *et al.* (1997). Wang *et al.* (2005) proposed a model to characterize the biviscous hysteretic force characteristics of a MR damper for vehicular suspension applications using symmetric and asymmetric sigmoid functions.

MR dampers have also been used in vibration reduction of various structural applications. Dyke *et al.* (1996) proposed a clipped-optimal control strategy based on acceleration feedback for controlling MR dampers to reduce the structural vibration under a seismic excitation and demonstrated the effectiveness of the controller through numerical simulations of a three-story building model. Experimental investigation was performed by the same authors (1998) to investigate the effectiveness of the proposed controller by comparing the measured peak and RMS responses with those of the system with a passive damper. The study concluded that MR damper is quite effective for structural vibration reduction. Spencer Jr. *et al.* (1998) analyzed the effectiveness of axisymmetric and parallel plate model for MR damper application in seismic vibration reduction of large structures. They also studied experimentally the effectiveness of the models with full scale (20-ton) MR damper. Yi *et al.* (2001) demonstrated experimentally the capabilities of multiple MR dampers for seismic control of a six-story structure using Lyapunov and clipped-optimal algorithms. Schurter and Roschke (2001) developed a fuzzy controller based on the acceleration feedback to reduce vibration of seismically

excited buildings equipped with MR dampers. It was concluded that MR dampers could yield superior performance when used with multiple-DOF structures for reduction of lateral acceleration compared to the passive systems.

The effectiveness of the sliding mode control system using the MR damper in reducing the vibration responses under seismic loading conditions was demonstrated numerically by Moon *et al.* (2003). The results attained for the MR-damper were compared with those of fully-active system and it was concluded that MR damper with sliding mode control is more effective than the active systems. Occhiuzzi *et al.* (2003) experimentally investigated the performance of four prototype MR dampers under harmonic displacement and imposed constant velocity tests and numerically validated the results using Bingham model for MR damper and suitability of those dampers for vibration response reduction of civil structures. Zhou *et al.* (2003) proposed an adaptive control strategy using MR damper for protecting the building against severe earth quakes and strong winds, and concluded that the combination of fuzzy controller and adaptive law for the MR damper provides robust control for non-linear structures. Hiemenz *et al.* (2003) analyzed numerically and experimentally the effectiveness of the MR braces installed in a three-story building in mitigation of earthquake hazards.

Yang *et al.* (2004) proposed a model for a full scale MR damper under dynamic loading conditions of large structures based on Bouc-Wen model by considering the fluid thinning and inertia effects. The study experimentally verified the model results in terms of force rolloff in the low velocity region, force overshoot when velocity changes sign and clockwise hysteresis loops. Yoshida and Dyke (2004) designed semi-active control system based on clipped optimal control strategy for reducing the vibration responses of

20-story building using MR damper. The study also compared the results with those obtained with an active and ideal semi-active damper (purely dissipative device capable of generating control forces) and concluded that the MR damper is more effective in attenuating the vibration than the active system and achieves a performance similar to the ideal semi-active system. Yoshida and Dyke (2005) further studied the effectiveness of a MR damper to control the vibration response of the full scale asymmetric buildings exhibiting coupled lateral and torsional motions using the genetic algorithm based control strategy. Tse and Chang (2004) investigated the effectiveness of the rotary type MR damper (Shear mode MR damper) in controlling the wind induced vibration of a building model in a wind tunnel and demonstrated experimentally that inverse dynamic model closely yields the required control force. Sahasrabudhe and Nagarajaiah (2005) investigated analytically and experimentally the effectiveness of the MR damper under several near fault earthquakes for a 1:20 scaled bridge model using the Lyapunov control algorithm. It was concluded that bearing displacement could be effectively reduced using a MR damper compared to that with a passive damper.

Jung *et al.* (2006) investigated the effectiveness of the various semi-active MR-damper based control systems including the modified clipped-optimal control, the maximum energy dissipation, the modulated homogeneous friction, and fuzzy logic-based control algorithms. It was concluded that the original clipped-optimal algorithm could be more effective in reducing the base displacement over a wide range of floor acceleration variations. The modified clipped-optimal algorithm, however, resulted in better performance under higher magnitudes of the floor acceleration. Yan and Zhou (2006) presented a numerical investigation of a control strategy based on genetic

algorithm with fuzzy controller to minimize both the maximum displacement and acceleration response of the structure equipped with a MR damper under earthquake like excitation. Loh *et al.* (2007) investigated the performance of a MR damper employing a wireless sensor and evaluated the control gains for a LQG controller applied to a three story building. Gu and Oyadiji (2008) developed and showed the effectiveness of an adaptive neuro-fuzzy interference system (ANFIS) controller for vibration reduction of multiple degree of freedom structure with MR damper under earthquake excitation.

The above reported studies have invariably concluded that MR fluid dampers can provide effective control of vibration in many applications, namely, vehicle suspension, buildings and bridge structures. The reported studies have employed a wide range of controllers and control algorithms to achieve controlled damping force for realizing the objectives of the respective studies. It is apparent that the MR-dampers can be most effectively applied in a semi-active control manner with only minimal external power. Furthermore, the bandwidth of the control and the MR-damper seems to adequate for the applications considered. Fewer studies, however, have explored the applications of MR-fluids as controllable damping treatment for structures. These studies are described in the following subsections.

#### **1.2.5. Application of ER/MR fluids in vibration reduction of sandwich construction**

In the past few years, the vast majority of the efforts in ER/MR fluids have been focused on designs of ER/MR dampers and evaluations of their potential benefits in vibration suppression in structures [Aldemir, 2004; Pranoto *et al.*, 2004; Zhang and Roschke, 1999; Dyke *et al.*, 1998; Stanway *et al.*, 1996; Makris *et al.*, 1996] and systems

[Choi, 1999; Choi, *et al.*, 2001; Peel *et al.*, 1996; Hong *et al.*, 2002; Du *et al.*, 2005; Yao *et al.*, 2002; Choi *et al.*, 2002]. In structure applications, the ER/MR fluid damping has been implemented either through lumped damping elements at selected discrete locations [Pahlavan and Rezaeepazhand, 2007; J. Dyke *et al.*, 1998; Pranoto *et al.*, 2004; Bashtovoi *et al.*, 2002] or through continuous MR/ER fluid layer treatments in selected structural members. The former approach may require multiple damping elements since vibration suppression in structures generally involves considerations of multiple modes of vibration. This may lead to higher weight and complex controller design. Alternatively, the ER/MR sandwich structures, achieved by embedding ER/MR material layers between two elastic/metal layers, can yield distributed control force along the treated structural member. This approach can facilitate the control of structural vibration over a broad range of frequencies through variations in distributed stiffness and damping properties in response to applied electric or magnetic field.

The developments in ER materials based sandwich structures was initiated by Gandhi *et al.* (1989). The study evaluated the dynamic characteristics of the sandwich structures experimentally and concluded that the structural damping ratio and the natural frequencies increase with increasing the electric field. Furthermore, the test specimen was tested at a temperature of 60<sup>0</sup>C to evaluate the effect of temperature on the elastodynamic characteristics of the specimen embedded with an ER fluid layer. Significant decrease in natural frequency and increase in damping ratio were observed at higher temperatures suggesting greater sensitivity of ER fluids to temperature variations. Choi *et al.* (1990) experimentally evaluated the effect of electric field on the rheological properties of the ER fluid under free vibration response of an ER sandwich structure. Different

compositions of ER fluid such as cornstarch-corn oil and Zeolite-silicone oil were considered to fabricate the test specimens. The study illustrated substantial variations in damping ratio of the ER sandwich beam with changes in the applied electric field. The effect of electric field on the rheological properties of the ER fluid under forced vibration response of an ER sandwich structure were also evaluated experimentally using the standard Oberst test for viscoelastic material (Choi *et al.*, 1992). Substantial increase in natural frequencies and reduction in vibration amplitude were observed corresponding to each mode. The study also suggested a simple on-off control methodology that could be implemented to control the vibration characteristics of ER sandwich beam.

Haiqing *et al.* (1993) experimentally analyzed the vibration characteristics of a cantilever beam locally linked by an ER fluid layer to the ground. It was concluded that the locally applied ER fluid layer serves as a complex spring and thus alters the damping and stiffness properties of the structures under the electric field. Leng *et al.* (1995) experimentally analyzed the vibration characteristics of the epoxy polymer matrix composite cantilever beam embedded with ER fluid and concluded that the damping ratio and natural frequencies corresponding to the first three modes were increased with increasing the electric field.

The above studies have mostly investigated the dynamic properties of the ER sandwich beams experimentally. Relatively fewer studies have investigated such properties via analytical means. Yalcintas and Coulter (1995) developed an analytical model using RKU (Ross-Kervin-Ungar) model for forced vibration of a simply supported ER sandwich beam and showed the significant effect of the electric field on vibration response of the structure, which was also verified through experimental measurements.

Yalcintas and Coulter (1995) extended their previous work by deriving an analytical model based on the sixth order transverse vibration equation developed using the Mead and Markus (1969) method to analyze the dynamic characteristics of the ER sandwich beam with different end conditions. The study investigated the dynamic characteristics of the beam in terms of natural frequencies, loss factor and the mode shapes. Haiqing and King (1997) further investigated the vibration response of a fully and partially treated ER beam clamped at both ends and concluded that the length of the ER fluid layer has a significant effect on the resonant frequencies and the loss factor. Rahn and Joshi (1998) employed the energy approach to develop an analytical model of an ER sandwich beam to predict the vibration response and proposed a controller synthesis. It was concluded that transient decay rate is significantly improved through implementation of the control law. Yalcintas and Coulter (1998) further proposed a nonhomogeneous sandwich beam comprising different ER materials along its axis and analyzed the variations in natural frequencies and loss factors under different electric field configurations. The structure was exposed to on-off control at each section and the control capability of the distributed non-homogeneous storage and loss modulus was illustrated.

Qiu and Khajika (1999) analyzed the vibration response of three- and five-layered beams with ER materials and concluded that the damping factor of a five-layer beam could be larger than that of a three-layer beam. The properties of a hybrid smart composite beam comprising carbon fiber reinforced plastics (CFRP) actuated by both the electro-rheological fluid and a piezoceramic actuator were investigated numerically and experimentally in a closed loop configuration by Fukuda *et al.* (2000). The study compared deflection and velocity feedback control strategies to control the deflection at

the free end of the cantilever beam and concluded that velocity feedback control strategy is the optimum for vibration suppression under sinusoidal excitations. Hybrid control of an ER sandwich beam was experimentally investigated by Shaw (2000) to reduce the vibration of the cantilever beam subjected to harmonic excitations. The study combined both semi-active controller based on fuzzy logic to tune the resonance frequencies and active controller based on plant disturbance cancellation to provide a negating force. The effect of spacing of parallel grooves on the local distribution of an electric field was experimentally investigated by Lee and Jwo (2001). The study analyzed the dynamic characteristics of the ER material within the parallel plate fixture and ER sandwich beam with different spacing of the grooves in the electrodes. Significant increase in the storage and loss moduli and the first two natural frequencies was observed with finer spacing of the grooves in the electrodes.

Harland *et al.* (2001) analyzed the free wave propagation through sandwich beam embedded with ER fluid numerically based on the sixth order transverse vibration equation developed by Mean and Markus (1969). The study derived the expressions for wave number, and the reflection and transmission coefficients for the first three modes, and concluded that the desired reflection and transmission could be achieved by tuning the electric field. Srikantha and Venkatraman (2003) investigated experimentally the behavior of an ER sandwich beam and estimated the viscous and non-viscous forces using the force-state mapping technique. The study also concluded that an increase in starch concentration in the ER fluid could yield greater damping factor of the sandwich beam.

The dynamic properties of sandwich structures embedded with ER fluid layers have been investigated in a large number of studies, while those employing MR fluid layers have been addressed in a relatively fewer studies. The sandwich structures with embedded MR fluid layer involve characterization of the MR fluid properties in the shear mode. Yalcintas and Dai (1999) analyzed the dynamic responses of a MR fluid adaptive structure using the energy approach and compared the responses with those of a structure employing the ER-fluid. It was concluded that the natural frequencies of MR fluid-based adaptive structure could be nearly twice those of the ER fluid-based adaptive structure. Harland *et al.* (2001) theoretically investigated the wave transmission through a structural member with ER and MR fluid filled insert. The comparisons of the responses of ER and MR inserts suggested that substantially greater changes in shear properties and reductions in wave transmission amplitude could be achieved using the MR fluid inserts compared to those ER fluid inserts.

Sun *et al.* (2003) analytically investigated the dynamic responses of a MR sandwich beam using the energy approach and compared the results with the measured data. Experiments were conducted to develop a relationship between the applied magnetic field and complex shear modulus of the MR fluid using oscillatory rheometry technique. Yeh and Shih (2006) analyzed the dynamic characteristics and instability of the MR adaptive structures under buckling loads based on the DiTaranto (1965) sixth-order partial differential equation together with the incremental harmonic balance method. Hu *et al.* (2006) analyzed the vibration characteristics of the MR sandwich beam using Mead and Markus (1969) model and concluded that the vibration amplitude of each mode decreases with increasing the magnetic field. Prieto *et al.* (2010) experimentally

analyzed the vibration responses of MR cantilever beam by activating the MR fluid fully and partially. They considered two different types of materials including aluminum and polyethylene terephthalate (PET) as face plates and concluded that PET beam showed higher shift in natural frequencies than the aluminum beam.

### **1.3 MOTIVATION AND OBJECTIVES**

From the review of the relevant studies, it is evident that controllable rheological fluids offer significant potential in control of vibration of structures. Furthermore, the MR fluids are more beneficial over the ER fluids due to their greater yield stress and temperature sensitivity. While the performance benefits of MR fluid dampers have been extensively explored for vehicular and structural applications, only limited analytical and experimental efforts have been made in developing MR-fluid treated sandwich or multi-layer structures. The vast majority of the studies have considered lumped MR/ER damping elements. In structural applications, it would be desirable to develop structures with distributed MR-fluid damping treatments in order to suppress the structural vibration corresponding to different modes. Furthermore, the analysis of MR-fluid sandwich structures have been reported for limited boundary conditions. Although a few analytical and experimental studies have contributed to the understanding of the vibration suppression capabilities of MR sandwich beams, these are mostly limited to simply supported end conditions. Furthermore, the effect of axial deformation of the MR fluid sandwich beam subjected to transverse vibration has been neglected in most of the studies. In addition, the effectiveness of the partial treatment of MR fluid in a sandwich structure on vibration control characteristics has not yet been explored theoretically and

experimentally, which would be highly desirable in view of the lower cost, controller design and implementations.

The present dissertation research thus aims to conduct fundamental investigations on the dynamic characteristics of MR fluid sandwich beams, vibration analysis of fully and partially treated MR fluid sandwich beams, design optimization of the partially treated MR sandwich beam in order to identify optimal locations of the MR fluid segments, and optimal closed loop control strategy for attenuation of vibration of the beam due to the external disturbances. The specific objectives of the proposed study are:

- (a) Formulate analytical model of a fully treated MR sandwich beam with different end conditions using the Ritz formulation and finite-element method, and to investigate the dynamic characteristics of the MR sandwich beam for different end conditions as a function of the applied magnetic field.
- (b) Design and fabricate prototype cantilever sandwich beams with a MR fluid layer and permanent magnets, and conduct experiments to characterize the dynamic properties and for model validation.
- (c) Formulate a relationship for the complex shear modulus of the MR fluid as a function of applied magnetic field by performing free oscillation experiments in the laboratory.
- (d) Formulate analytical models of a partially treated MR sandwich beam with different end conditions, and evaluate its dynamic characteristics as functions of the MR fluid segments and the magnetic field.

- (e) Formulate an optimization problem to determine optimal locations of the MR fluid segments to maximize the modal damping factors corresponding to individual and multiple modes for different end conditions.
- (f) Formulate an optimal closed loop control strategy using Linear Quadratic Regulator (LQR) based on a full and reduced order observers for suppression of vibration of the fully and partially treated MR sandwich beams under impulsive and random excitations.

#### **1.4 ORGANISATION OF THE DISSERTATION-MANUSCRIPT BASED FORMAT**

This “Manuscript-based” dissertation is organized in six chapters. Four of the chapters present four articles that illustrate the dissertation work in a sequential manner and address the objectives stated in section 1.3. Three of these articles have been published in peer-reviewed journals, while one is expected to be submitted for review very shortly to a journal. Each of these articles present a portion of the dissertation research and contents of the articles are interrelated as per the stated scope and the rules and requirements defined in “Thesis Preparation and Thesis Examination Regulation” booklet of the School of graduate Studies at Concordia University.

The first chapter summarizes the highlights of the relevant reported studies on controllable rheological fluids, dynamic characteristics of the MR and ER fluids, and their potential applications for attenuation of vibration of vehicles and structures, and the analytical and experimental methods developed. The scope of the dissertation research is subsequently formulated on the basis of the reviewed studies.

The four journal articles are reproduced in chapters 2 to 5, while their contents have been modified in order to reduce repetitions. In particular, the ‘Introduction’ section in each article is substantially modified. Furthermore, the citations in all of the articles are presented in the re-organized ‘References’ section of the dissertation. Despite these reorganizations, repetitions in the experimental setup could not be avoided since these were incorporated in most of the articles to illustrate subsequent developments. Furthermore, some repetitions in analytical formulations are also evident. Although each article presents the related formulations focusing on different aspects of the dissertation work, the formulations in subsequent articles are generally based on those reported in the previous article. Chapter 2 presents the following article published in the Journal of Smart Materials and Structures:

“Vibration analysis of a multi-layer beam containing magnetorheological fluid”, *Smart Materials and Structures*, Vol. 19, 2010, 015013 (12 p).

This article presents the finite element and Ritz formulations for the fully treated MR-fluid sandwich beam, and the design of the prototype beam for laboratory experiments. The experiment design and methods are described and the model validity is demonstrated in terms of natural frequencies corresponding to lower modes. Furthermore, a relationship between the magnetic field and the complex shear modulus of the MR materials in the pre-yield regime is presented on the basis of the measured free oscillation response data. The results attained from a parametric study are presented to characterize the dynamic properties of the MR-fluid treated structure and the factors that affect the properties in terms of variations in the natural frequencies and loss factor are discussed for various boundary conditions. These included the applied magnetic field and thickness

of the MR-fluid layer. The forced vibration response of the MR sandwich beam is also briefly discussed under harmonic excitations.

Chapter 3 presents the following article published in the Journal of Sound and Vibration:

“Vibration analysis of a partially treated multi-layer beam with magnetorheological fluid”, *Journal of Sound and Vibration*, Vol. 329, 2010, pp.3451-3469.

This article presents the concept of a partially-treated MR fluid sandwich beam and an analytical formulation to study the vibration properties of the partially-treated structure. The finite element and Ritz formulations developed in Chapter 2 are extended for the partially treated MR fluid sandwich beam by considering the strain energy associated with different segments of the MT-fluid. The validity of the proposed finite element formulation is demonstrated by comparing the results with those obtained from the Ritz formulation and the laboratory-measured results attained for a partially-treated beam. This article particularly focuses on the influences of the location and size of the MR-fluid segments in the partially treated MR sandwich beam for different end conditions. These are presented in terms of variations in the natural frequencies and loss factor as a function of location and size of the fluid segments apart from the applied magnetic field for different end conditions. Furthermore, the effects of locations of the MR fluid treatments on the deflection mode shapes and forced vibration responses are also presented and discussed.

Chapter 4 presents the following article published in the Journal of Smart Materials and Structures:

“Optimum design of a multi-layer beam partially treated with magnetorheological fluid”, *Smart Materials and Structures*, Vol. 19, 2010, 065002(15pp).

This article focuses on the modal damping characteristics of beams partially treated with magneto-rheological (MR) fluid elements using the modal strain energy approach and the finite element method. The significance of the location of MR fluid segments on the modal damping factor is particularly discussed for different end conditions. Two different optimization problems are formulated to identify optimal locations of MR-fluid segments to achieve maximum modal damping factors corresponding to the first five flexural modes, individually and simultaneously. The solutions attained from the genetic algorithm (GA) and sequential quadratic programming (SQP) methods are compared and discussed for different end conditions. The study showed that localized MR-fluid segments could significantly alter the deflection modes and the effects of the end-conditions.

Chapter 5 presents the draft article, “Optimal vibration control of beams with total and partial MR-fluid treatments” to be submitted in the *Journal of Intelligent Material Systems and Structures*. The article presents a numerical study on semi-active vibration control of a multilayer beam, treated either fully and partially with the MR fluid. An optimal control strategy based on the linear quadratic regulator (LQR) is formulated to seek active vibration suppression under limited maximum magnetic field intensity. The controller syntheses are formulated using two different methods. These included a full order observer and a limited-state approach based on the flexural mode shape (FMS) of the beam. The effectiveness of both the full observer- and the FMS-based LQR control

strategies are demonstrated by investigating the tip displacement response under impulsive and white noise random excitations.

The major conclusions drawn from the dissertation research are summarized in Chapter 6 together with a few recommendations and suggestions for further studies in the field.

## CHAPTER 2

# VIBRATION ANALYSIS OF A MULTI-LAYER BEAM WITH MAGNETORHEOLOGICAL FLUID

### 2.1 INTRODUCTION

The Magnetorheological (MR) materials exhibit rapid variations in their rheological properties, when subjected to varying magnetic field and thus offer superior potential for applications in smart structures requiring high bandwidth. MR sandwich structures can apply distributed control force to yield variations in stiffness and damping properties of the structure in response to the intensity of the applied magnetic field and could thus provide vibration suppression over a broad range of external excitation frequencies. The properties of sandwich structures employing ER fluid layers have been investigated in a large number of studies, while those employing MR fluid layers have been addressed in a relatively fewer studies. Yalcintas and Dai (1999, 2004) analyzed the dynamic responses of a MR fluid adaptive structure using the energy approach and compared the responses with those of a structure employing ER-fluid. It was concluded that the natural frequencies of MR fluid-based adaptive structure could be nearly twice those of the ER fluid-based adaptive structure. Sun *et al* (2003) analytically investigated the dynamic responses of a MR sandwich beam using energy approach and compared the results with the measured data. Experiments were conducted to develop the relationship between the applied magnetic field and complex shear modulus of the MR fluid using oscillatory rheometry technique. Yeh and Shih (2006) analyzed the dynamic characteristics and instability of MR adaptive structures under buckling loads based on

the DiTaranto (1965) sixth-order partial differential equation together with the incremental harmonic balance method.

In this chapter, the governing equations of a multi-layer beam structure employing MR-fluid layer are presented in the finite element form and Ritz formulation. The relationship between the magnetic field and the complex shear modulus of the MR material in the pre-yield regime is estimated by modeling the MR sandwich beam as a damped harmonic oscillator and measurements of free oscillations. The validity of the finite element formulations is demonstrated by comparing the results with those obtained from the Ritz formulation and laboratory measurements performed on a prototype beam. Simulations are performed to derive the essential properties of the multi-layered structure, namely natural frequencies and loss factors, as functions of the applied magnetic field and thickness of the MR-fluid layer under different boundary conditions. The dynamic responses of the structure are also presented under harmonic force excitations.

## **2.2 MATHEMATICAL MODELING OF THE MULTI-LAYER BEAMS**

A three-layer beam structure comprising a MR-fluid layer as the core between the two elastic layers (Figure. 2.1) is considered for development of the finite element model and Ritz formulation. The normal stresses in the fluid layer are neglected considering that the Young's modulus of the MR-fluid is nearly negligible compared to that of the elastic layers. The fluid layer thickness  $h_2$  is assumed to be very small compared to its length  $L$ , while the slippage between the elastic and fluid layers is neglected. The shear strain in the elastic layers is also assumed to be negligible considering that the thickness  $h_1$  and  $h_3$  are

very small compared to the length of the beam. The damping due to elastic layers is also assumed to be negligible. Furthermore, the transverse displacement  $w$  in a given cross-section is assumed to be uniform.

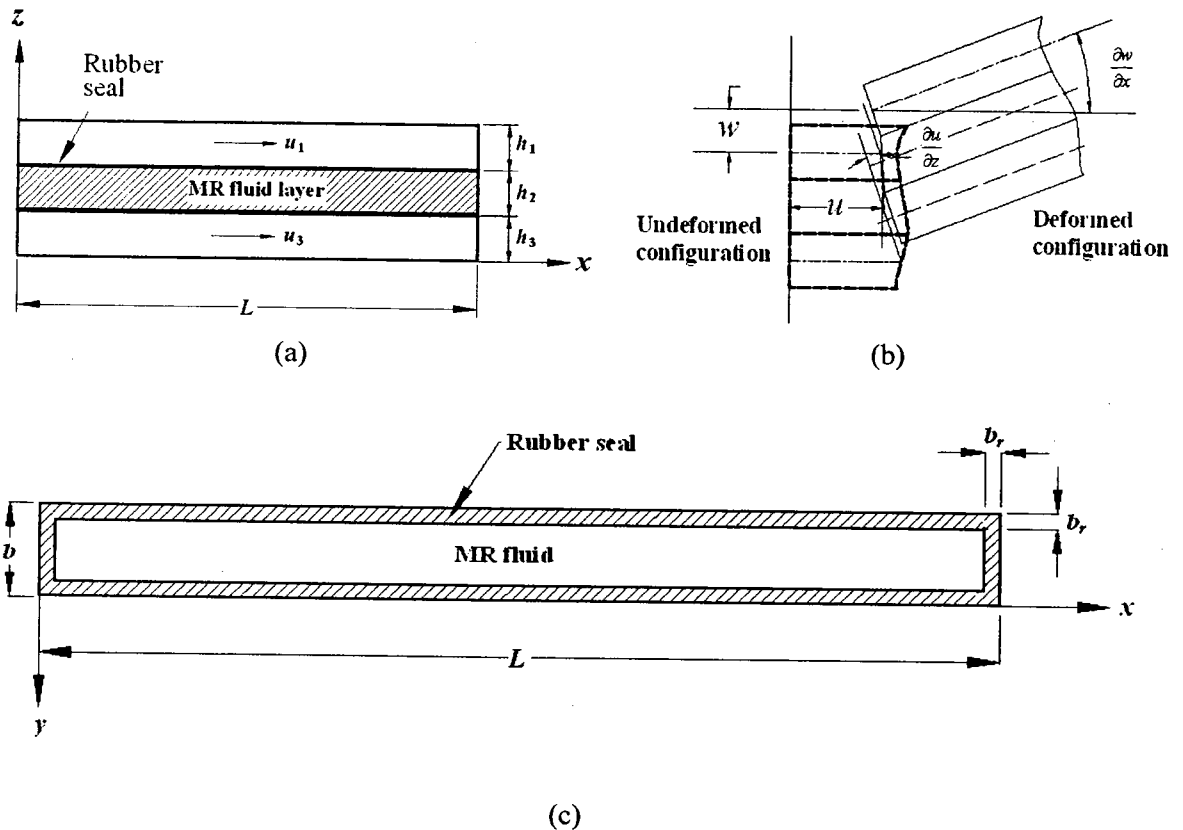


Figure 2.1: (a) The sandwich beam with a MR-fluid layer; (b) Deformed and undeformed beam cross sections; and (c) Plan view of mid-layer of the sandwich beam.

Let the longitudinal displacements of the mid-planes of the elastic layers in  $x$ -direction be  $u_1$  and  $u_3$  and the longitudinal displacement component of any point in the MR fluid be  $u$ . The mid layer is further assumed as a neutral layer in the transverse plane. The top and bottom surfaces are thus considered to undergo axial compression and tension, respectively. Consequently, the axial displacement of the sandwich beam is considered to be equivalent to the axial displacement at the MR-fluid layer of the beam.

The strains and displacements in the axial and transverse directions are shown in Figure 2.1(b). The shear strain  $\gamma$  in the MR layer can be derived from [Mead and Markus, 1969]:

$$\gamma = \frac{\partial w}{\partial x} + \frac{\partial u}{\partial z} \quad (2.1)$$

where

$$\frac{\partial u}{\partial z} = \frac{(h_1 + h_3)}{2h_2} \frac{\partial w}{\partial x} + \frac{(u_1 - u_3)}{h_2} \quad (2.2)$$

which yields shear strain as a function of the layers' thickness as:

$$\gamma = \frac{D}{h_2} \frac{\partial w}{\partial x} + \frac{u_1 - u_3}{h_2} \quad (2.3)$$

where  $D = h_2 + \frac{1}{2}(h_1 + h_3)$ .

Let the longitudinal forces in each of the elastic layers be denoted by  $F_1$  and  $F_3$  with their lines of action in the mid-planes of the elastic layers. These forces can be expressed as:

$$F_1 = E_1 A_1 \frac{\partial u_1}{\partial x}; \quad F_3 = E_3 A_3 \frac{\partial u_3}{\partial x} \quad (2.4)$$

where  $A_1$  and  $A_3$  are the cross sectional areas of layers 1 and 3, respectively and  $E_1$  and  $E_3$  are the corresponding Young's moduli. Since the beam is assumed to be free of longitudinal forces, i.e.,  $F_1 + F_3 = 0$ ., Eq. (2.4) yields the following relationship between the longitudinal deflection of the elastic layers:

$$E_1 A_1 \frac{\partial u_1}{\partial x} = - E_3 A_3 \frac{\partial u_3}{\partial x} \quad (2.5)$$

By integrating with respect to  $x$ , the above relation can be simply expressed as a function of the longitudinal deflections:

$$u_3 = -eu_1 \quad (2.6)$$

where  $e = \frac{E_1 A_1}{E_3 A_3}$ .

A sealant material, Buna-N rubber, is also considered around the edges of the MR-fluid layer to ensure uniform layer thickness and containment of the MR fluid within the sandwich beam. The thin layer of the sealant rubber used around the edges is illustrated in the plan view of the beam in Figure 2.1(c). The mid-layer of the sandwich beam comprising the rubber seal and the MR fluid, however, is modeled as a homogeneous material layer with equivalent shear modulus expressed by moduli and widths of the two materials, such that:

$$\bar{G} = G_r \left( \frac{b_r}{b} \right) + G^* \left( 1 - \frac{b_r}{b} \right) \quad (2.7)$$

where  $\bar{G}$  is the equivalent shear modulus of the homogeneous layer,  $b_r$  and  $b$  are the widths of the rubber and entire beam, respectively, and  $G_r$  and  $G^*$  are the shear modulus of the rubber and MR fluid, respectively.

The shear modulus of the MR fluid has been described in a number of studies on the basis of measured shear stress-shear strain properties [Li *et al.*, 1999; Choi *et al.*, 2005], which have been characterized by two distinguished regions, referred to as ‘pre-yield’ and ‘post-yield’ regions, as shown in Figure 1.3. Although the shear stress-strain

properties of the MR material strongly depend upon the applied magnetic field, the measured properties generally exhibit quite comparable patterns. In the pre-yield regime, the MR material demonstrates viscoelastic behavior, which has been described by the complex modulus  $G^*$ , given by [Li *et al.*, 1999]:

$$G^* = G' + iG'' \quad (2.8)$$

where  $G'$  is storage modulus of the MR fluid, which is related to the average energy stored per unit volume of the material during a deformation cycle, and  $G''$  is the loss modulus, a measure of the energy dissipated per unit volume of the material over a cycle. The post-yield behavior of the MR material has been approximately characterized by the Bingham plastic model, such that [Choi *et al.*, 2005]:

$$\tau = \tau_y + \eta \dot{\gamma} \quad (2.9)$$

where  $\tau_y$  is the magnetic field induced dynamic yield stress,  $\eta$  is the plastic viscosity and  $\dot{\gamma}$  is the shear strain rate.

### 2.2.1 Formulation of energy equation

The governing equations of motion for the MR sandwich beam are formulated in the finite element form using Lagrange's energy approach. To accomplish this, the total strain and kinetic energy of the system are derived. The strain energy due to elastic layers,  $V_{1,3}$ , can be expressed as:

$$V_{1,3} = \frac{1}{2} \int_0^L (E_1 A_1 + E_3 A_3 e^2) \left( \frac{\partial u}{\partial x} \right)^2 dx + \frac{1}{2} \int_0^L (E_1 I_1 + E_3 I_3) \left( \frac{\partial^2 w}{\partial x^2} \right)^2 dx \quad (2.10)$$

where  $I_1$  and  $I_3$  are the second moment of inertia at the centroid of the elastic layers 1 and 3, respectively.

Considering the very small thickness of the MR-fluid layer, it is assumed that the MR-fluid would yield very low loss factors and primarily affect the sandwich beam stiffness property. The shear strain energy of the mid-layer comprising of the MR-fluid and the rubber compound is thus obtained as:

$$V_2 = \frac{1}{2} \int_0^L G A_2 \left[ \frac{D}{h_2} \frac{\partial w}{\partial x} - \frac{(1+e)u}{h_2} \right]^2 dx \quad (2.11)$$

where  $A_2 = b \cdot h_2$  is the total cross sectional area of layer 2 which includes both rubber material and MR fluid.

The total strain energy  $V$  of the sandwich beam structure is the sum of those due to elastic and fluid layers, such that:

$$V = V_1 + V_2 + V_3 \quad (2.12)$$

The kinetic energy includes those associated with: (i) the transverse motion of the elastic layers and the MR layers ( $T_1$ ); (ii) the axial deformations of the elastic layers ( $T_2$ ); and (iii) the rotational deformation of the MR layer due to the strain displacement ( $T_3$ ). The kinetic energy associated with the transverse motions of the elastic and fluid layers,  $T_1$ , and axial deflections of the elastic layers,  $T_2$ , can be expressed as:

$$T_1 = \frac{1}{2} \int_0^L (\rho_1 A_1 + \rho_2 A_2 + \rho_r A_r + \rho_3 A_3) \left( \frac{\partial w}{\partial t} \right)^2 dx \quad (2.13)$$

$$T_2 = \frac{1}{2} \int_0^L (\rho_1 A_1 + e^2 \rho_3 A_3) \left( \frac{\partial u}{\partial t} \right)^2 dx \quad (2.14)$$

where  $\rho_1$  and  $\rho_3$  are mass densities of the elastic layers, and  $\rho_2$  and  $\rho_r$  are the mass densities of the fluid and the rubber materials, respectively .

The kinetic energy associated with the rotation of the MR-fluid layer,  $T_3$ , can be expressed by:

$$T_3 = \frac{1}{2} \int_0^L I_2 \rho_2 \left[ \frac{-(1+e)}{h_2} \frac{\partial u}{\partial t} + \frac{D}{h_2} \frac{\partial^2 w}{\partial x \partial t} \right]^2 dx \quad (2.15)$$

where  $I_2$  is the second moment of inertia at the centroid of the MR-fluid layer.

The total kinetic energy  $T$  of the sandwich beam can then be obtained from:

$$T = T_1 + T_2 + T_3 \quad (2.16)$$

Apart from the strain and kinetic energies, the work done by the excitation force, if present, also needs to be considered in the formulation.

### 2.2.2 Finite element formulation

In the finite element formulation, a standard beam element with two end nodes and three-DOF per node is considered. The DOF include the transverse  $w$ , axial  $u$  and rotational  $\theta$  displacements of the beam. The transverse and axial displacements can be expressed in terms of nodal displacement vectors and shape functions, as:

$$u(x,t) = N_u(x) \{d(t)\} \quad (2.17)$$

$$w(x,t) = N_w(x) \{d(t)\} \quad (2.18)$$

where  $d(t) = \{u^1, w^1, \theta^1, u^2, w^2, \theta^2\}$  is the nodal displacement vector and  $N_u(x)$  and  $N_w(x)$  are common beam shape functions.

Lagrange's equations are used to develop the governing differential equations in finite element form. In general form, Lagrange's equation can be written as:

$$\frac{d}{dt} \left( \frac{\partial T}{\partial \dot{q}_i} \right) - \frac{\partial T}{\partial q_i} + \frac{\partial V}{\partial q_i} = Q_i, \quad i=1, \dots, n \quad (2.19)$$

where  $n$  is the total DOF considered in the formulation and  $Q_i$  is the generalized force corresponding to the  $i^{\text{th}}$  DOF. Upon substituting for energy expressions in Eqs. (2.12) and (2.16) together with the deflection functions in Eqs. (2.17) and (2.18), the governing equations of motion for the MR sandwich beam element in the finite element form can be obtained as:

$$[m^e] \{\ddot{d}\} + [k^e] \{d\} = \{f^e\} \quad (2.20)$$

where  $[m^e]$  and  $[k^e]$  are the element mass matrix and stiffness matrix, respectively, which are presented in Appendix A, and  $\{f^e\}$  is the element force vector. Assembling the mass and stiffness matrices and the force vector for all the elements yields the system governing equations of motion of the MR sandwich beam in the finite element form, which can be expressed in the following general form:

$$[M] \{\ddot{d}_g\} + [K] \{d_g\} = \{F\} \quad (2.21)$$

where  $[M]$ ,  $[K]$ ,  $\{F\}$  and  $\{d_g\}$  are the system mass and stiffness matrices, and the force and displacement vectors, respectively.

### 2.2.3 Ritz formulation

The equations of motion of the sandwich beam are also formulated using the Ritz method to analytically obtain the free vibration properties of the sandwich beam, which are further applied to examine the validity of the proposed finite-element formulation. Based on Ritz formulation, the maximum strain energy must be equal to the maximum kinetic energy which can be stated as:

$$\delta(T - V) = 0 \quad (2.22)$$

In Ritz method, a solution is sought by summing  $N$  weighted functions in order to approximate the transverse and axial deflections in the following forms:

$$w(x) = \sum_{i=1}^N c_i \phi_i; \text{ and } u(x) = \sum_{j=1}^N c_j \Psi_j \quad (2.23)$$

where  $c_i$  and  $c_j$  are coefficients to be determined, and  $\phi_i$  and  $\Psi_j$  are the interpolation deflection functions satisfying atleast the geometrical boundary conditions. Substituting Eqs. (2.23) into (2.22), and application of the stationary condition yields algebraic equations of the form:

$$[[K_R] - \omega^2 [M_R]]\{c\} = 0 \quad (2.24)$$

The solution of the above equation yields the natural frequencies and mode shapes of the sandwich system. It should also be noted that the dissipated energy due to the MR fluid has been neglected in the strain energy formulation term in the Ritz's formulation. The negligible contributions due to dissipated energy was also verified by comparing the natural frequencies of the structure model with and without the loss factor due to MR-fluid. The natural frequencies corresponding to the first five modes of the two models were found to be within 0.05%.

### 2.3 EXPERIMENTAL METHOD AND DATA ANALYSIS

Laboratory experiments were performed on a prototype MR sandwich beam to investigate the vibration properties of the beam and to examine the validity of the proposed finite element model and Ritz formulation. A cantilever sandwich beam was fabricated using two thin aluminum strips (300 mm x 30 mm x 0.9 mm) with zero magnetic permeability. The strips were arranged to create a uniform 1.15 mm gap for the MR fluid (MRF-122EG), used as the core material. In order to maintain the uniform gap and contain the fluid in between the two strips, 1.15 mm thick high strength Buna-N rubber was applied as an adhesive around the edges. The width of this rubber layer was in the order of 1.5 mm. The sandwich beam was clamped to a support that was mounted on an electro-dynamic vibration exciter. Permanent magnets were used to generate the magnetic field over the beam. A single-axis accelerometer, oriented along the z-axis, was installed close to the free edge of the beam, to measure the acceleration response. A single-axis accelerometer was also installed at the support to measure the acceleration due to excitation. This acceleration signal also served as the feedback for the vibration exciter controller. The experimental setup is shown in Figure 2.2.

Two different experiments were conducted to study the free and forced vibration responses of the beam under different intensities of the magnetic field, which were realized by varying the vertical position of the permanent magnets with respect to the beam. The magnetic field intensity was measured near the beam surfaces using a Gauss meter. The measurements were performed in the absence of permanent magnets (0 Gauss) and four different positions of the magnets leading to field intensities of approximately 75, 175, 400 and 500 Gauss at the beam surfaces. In the first experiment,

the free vibration responses were measured under the selected magnetic field intensities. The data acquired were also used to estimate the complex shear modulus of the MR-fluid. In the second experiment, the forced vibration responses of the beam were measured under a white-noise vibration spectrum with nearly constant power spectrum density (PSD) in the 1-300 Hz frequency range at three different magnetic field intensities (0, 75 and 175 Gauss). The forced responses were measured in terms of the transfer function of the accelerations at the free end and the support, using the  $H_1$  function of the signal analyzer (Bruel & Kjaer 2035). The measured acceleration signals were analyzed in the signal analyzer using the frequency span of 800 Hz with a resolution of 1 Hz. The natural frequencies of the sandwich beam were subsequently identified from the peaks in the frequency response function.

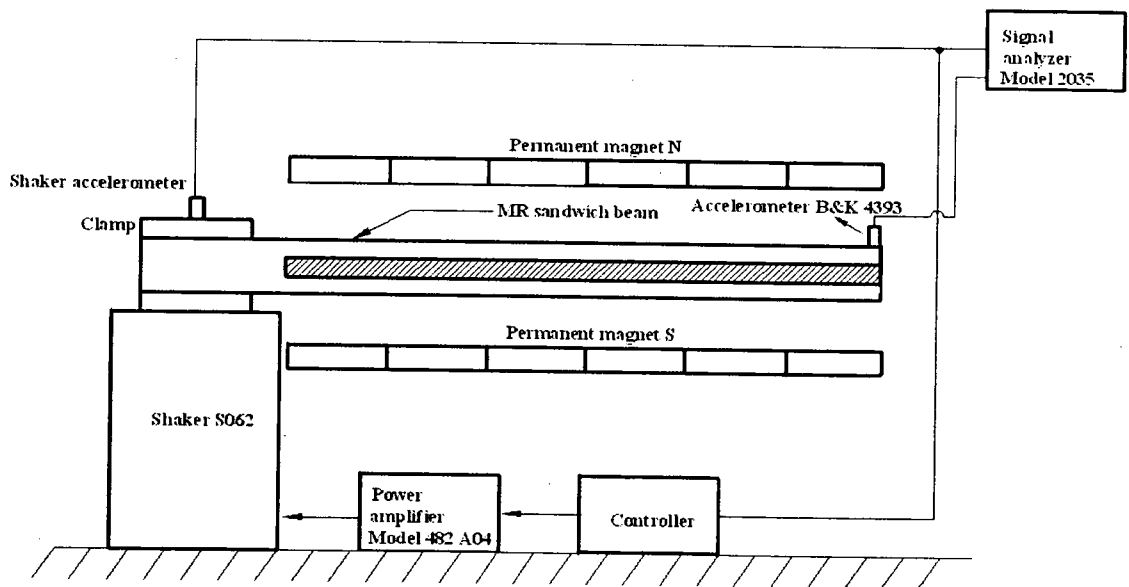


Figure 2.2. Experimental set-up.

### 2.3.1. Estimation of complex shear modulus and model validations

The measured free-vibration response data were analyzed to obtain an estimate of the complex shear modulus of the MR-fluid used in the prototype beam, which is essential for deriving the strain energy  $V_2$  in Eq. (2.11). The shear modulus of the MR-fluid is estimated using the methodology proposed by Choi *et al.* (1990) for the ER fluid. The method is based on the single-DOF free vibration behavior of the sandwich beam, and assumes that the shear modulus of the elastic layer is negligible compared to the fluid layer. Furthermore, the elastic modulus of the sandwich beam can be considered equivalent to the storage modulus  $G'$ , which is proportional to the average energy stored per unit volume of the material during a deformation cycle. For the single-DOF consideration, the natural frequency of the MR sandwich beam can be expressed in terms of the storage modulus, as:

$$\omega_n = \sqrt{\frac{k}{m}} = \sqrt{3G'I / L^3 m_{eff}} \quad (2.25)$$

where  $m_{eff} = 0.236 m$  is the effective lumped mass located at the end of the cantilever beam of mass  $m$  and length  $L$  [Thomson and Dahleh, 1998].

Since the loss modulus  $G''$  is proportional to the energy dissipated per unit volume of material over a cycle, a relation between the storage and the loss moduli has been defined as [Rao, 1995]:

$$\frac{G''}{G'} = \frac{\delta}{\pi} \quad (2.26)$$

where  $\delta$  is the logarithmic decrement.

The storage and loss moduli of the sandwich beam are obtained from the measured  $\omega_n$  and  $\delta$  using Eqs. (2.25) and (2.26), respectively. The complex shear modulus of the MR fluid is then expressed as:

$$G^* = G' + iG'' \quad (2.27)$$

The storage and loss moduli of the MR-fluid were estimated corresponding to different magnetic field intensities (0, 75, 175, 400 and 500 Gauss). The linear regressions were subsequently used to express the moduli as a function of the magnetic field intensity. Both the storage and shear moduli were expressed by the following 2<sup>nd</sup> order polynomial functions with respect to the field intensity as:

$$G'(B) = -3.7434B^2 + 4543.2B + 0.95 \times 10^6$$

$$G''(B) = -B^2 + 0.0009 \times 10^6 B + 0.2095 \times 10^6$$

and 
$$G^* = G'(B) + iG''(B) \quad (2.28)$$

where  $B$  is the intensity of magnetic field in Gauss.

The validity of the estimated complex shear modulus was examined by comparing the measured natural frequencies of the sandwich beam with those derived from the proposed finite-element formulation employing the identified complex shear modulus of the MR fluid. The natural frequencies of the beam corresponding to the first 4 modes were obtained from the measured frequency response functions under 0 and 75 Gauss field intensity. The finite-element simulation was also conducted for the same field intensities, while the material properties were considered as:  $\rho_1 = \rho_3 = 2700 \text{ kg/m}^3$ ;  $E_1 =$

$E_3 = 68$  GPa;  $\rho_r = 1.233$  kg/m<sup>3</sup> and  $\rho_2 = 3500$  kg/m<sup>3</sup>. The estimated and measured frequencies corresponding to 0 and 75 Gauss are compared in Table 2.1. The comparisons suggest reasonably good agreements in the frequencies corresponding to higher modes for both magnetic fields, while considerable deviation is evident in the fundamental mode frequency. This may be partly attributed to consideration of the single-DOF response for estimation of the complex modulus, and in part to the assumption of negligible contributions due to shear property of the elastic layers [Choi *et al.*, 1990]. Furthermore, the shear properties of the rubber seal may contribute to the overall complex shear modulus, although its dimensions are very small compared to the beam dimensions.

Table 2.1: Comparisons of measured natural frequencies of the cantilever MR sandwich beam with those derived from the finite-element formulation employing estimated and refined complex shear moduli of the MR fluid.

Field intensity (Gauss)	Mode	Natural frequencies (Hz)				
		Measured	FEM (estimated G*)	% deviation	FEM (refined G*)	% deviation
0	1	10	13.87	27.90	10.77	7.15
	2	60	64.69	7.24	61.90	3.07
	3	137	141.38	3.10	135.87	0.82
	4	240	242.03	0.84	234.34	2.35
75	1	12	14.63	17.97	12.11	0.91
	2	63	68.00	7.35	65.85	4.33
	3	144	147.82	2.58	143.40	0.42
	4	252	250.00	0.79	243.55	3.35

The prediction ability of the FE model could be enhanced through identification of a more accurate complex shear modulus function. An error minimization problem was thus formulated to seek coefficients of the quadratic storage and shear moduli functions that would yield minimal error in the measured and the computed natural frequencies.

The minimization problem was formulated to minimize the sum of squared deviations in the frequencies corresponding to the first four modes under the two field intensities (0 and 75 Gauss), such that:

$$\text{Minimize } [E(\bar{X})] = \sum_{i=1}^4 \alpha_i (f_i - f_i^m)^2 \quad (2.29)$$

where  $f_i$  is the natural frequency corresponding to mode  $i$  ( $i=1, \dots, 4$ ) estimated from the FE model,  $f_i^m$  is the corresponding measured frequency.  $\alpha_i$  denotes the weighting factor corresponding to mode  $i$ ,  $E$  is the weighted minimization function and  $\bar{X} = \{a, b, c, d, e, f\}$  is the design vector of quadratic storage and shear moduli functions, given by:

$$G'(B) = -aB^2 + bB + c; \text{ and } G''(B) = -dB^2 + eB + f \quad (2.30)$$

The minimization problem was solved using the Sequential Quadratic Programming (SQP) technique available in MATLAB optimization toolbox subject to limit constraints on the design variables, and assuming unity weighting factors. The design variables were limited to variations of  $\pm 15\%$  of those estimated from the measured data and presented in Eq. (2.28). The optimization problem was solved in two sequential steps corresponding to 0 and 75 Gauss field intensities. The solution in the absence of a magnetic field converged to the constant coefficients  $c$  and  $f$ , and those under 75 Gauss resulted in values of  $a$ ,  $b$ ,  $d$  and  $e$ . Solutions in each case were attained for different starting values of the design vector, which converged to comparable optimal results:  $\bar{X} = \{3.3691, 4.9975 \times 10^3, 0.873 \times 10^6, 0.9, 0.8124 \times 10^3, 0.1855 \times 10^6\}$ . These identified parameters differ only slightly from the estimated parameters, in the 8 to 11%

range, which suggests relatively small contributions due to shear properties of the rubber seal and the elastic layers, and that a single-DOF approximation may suffice.

Table 2.2. Comparisons of natural frequencies of a cantilever MR-sandwich beam derived from the finite-element and Ritz formulations with the measured frequencies.

Field intensity (Gauss)	Mode	Natural Frequencies (Hz)		
		Measured	FEM (% deviation)	Ritz method (% deviation)
0	1	10	10.77 (7.15)	10.99 (9.00)
	2	60	61.90 (3.06)	62.06 (3.32)
	3	137	135.87 (0.82)	136.80 (0.15)
	4	240	234.34 (2.35)	235.17 (2.01)
75	1	12	12.11 (0.91)	13.14 (8.68)
	2	63	65.85 (4.33)	65.19 (3.36)
	3	144	143.40 (0.42)	144.89 (0.61)
	4	252	243.55 (3.35)	244.67 (2.91)
175	1	13	12.97 (0.23)	14.41 (9.78)
	2	65	69.81 (6.89)	69.43 (6.38)
	3	148	151.30 (2.18)	152.49 (2.94)
	4	257	253.59 (1.33)	252.08 (1.91)
400	1	14	14.04 (0.28)	15.01 (6.73)
	2	79	75.29 (4.69)	75.49 (4.44)
	3	161	162.74 (1.07)	163.76 (1.69)
	4	-	268.82(-)	270.28(-)
500	1	15	15.29 (1.90)	15.98 (6.13)
	2	80	76.66 (4.18)	77.03 (3.71)
	3	165	165.68 (0.41)	166.70 (1.02)
	4	-	272.87(-)	274.17(-)

The validity of the refined complex shear modulus model was further examined by comparing the natural frequencies derived from the FE model employing the refined complex modulus with the measured data (Table 2.2). The comparisons show substantial reduction in the deviation in the fundamental mode frequency compared to those obtained for the model based on complex shear modulus estimated directly from the measured data. The results also show the refined model yields better agreements in the higher

modes frequencies, except for the 4<sup>th</sup> mode, where a relatively larger deviation is observed, irrespective of the field intensity considered.

The validity of the proposed finite element and Ritz formulations were further examined under different magnetic field intensities in the 0 to 500 Gauss range by comparing the computed natural frequencies with the frequencies identified from the measured transfer functions under excitations at the support. The measurements, however, could not be performed under higher intensities (400 and 500 Gauss) due to very small clearance between the beam and the magnets, which caused repetitive contacts of the beam with the magnets. The frequencies under these fields were thus extracted from the frequency spectrum of the free vibration response to a very low-level perturbation. The peak corresponding to the 4<sup>th</sup> mode, however, could not be clearly identified due to low magnitude perturbation.

The comparisons of the natural frequencies obtained from the FE and Ritz formulations with the measured data under the selected field intensities are presented in Table 2 together with the percent deviations. The comparisons show reasonably good agreements between the computed and measured frequencies, irrespective of the field intensity and the mode. Furthermore, the results obtained from the proposed finite element model are in good agreement with those derived from the Ritz method for the range of field intensities and modes considered.

## **2.4 RESULTS AND DISCUSSION**

The properties of a sandwich MR beam are strongly influenced by many fluid and structure-related parameters, which may include field intensity, fluid layer thickness,

complex shear modulus of the MR fluid, beam geometry, boundary conditions, elastic layer thickness, etc. The proposed FE model is used to study the effects of variations in the magnetic field intensity and the MR-fluid layer thickness on the properties of the beam in terms of natural frequencies and the loss factors for different boundary conditions. The influence of variations in the field intensity on the forced vibration response of a simply-supported MR sandwich beam is also evaluated under harmonic force excitations. The simulation results are obtained by considering identical baseline thickness of 1mm of the elastic and fluid layers, while the material and all other geometric properties of the layers are identical to those described in section 2.3.1

#### **2.4.1. Influences of magnetic field intensity**

Table 2.3 summarizes the influence of variations in the magnetic field intensity on the natural frequencies of a MR-fluid sandwich beam structure with different boundary conditions, including the simply-supported (SSB), clamped free (CFB) and clamped – clamped (CCB) conditions. The results are presented for the first 5 modes under three different field intensities: 0, 250 and 500 Gauss. The results consistently show that the natural frequencies corresponding to all the modes increase with increase in the magnetic field, irrespective of the boundary condition, as observed earlier in Table 2.2. A similar trend in the natural frequencies has also been reported in a few earlier studies on simply-supported beams based on analytical approach [Yalcintas and Dai, 1999; Sun *et al.*, 2003]. The upward shift in the natural frequencies with increasing magnetic field is attributable to increase in the complex shear modulus of the MR fluid and thus the structure stiffness under higher magnetic field, which is evident from the element stiffness matrix presented in Appendix A. The results also show the important effect of

the boundary condition. As expected, the clamped-clamped condition yields the highest natural frequencies, while the natural frequencies of the clamped-free beam are the lowest for all modes considered, irrespective of the magnetic field intensity. The results also suggest that an increase in the field intensity generally yields the largest stiffness increase for all the modes for the relatively soft clamped-free condition, and relatively smallest change in stiffness for the relatively stiff clamped-clamped beam.

Table 2.3. Influence of variations in the magnetic field intensity on the natural frequencies of the MR sandwich beam for different boundary conditions.

Field intensity (Gauss)	Boundary conditions	Natural frequency (Hz)				
		Mode				
		1	2	3	4	5
0	SSB	40.31	103.10	200.07	332.45	501.67
	CFB	12.12	67.35	151.22	265.26	415.97
	CCB	57.66	139.66	255.93	407.71	596.36
250	SSB	50.92	120.32	222.24	357.33	528.15
	CFB	14.36	77.58	171.1	289.87	443.37
	CCB	66.52	154.74	275.59	430.01	620.37
500	SSB	55.89	128.95	233.97	371.00	543.05
	CFB	16.23	82.20	180.78	302.78	458.30
	CCB	70.80	162.51	286.22	442.44	634.02

The loss factor due to the MR-fluid sandwich beam is computed as the ratio of the square of the imaginary component of the complex natural frequency to that of the real component [Yalcintas and Dai, 1999; Yeh and Shih, 2006]. Figure 2.4 illustrates variations in the loss factors of the beam with simply-supported and clamped-free boundary conditions for different field intensities corresponding to the first 5 modes. The results generally show an increase in the loss factors with increase in the magnetic field for both the boundary conditions, except for the lower modes. The loss factor is merely the ratio of energy dissipated per radian to the total strain energy  $V$ , both of which

increase with the magnetic field. Furthermore, the dissipated energy is directly related to the loss modulus, which increases with the field intensity as seen in Eq. (2.28). The relative increase in the loss modulus and thus the dissipated energy with increase in the magnetic field, however, is greater than that in the total strain energy, particularly for the higher modes, which leads to higher loss moduli under increasing magnetic field.

The above trend, however, is not evident for the fundamental mode loss factor, which can be related to relative changes in the dissipated and strain energy corresponding to the lower modes. The increase in the strain energy corresponding to the lower modes with the magnetic field would be relatively larger, which can be observed from the relatively greater changes in the lower mode frequencies (Table 2.3). This may lead to either negligible or decreasing effect of magnetic field on the loss factor. For the simply supported end conditions, the fundamental mode loss factor increases considerably under the application of a magnetic field of intensity up to nearly 200 Gauss but it decreases slightly with further increase in the field intensity. A similar trend has also been reported in [Yalcintas and Dai, 1999; Sun *et al.*, 2003; Yeh and Shih, 2006] for a simply supported beam. The fundamental mode loss factor of the clamped-free beam, however, decreases consistently with increasing field intensity, as seen in Figure 2.3(b). The effect of boundary condition on the loss factor is further illustrated in Figure 2.4 corresponding to a fixed field intensity of 500 Gauss. The results clearly show the important effect of the boundary conditions on the loss factors, particularly for the lower modes. The loss factors of the simply-supported and clamped-clamped beams decrease monotonically with increasing mode number. This trend for the clamped-free condition, however, could be observed only for the higher modes. As it is observed earlier, the increase in the total

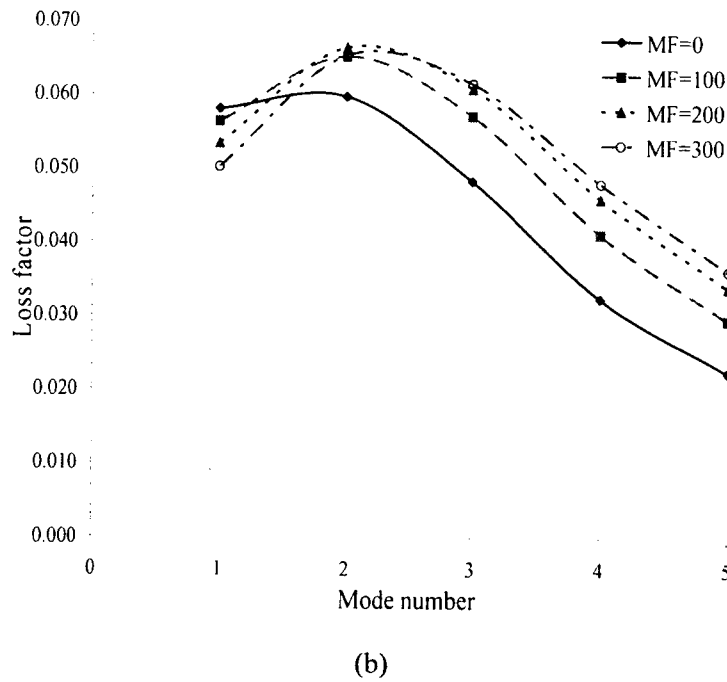
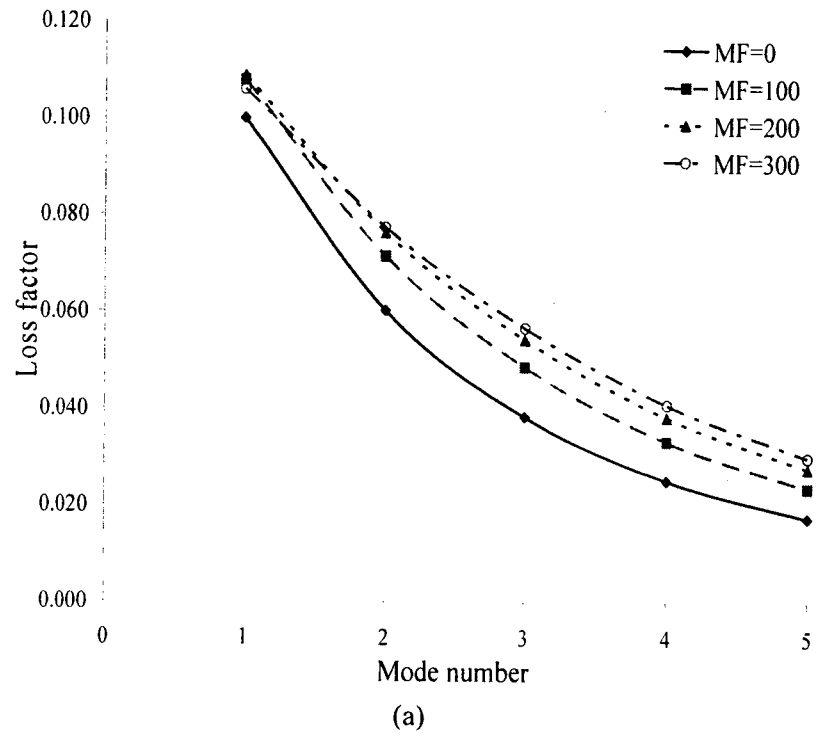


Figure 2.3: Influence of variations in the magnetic field intensity on the loss factor corresponding to different modes: (a) simply-supported beam; and (b) clamped - free beam.

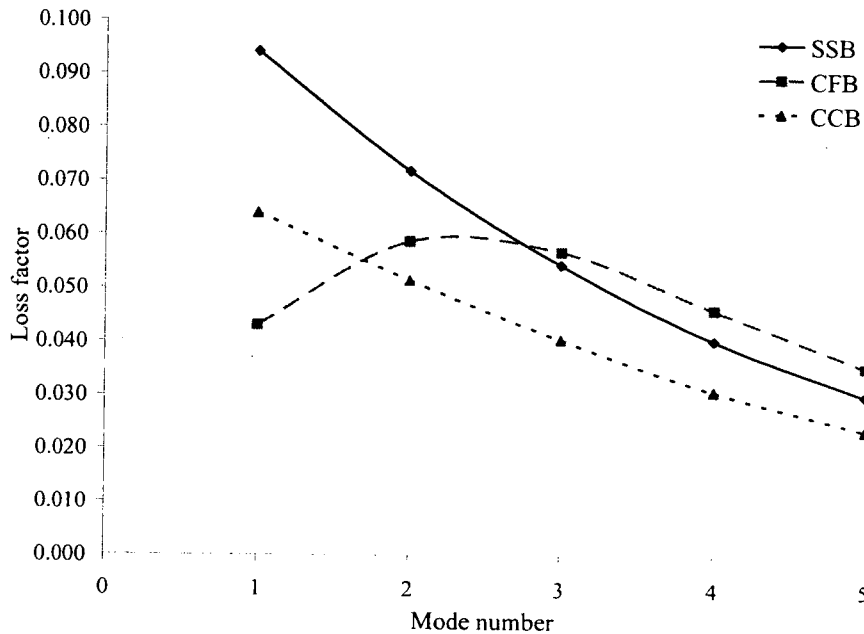


Figure 2.4: Effect of boundary conditions on loss factors corresponding to first five modes.

strain energy related to the first two modes with the magnetic field would be relatively larger compared to that of the energy dissipated resulting the increase in loss factor. The results also show that the loss factor at the higher modes for the clamped-free end conditions is always higher than those of simply supported and clamped-clamped end conditions which can be attributed to the fact that the relative change in the strain energy of clamped-free beam with magnetic field is lower than those of simply supported and clamped clamped beams.

#### 2.4.2 Influences of MR layer thickness

A comparison of the natural frequencies of the beam structures with different thicknesses of MR layer at magnetic field of 500 Gauss for the simply supported end conditions for

the first five modes has been performed and the results are shown in Figure 2.5. The results generally show a decrease in the natural frequencies with increase in thickness of the MR layer. A significant variation can be observed in higher modes compared to that of lower modes. This can be attributed to the fact that the relative change in the effective mass of the structure is higher than that of the effective stiffness when the thickness of the MR fluid layer increases. Such type of variation has also been reported in [Yeh and Shih, 2006].

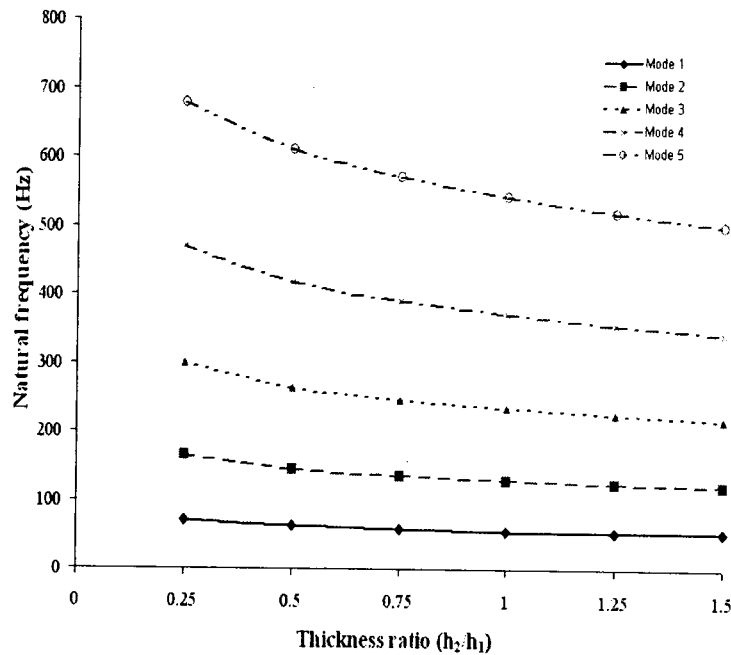


Figure 2.5. Influence of the thickness ratio ( $h_2/h_1$ ) of the MR fluid layer on the natural frequencies at magnetic field of 500 Gauss under simply supported end conditions.

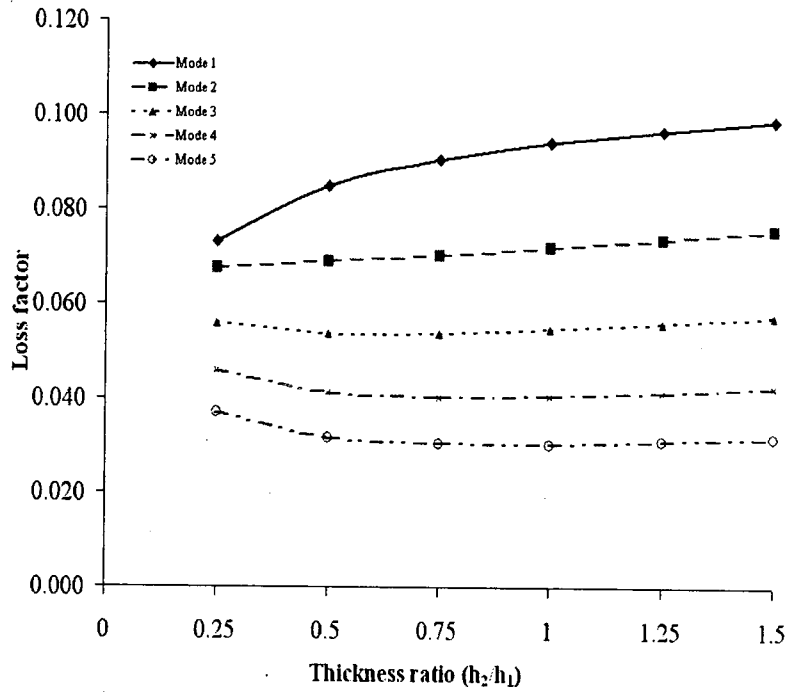
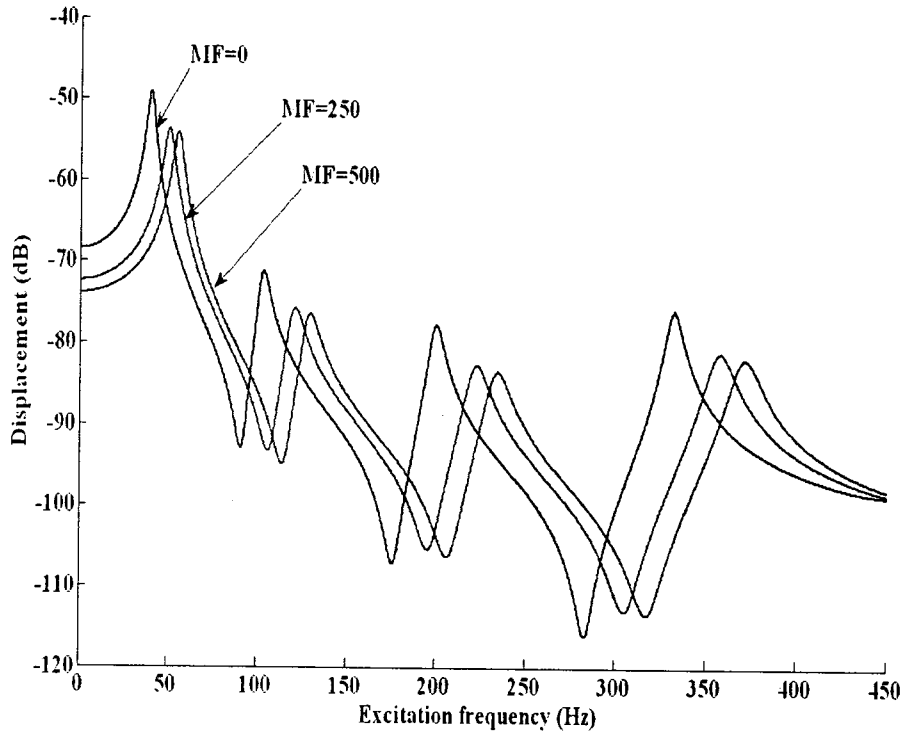


Figure 2.6. Influence of the thickness ratio ( $h_2/h_1$ ) of the MR fluid layer on the loss factor at magnetic field of 500 Gauss under simply supported end conditions.

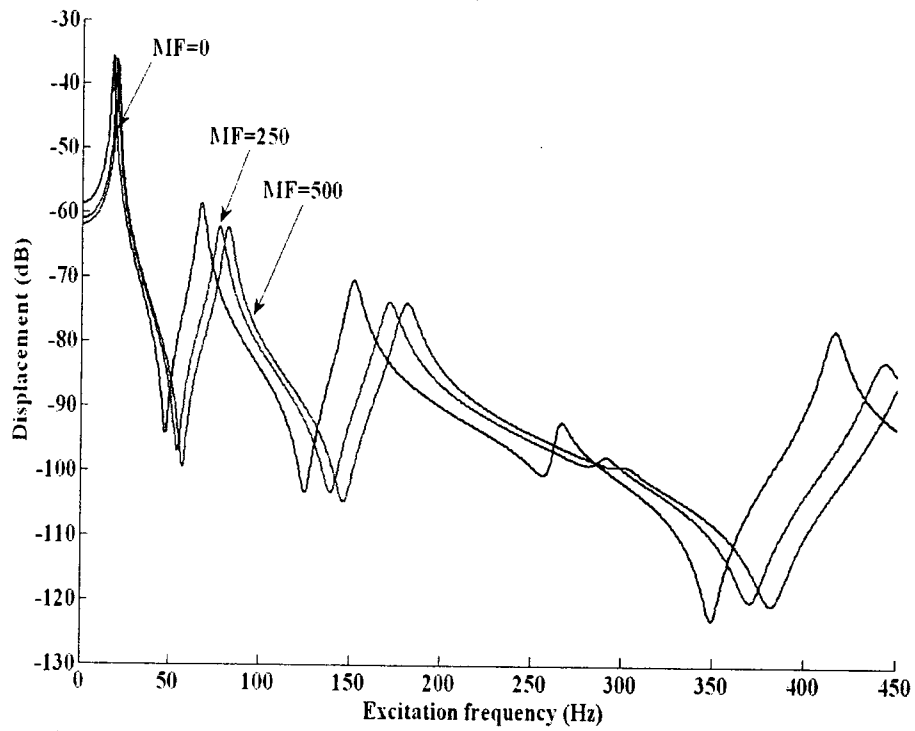
A comparison of the loss factor of the beam structures with different thickness of MR layer at magnetic field of 500 Gauss for the simply supported end conditions is presented in Figure 2.6. The results show that the loss factor always increases at first two modes as the thickness of the MR layer increases. The trend for the higher modes however is not the same. Such type of variation can also be observed in [Yeh and Shih, 2006]. When the thickness of the MR layer is increased, both the dissipated energy and the strain energy are increased. Hence, with increase in the thickness of the MR layer, the relative change in the dissipated energy would be considerably higher than that of the strain energy which results the increase in the loss factor in the first two modes. The same trend can be observed at higher modes when the thickness ratio is increased from 0.5.

### 2.4.3 Effect of magnetic field intensity on the transverse response of the beam

The effect of magnetic field on the transverse response of the simply-supported and clamped free MR sandwich beams is investigated by considering a sinusoidal force excitation acting at a distance of 175 mm from the left support. The response characteristics of the beam were evaluated under a 1N force excitation over the frequency range of 1-450 Hz for three different magnetic field intensities (0, 250 and 500 Gauss). Figure 2.7 illustrates the amplitude spectrum of the transverse displacement response evaluated at a distance of 194 mm from the left support. The results show increase in the natural frequencies (frequencies corresponding to response peaks) with increase in the magnetic field, as observed from the free vibration responses. The peak response magnitudes corresponding to all the modes also decrease with increasing the magnetic field, which may be attributed to higher loss factors under higher magnetic fields. The changes in the peak magnitudes, however, appear to be nonlinear functions of the magnetic field. An increase in the magnetic field from 0 to 250 Gauss yields substantial reduction in the peak amplitudes, which are approximately 9.5%, 6.5%, 6.4% and 7.6%, respectively, for the first 4 modes of simply supported MR sandwich beam and 1.6%, 5.9%, 4.8%, 5.9% and 6.2% respectively, for the first five modes of clamped free MR sandwich beam considered in the analysis. A similar trend in the response peaks has also been observed for simply supported MR sandwich beam in [Yalcintas and Dai, 1999; Sun *et al.*, 2003]. A further increase in the field intensity, however, yields relatively smaller reductions in the response magnitudes corresponding to all the modes. Such a saturation tendency is also evident from the loss factors presented in Figure 2.3. The relatively



(a)



(b)

Figure 2.7. Influence of magnetic field on the transverse response: a) simply supported beam b) Clamped free beam

smaller reduction of amplitude at the fundamental mode of a clamped free beam is mainly due to the decrease of loss factor with increasing magnetic field as shown in Figure 2.3 (a).

## 2.5 CONCLUSIONS

In this study, vibration response of a multi-layered beam with MR fluid as a sandwich layer between two layers of the continuous elastic structure has been analyzed. Mathematical modeling was developed in finite element form and Ritz formulation to simulate the dynamic response of the MR sandwich beam. The relationship between the magnetic field and the complex shear modulus of the MR material was estimated by first modeling the MR sandwich beam as a damped harmonic oscillator, then performing a free oscillation experiment and finally minimizing the error using constrained optimization technique. The validity of the developed finite element formulation has been demonstrated by comparing the results with those obtained from the Ritz formulation and the experimental investigation. The controllable capabilities of MR fluid in continuous elastic structure were also investigated through conducting various parametric studies. It has been shown that the natural frequencies for all the modes and loss factor at the higher modes of the MR multilayer beam could be increased by increasing the strength of the magnetic field. It has also been observed that the clamped - clamped and clamped- free beams yield the highest and lowest natural frequencies, respectively, irrespective of the magnetic field. It has also been shown that the simply supported and clamped – free end conditions yield the highest loss factor at lower and higher modes, respectively. Furthermore, it has also been demonstrated that the thickness of MR layer plays an important role in variation of natural frequencies and loss factors. It has been observed

that the natural frequency at all modes decreases with increase in the thickness of the MR layer. However, the loss factor increases with increase in thickness of the MR layer at the first two modes and for the higher modes, the loss factor could be increased when the thickness ratio of the MR layer with the elastic layer exceeds certain value. Transverse response of the MR sandwich beam also confirms that the amplitude of vibration could be considerably reduced using controllable MR fluids. This shows that MR fluids can be effectively used in vibration control of multilayer structures.

# CHAPTER 3

## VIBRATION ANALYSIS OF A PARTIALLY TREATED MULTI-LAYER BEAM WITH MAGNETORHEOLOGICAL FLUID

### 3.1 INTRODUCTION

Semi-active vibration control based on Magnetorheological (MR) materials offers excellent potential for high bandwidth control through rapid variations in the rheological properties of the fluid under varying magnetic field. While a number of studies have analyzed sandwich structures with ER fluids [Gandhi *et al.*, 1989; Choi *et al.*, 1990; Yalcintas and Coulter, 1995; Yalcintas and Coulter, 1998], the application of MR materials in sandwich structures have been explored in a very few studies. Such fluids may be conveniently applied to partial or more critical components of a large structure to realize more efficient and compact vibration control mechanism with variable damping. Haiqing *et al.* (2003) experimentally analyzed the vibration characteristics of a cantilever beam locally linked by ER fluid layer to the ground. It was concluded that the locally applied ER fluid layer serves as a complex spring and thus alters the damping and stiffness properties of the structures under the electric field. The study also concluded that the cantilever beam with such local treatment exhibits greater sensitivity than the full treatment with regards to the natural frequencies and loss factors. Haiqing and King (1997) investigated the vibration response of a fully and partially treated ER beam clamped at both ends and concluded that the length of the ER fluid layer has a significant

effect on the resonant frequencies and the loss factor. The effectiveness of partial treatment of MR fluids in sandwich structures, however, has not yet been explored.

In Chapter 3, the dynamic properties of a MR sandwich beam were investigated using finite element and Ritz formulations and the results are compared with those obtained using the experimental investigations. A free oscillation experiment was also performed to estimate the complex shear modulus of the MR fluid. Furthermore, the effectiveness of the MR fluids in controlling the vibration of fully treated MR fluid multilayer structures was demonstrated.

In this chapter, the properties and vibration responses of a partially-treated multilayer MR fluid beam is investigated. The governing equations of a partially-treated multilayered MR beam are formulated using finite element method and Ritz formulation. The validity of the proposed finite element formulations is demonstrated by comparing the results with those obtained from the Ritz formulation and the experimental measurements. The properties of different configurations of a partially treated MR-fluid beam are evaluated to investigate the influences of the location and length of the MR-fluid for different boundary conditions. The properties in terms of natural frequencies and loss factors corresponding to various modes are evaluated under different magnetic field intensities and compared with those of the fully-treated beams. The effect of location of the fluid treatment on deflection mode shapes is also investigated. The forced vibration responses of the various configurations of partially treated MR sandwich beam are also evaluated under harmonic force excitations.

### 3.2 DYNAMIC MODEL OF A PARTIALLY TREATED MULTI-LAYER BEAM

A partially-treated sandwich beam structure can be modeled on the basis of those developed for a fully treated beam. The beam structure with multiple MR-fluid segments can be modeled by treating each segment independently and then coupling with the adjacent segments to assure compatible deformation and continuous response of the composite structure. This could be achieved by imposing compatibility conditions which are identical displacements and the slopes at the boundaries of the two adjacent segments. A three – layer beam structure comprising a MR-fluid layer over the entire beam length between two elastic layers, as shown in Figure 3.1(a), is considered as the basis for developing the finite element model and Ritz formulation for the partially treated MR sandwich beam shown in Figure 3.1(b). The mid-layer of the partially-treated sandwich beam is comprised of elastic layers of lengths  $L_1$  and  $L_3$  and a MR fluid layer segment of length  $L_2$ . Considering that the Young's modulus of the MR-fluid is nearly negligible compared to that of the elastic layers, the normal stresses in the fluid layer are considered to be neglected. The elastic and fluid layers thickness,  $h_1$ ,  $h_2$  and  $h_3$ , are considered to be very small compared to the length of the beam. The shear strain and the damping in the elastic layers are also assumed to be negligible. The slippage between the elastic and fluid layers is further assumed to be negligible. Furthermore, the variation of the through the thickness displacement is assumed to be negligible and thus the transverse displacement  $w$  is considered to be uniform throughout the given cross section.

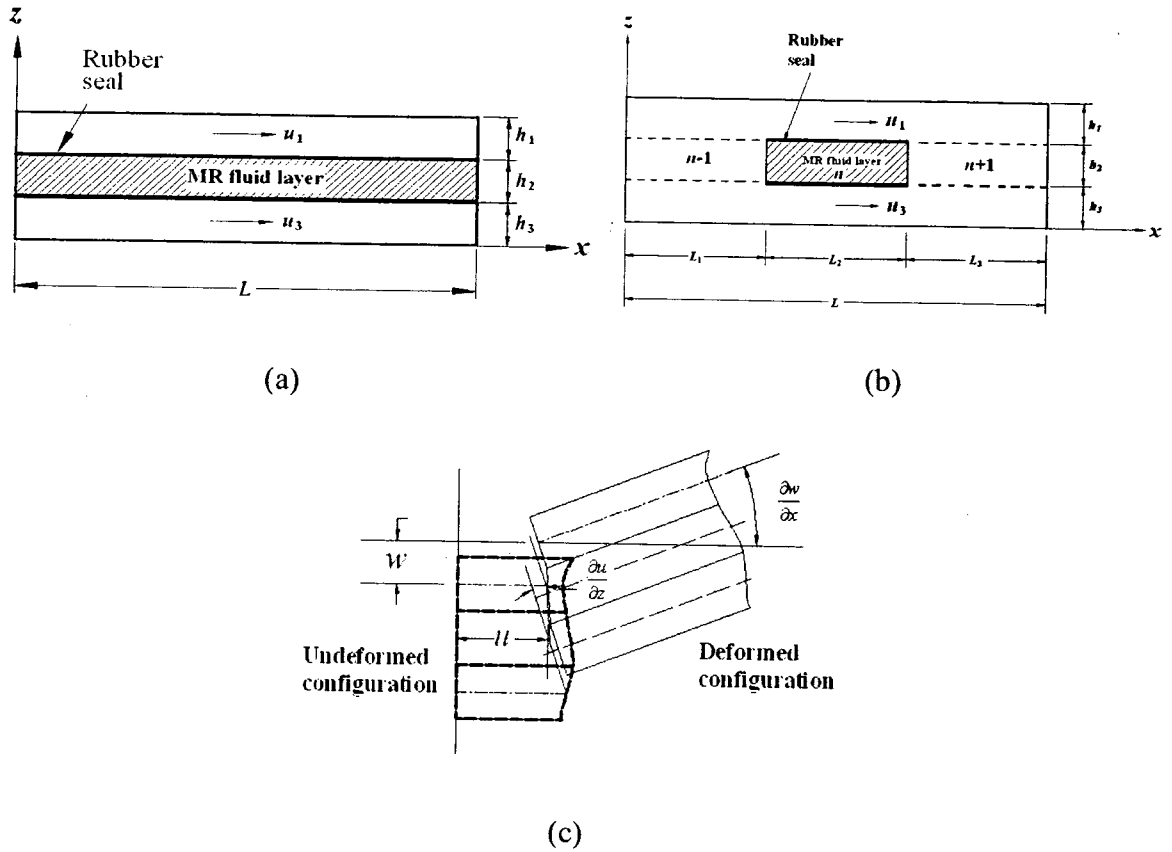


Figure 3.1: (a) Fully treated MR sandwich beam. (b) Partially treated MR sandwich beam  
(c) Deformed and undeformed beam cross section

Let the longitudinal displacements of the mid-planes of the top, middle and bottom layers in the  $x$ -direction be  $u_1$ ,  $u$  and  $u_3$  respectively. As the mid layer is assumed as a neutral layer in the transverse plane, the top and bottom surfaces are considered to experience axial compression and tension, respectively. Consequently, the axial displacement of the sandwich beam is considered to be equivalent to the axial displacement at the mid-layer of the beam. The strains and displacements in the axial and transverse directions are shown in figure 3.1(c). The shear strain  $\gamma$  in the MR layer can be derived from [Mead and Markus, 1969]:

$$\gamma = \frac{\partial w}{\partial x} + \frac{\partial u}{\partial z} \quad (3.1)$$

where

$$\frac{\partial u}{\partial z} = \frac{(h_1 + h_3)}{2h_2} \frac{\partial w}{\partial x} + \frac{(u_1 - u_3)}{h_2} \quad (3.2)$$

and  $w$  is the transverse displacement.

Substituting Eq. (3.2) into Eq. (3.1) yields shear strain as a function of the layers' thickness as:

$$\gamma = \frac{D}{h_2} \frac{\partial w}{\partial x} + \frac{u_1 - u_3}{h_2} \quad (3.3)$$

where  $D = h_2 + \frac{1}{2}(h_1 + h_3)$ .

Let  $F_1$  and  $F_3$  be the longitudinal forces in each of the elastic layers with their lines of action in the mid-planes of the elastic layers, such that:

$$F_1 = E_1 A_1 \frac{\partial u_1}{\partial x}; \quad F_3 = E_3 A_3 \frac{\partial u_3}{\partial x} \quad (3.4)$$

where  $A_1$  and  $A_3$  are the cross section areas of layers 1 and 3, respectively and  $E_1$  and  $E_3$  are the corresponding Young's moduli. Since the beam is assumed to be free of longitudinal forces, i.e.,  $F_1 + F_3 = 0$ , Eq. (3.4) yields the following relationship between the longitudinal deflections of the top and bottom layers:

$$E_1 A_1 \frac{\partial u_1}{\partial x} = -E_3 A_3 \frac{\partial u_3}{\partial x} \quad (3.5)$$

Integration of the above relation with respect to  $x$  yields the following relation between the longitudinal displacements at the top and bottom layers, as:

$$u_3 = -e u_1 \quad (3.6)$$

where  $e = \frac{E_1 A_1}{E_3 A_3}$ .

Buna-N rubber is considered as a sealant material around the edges of the MR-fluid layer segment to contain the MR fluid within the two elastic layers of the sandwich beam and maintain uniform thickness. The rubber seal and the MR fluid, however, are modeled as a homogeneous material layer with equivalent shear modulus expressed as:

$$\bar{G} = G_r \left( \frac{b_r}{b} \right) + G^* \left( 1 - \frac{b_r}{b} \right) \quad (3.7)$$

where  $\bar{G}$  is the equivalent shear modulus of the homogeneous layer,  $b_r$  and  $b$  are the widths of the rubber and the entire beam, respectively, and  $G_r$  and  $G^*$  are the shear modulus of the rubber and MR fluid, respectively.

The shear stress–shear strain properties of MR fluids have been described in many studies [Li *et al.*, 1999; Choi *et al.*, 2005] and characterized by two distinguished regions, referred to as ‘pre-yield’ and ‘post-yield’ regions, as shown in Figure 1.3. MR materials experience different levels of stress and strain in response to the applied magnetic field and follow a similar pattern in its rheological behavior. In the pre-yield regime, the MR material demonstrates viscoelastic behavior and is described by the complex modulus as [Li *et al.*, 1999]:

$$G^*(B) = G'(B) + iG''(B) \quad (3.8)$$

While the storage modulus  $G'(B)$  is proportional to the average energy stored during a cycle of deformation per unit volume of the material, the loss modulus  $G''(B)$  is proportional to the energy dissipated per unit volume of the material over a cycle. Moreover, both the moduli are functions of the magnetic field intensity  $B$ . The post-yield behavior of MR materials is approximately characterized by the Bingham plastic model, such that [Choi *et al.*, 2005]:

$$\tau = \tau_y + \eta \dot{\gamma} \quad (3.9)$$

where  $\tau$  is the shear stress,  $\tau_y$  is the magnetic field induced dynamic yield stress,  $\eta$  is the plastic viscosity and  $\dot{\gamma}$  is the shear strain rate. Due to the application of the magnetic field through MR fluid, the ferrous particle suspended in the viscous fluid produces particle chain and yield stress is thus developed [Goncalves *et al.*, 2006]. As a result, both storage and loss moduli (Eq. (3.8)) increase with increasing the magnetic field. Consequently the stiffness and damping properties can be controlled using the applied magnetic field. This enables an effective mechanism to suppress the vibration of the structural systems [Yalcintas and Dai, 1999].

### 3.2.1. Formulation of energy equations

Lagrange's energy approach has been implemented to formulate the governing equations of motion for the partially treated MR sandwich beam in the finite element form. To accomplish this, the total strain and kinetic energy of the system are derived. The strain energy due to elastic layers located at top and bottom of the sandwich beam,  $V_{1,3}$  can be expressed as:

$$V_{1,3} = \frac{1}{2} \int_0^L (E_1 A_1 + E_3 A_3 e^2) \left( \frac{\partial u}{\partial x} \right)^2 dx + \frac{1}{2} \int_0^L (E_1 I_1 + E_3 I_3) \left( \frac{\partial^2 w}{\partial x^2} \right)^2 dx \quad (3.10)$$

where  $I_1$  and  $I_3$  are the second moment of inertia at the centroid of the top and bottom elastic layers 1 and 3, respectively.

As shown in Figure 3.1 (b), the middle layer of the beam consists of elastic and MR fluid segments together with the rubber sealant material and thus the total strain energy of the middle layer of the beam can be expressed as the sum of the strain energy of the MR fluid layer with rubber material,  $V_{2f}$  and that of elastic sections,  $V_{2e}$ , such that:

$$V_2 = V_{2f} + V_{2e} \quad (3.11)$$

The above strain energies for a beam structure with one MR-fluid segment shown in Figure 3.1(b) can be expressed as:

$$V_{2f} = \frac{1}{2} \int_{L_1}^{L_1+L_2} G b h_2 \left[ \frac{D}{h_2} \frac{\partial w}{\partial x} - \frac{(1+e)u}{h_2} \right]^2 dx \quad \text{and}$$

$$V_{2e} = \frac{1}{2} \int_0^{L_1} E_{2e} A_{2e} \left( \frac{\partial u}{\partial x} \right)^2 dx + \frac{1}{2} \int_0^{L_1} E_{2e} I_{2e} \left( \frac{\partial^2 w}{\partial x^2} \right)^2 dx + \frac{1}{2} \int_{L_1+L_2}^L E_{2e} A_{2e} \left( \frac{\partial u}{\partial x} \right)^2 dx$$

$$+ \frac{1}{2} \int_{L_1+L_2}^L E_{2e} I_{2e} \left( \frac{\partial^2 w}{\partial x^2} \right)^2 dx \quad (3.12)$$

where  $E_{2e}$ ,  $A_{2e}$  and  $I_{2e}$  are the Young's modulus, cross sectional area and second moment of inertia, respectively, of the elastic segments within the mid layer of the sandwich beam.

The total strain energy  $V$  of the sandwich beam structure is expressed as the sum of those due to top, bottom and middle layers, such that:

$$V = V_1 + V_2 + V_3 \quad (3.13)$$

The kinetic energy of the sandwich beam structure is derived considering: (i) the transverse motion of the top and bottom elastic layers ( $T_{1TBL}$ ) (ii) the transverse motion of the middle layer which comprises of elastic layer, MR fluid layer and rubber material ( $T_{1ML}$ ) (iii) the axial deformations of the top and bottom elastic layers ( $T_2$ ) and (iv) the rotational deformation of the MR fluid segment due to strain displacement ( $T_3$ ).

The kinetic energy associated with the transverse motions of the top and bottom elastic layers,  $T_{1TBL}$  can be expressed as:

$$T_{1TBL} = \frac{1}{2} \int_0^L (\rho_1 A_1 + \rho_3 A_3) \left( \frac{\partial w}{\partial t} \right)^2 dx \quad (3.14)$$

where  $\rho_1$  and  $\rho_3$  are mass densities of the top and bottom elastic layers, respectively.

The kinetic energy associated with the transverse motions of the middle layer of the sandwich beam,  $T_{1ML}$ , which comprises of elastic and MR fluid layer segments, and rubber material, can be expressed as the sum of the kinetic energy due to transverse motion of the elastic layer,  $T_{1f}$ , and that of due to MR fluid layer and rubber material,  $T_{1e}$ , such that:

$$T_{1ML} = T_{1f} + T_{1e} \quad (3.15)$$

where,

$$T_{1f} = \frac{1}{2} \int_{L_1}^{L_1+L_2} (\rho_2 A_2 + \rho_r A_r) \left( \frac{\partial w}{\partial t} \right)^2 dx$$

$$T_{1e} = \frac{1}{2} \int_0^{L_1} \rho_{2e} A_{2e} \left( \frac{\partial w}{\partial t} \right)^2 dx + \frac{1}{2} \int_{L_1+L_2}^L \rho_2 A_{2e} \left( \frac{\partial w}{\partial t} \right)^2 dx$$

where  $\rho_2$ ,  $\rho_{2e}$  and  $\rho_r$  are the mass densities of the MR fluid, elastic layer and the rubber materials, respectively.

The kinetic energy associated with axial deformation of the top and bottom elastic layers,  $T_2$ , can be expressed as:

$$T_2 = \frac{1}{2} \int_0^L (\rho_1 A_1 + e^2 \rho_3 A_3) \left( \frac{\partial u}{\partial t} \right)^2 dx \quad (3.16)$$

and the kinetic energy associated with the rotation due to shear strain of the MR-fluid layer,  $T_3$ , is expressed by:

$$T_3 = \frac{1}{2} \int_{L_1}^{L_1+L_2} I_2 \rho_2 \left[ \frac{-(1+e)}{h_2} \frac{\partial u}{\partial t} + \frac{D}{h_2} \frac{\partial^2 w}{\partial x \partial t} \right]^2 dx \quad (3.17)$$

where  $I_2$  is the second moment of inertia at the centroid of the MR-fluid layer.

The total kinetic energy  $T$  of the sandwich beam is then obtained from:

$$T = T_1 + T_2 + T_3 \quad (3.18)$$

It should be noted that apart from the strain and kinetic energies, the work done by the excitation force, if present, also needs to be considered in the formulation. It should be noted that the above energy formulations are also applicable to multiple partial MR-fluid segments within the mid-layer.

### 3.2.2. Finite element formulation

In the finite element analysis (FEM), a standard beam element with two end nodes with three degrees-of- freedom (DOF) for each node is considered. The DOF include the transverse  $w$ , axial  $u$  and the rotational  $\theta$  displacements of the beam. The transverse and axial displacements can be expressed in terms of nodal displacement vectors and shape functions, as follows:

$$u(x,t) = N_u(x) d(t) \quad (3.19)$$

$$w(x,t) = N_w(x) d(t) \quad (3.20)$$

where  $d(t) = \{u^1, w^1, \theta^1, u^2, w^2, \theta^2\}$  and  $N_u(x)$  and  $N_w(x)$  are common linear and cubic polynomial beam shape functions represented as [Rao, 1999]:

$$\begin{aligned} N_1(x) &= 1 - \frac{x}{l_e}; \quad N_2(x) = 1 - \frac{3x^2}{l_e^2} + \frac{2x^3}{l_e^3}; \quad N_3(x) = x - \frac{2x^2}{l_e} + \frac{x^3}{l_e^2}; \\ N_4(x) &= \frac{x}{l_e}; \quad N_5(x) = \frac{3x^2}{l_e^2} - \frac{2x^3}{l_e^3}; \quad N_6(x) = -\frac{x^2}{l_e} + \frac{x^3}{l_e^2}; \end{aligned} \quad (3.21)$$

where  $l_e$  is the length of the element.

Upon substituting Eqs. (3.19) and (3.20) into Eqs. (3.13) and (3.18), and subsequently into the Lagrange's equations, described as:

$$\frac{d}{dt} \left( \frac{\partial T}{\partial \dot{q}_i} \right) - \frac{\partial T}{\partial q_i} + \frac{\partial V}{\partial q_i} = Q_i, \quad i = 1, 2, 3, n \quad (3.22)$$

the governing equations of motion for the undamped partially or fully-treated MR sandwich beam element in the finite element form can be obtained as:

$$[m^e]\{\ddot{d}\} + [k^e]\{d\} = \{f^e\} \quad (3.23)$$

where  $n$  is the total DOF considered in the formulation and  $Q_i$  is the generalized force corresponding to the  $i$ th DOF,  $[m^e]$  and  $[k^e]$  are the element mass and stiffness matrices respectively, and  $\{f^e\}$  is the element force vector. The stiffness and mass matrices of the sandwich beam element containing the MR fluid within its mid-length are summarized in Appendix B. The element matrices of the sandwich beam containing the elastic material within its mid-layer are not presented since the standard matrices are available for such elements. Assembling the mass and the stiffness matrices and the force vector for all the elements, yields the global governing equations of motion of MR sandwich beam which can be expressed in the finite element form as:

$$[M]\{\ddot{d}_g\} + [K]\{d_g\} = \{F\} \quad (3.24)$$

where  $[M]$ ,  $[K]$ ,  $\{F\}$  and  $\{d_g\}$  are the global system mass and stiffness matrices and global force and displacement vectors, respectively.

For the partially-treated sandwich beam, the matrices  $[M]$  and  $[K]$  are formulated by imposing compatibility conditions which are identical transverse and axial displacements and the slopes at the interfaces of the elastic material and MR-fluid segments within the mid-layer of the beam. For instance, for the beam with three mid-layer segments, as shown in Figure 3.1(b), these conditions can be expressed as:

$$\begin{aligned}
w_{n-1}(x=L_1) &= w_n(x=L_1); & w_n(x=L_1+L_2) &= w_{n+1}(x=L_1+L_2); \\
u_{n-1}(x=L_1) &= u_n(x=L_1); & u_n(x=L_1+L_2) &= u_{n+1}(x=L_1+L_2); \\
\theta_{n-1}(x=L_1) &= \theta_n(x=L_1); & \theta_n(x=L_1+L_2) &= \theta_{n+1}(x=L_1+L_2);
\end{aligned} \quad (3.25)$$

where  $w_n$ ,  $u_n$  and  $\theta_n$  refers to the transverse, axial displacements and slope, respectively, of the segment  $n$ .

### 3.2.3 Ritz formulation

The governing equations of motion of the partially treated MR sandwich beam are also formulated using the Ritz method to analytically obtain the free vibration properties of the partially treated MR sandwich beam, and to examine the validity of the proposed finite-element formulation. Based on Ritz formulation, the maximum strain energy must be equal to the maximum kinetic energy and consideration of  $\delta(T - V) = 0$ , a solution of the following form can be expressed as:

$$w(x) = \sum_{i=1}^N c_i \phi_i; \text{ and } u(x) = \sum_{j=1}^N c_j \Psi_j \quad (3.26)$$

where  $c_i$  and  $c_j$  are coefficients to be determined, and  $\phi_i$  and  $\Psi_j$  are the interpolation functions satisfying the boundary conditions. A minimization problem relative to the undetermined coefficients can be established by the application of the stationary condition and yields a set of  $N$  simultaneous linear algebraic equations in coefficients  $c_1, c_2 \dots c_n$  such that:

$$[[K_R] - \omega^2 [M_R]]\{c\} = 0 \quad (3.27)$$

The solution of the above equation yields the natural frequencies and mode shapes of the partially treated MR sandwich beam. It should also be noted that the dissipated energy due to the MR fluid has been neglected in the strain energy formulation term in the Ritz's

formulation. The negligible contributions due to dissipated energy was also verified by comparing the natural frequencies of the structure model with and without the loss factor due to MR-fluid. The natural frequencies corresponding to the first five modes of the two models were found to be within 0.05%.

As it can be realized from Eq. (3.8), both the storage modulus  $G'$  and loss modulus  $G''$  are directly dependent on the applied magnetic field  $B$ . Thus by changing the magnetic field the stiffness and damping of the MR sandwich beam can be controlled and vibration attenuation can be achieved. The detailed effect of magnetic field on the stiffness matrix can also be realized from the developed element stiffness matrices provided in the Appendix B.

### **3.3 EXPERIMENTAL STUDY AND VALIDATION OF THE DEVELOPED FINITE ELEMENT FORMULATION**

Laboratory experiments were performed on a partially treated MR sandwich beam to investigate its essential properties and to examine the validity of the proposed finite element model and Ritz formulation. Two thin aluminum strips (300 mm x 30 mm x 0.9 mm) with zero magnetic permeability were used to fabricate a partially treated MR sandwich beam. The strips were arranged to create a uniform 1.15 mm gap for the MR fluid (MRF-122EG), which was filled only at the center of the mid-layer of the beam over a length of 100 mm and aluminum was located at the remaining portion of the mid-layer, as shown in Figure 3.2. In order to maintain the uniform gap and contain the fluid in between the top and bottom layers, 1.15 mm thick high strength Buna-N rubber was applied around the edges using an adhesive. The width of this rubber layer was in the order of 1.5 mm. The sandwich beam was clamped to a support that was mounted on an

electro-dynamic vibration exciter, while permanent magnets were used to generate the magnetic field over the beam. Different magnetic field intensity was realized by varying the vertical position of the permanent magnets with respect to the beam, which was measured near the beam surfaces using a Gauss meter. The measurements were performed in the absence of permanent magnets (0 Gauss) and four different positions of the magnets leading to field intensities of approximately 75, 175, 400 and 500 Gauss at the beam surfaces.

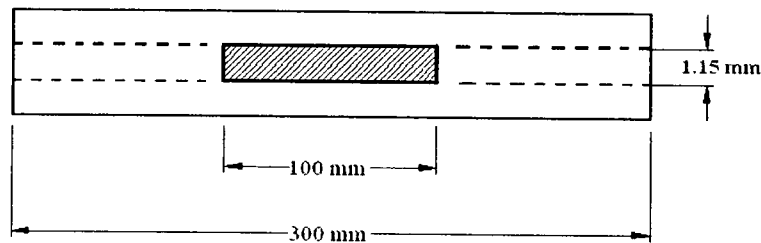
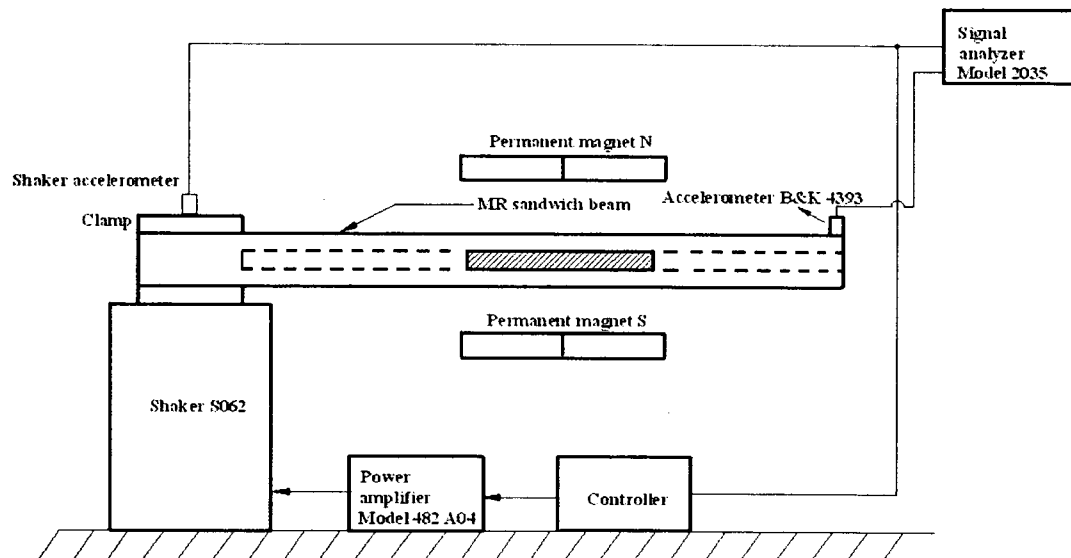


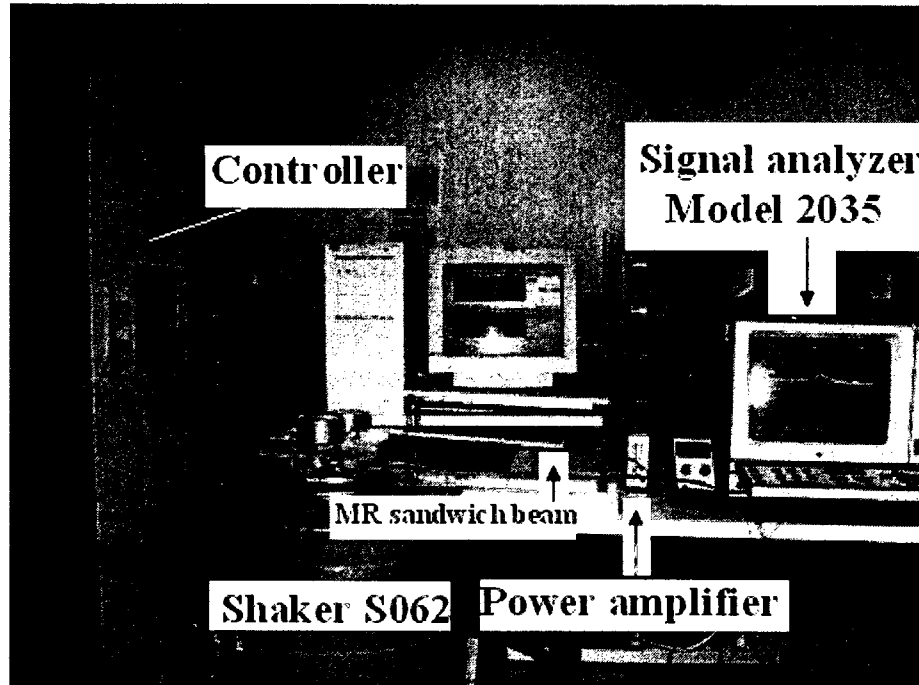
Figure 3.2. The test specimen of a partially treated MR fluid sandwich beam

Both free and forced vibration responses of the partially treated MR sandwich beam were measured. For the measurement of forced response, a single-axis accelerometer, oriented along the  $z$ -axis, was installed close to the free edge of the beam, to measure the acceleration response. A single-axis accelerometer was also installed at the support to measure the acceleration due to the excitation. This acceleration signal also served as the feedback for the vibration exciter controller. The schematic and photograph of the experimental setup is shown in Figure 3.3. The forced vibration responses of the partially treated MR sandwich beam were measured under a white-noise vibration spectrum with nearly constant power spectrum density (PSD) in the 1-300 Hz frequency range at three different magnetic field intensities (0, 75 and 175 Gauss). The forced responses were measured in terms of the transfer function of the accelerations at

the free end and the support, using the  $H_1$  function of the signal analyzer (Bruel & Kjaer 2035). The natural frequencies of the sandwich beam were subsequently identified from the peaks in the frequency response function. The forced vibration response could not be performed under higher magnetic field intensities (400 and 500 Gauss) due to the very small clearance between the beam and magnets, which caused repetitive locking of the beam with the magnets. The natural frequencies under these fields were thus extracted from the frequency spectrum of the free vibration response of the partially treated MR sandwich beam to a very low-level perturbation. It should be noted that the complex shear modulus of the MR fluid, MRF-122EG, used in the test specimen was estimated by performing a free oscillation experiment on the fully treated MR sandwich beam, as mentioned in section 2.3.1.



(a)



(b)

Figure 3.3. Experimental set-up. (a) Block diagram of the experimental setup  
 (b) Photograph of the partially treated MR sandwich beam experimental set up

Thus both the storage and shear moduli were expressed by the following 2<sup>nd</sup> order polynomial function with respect to the magnetic field intensity as:

$$G'(B) = -3.3691B^2 + 4997.5B + 0.873 \times 10^6$$

$$G''(B) = -0.9B^2 + 0.8124 \times 10^3 B + 0.1855 \times 10^6 \quad (3.28)$$

Now the developed finite element and Ritz formulations for the partially treated MR sandwich beam are validated by comparing the computed natural frequencies with those identified from the free and forced vibration responses of the beam. The simulations were performed by considering the material properties as:  $\rho_1 = \rho_3 = 2700$

kg/m<sup>3</sup>;  $E_1 = E_3 = 68$  Gpa;  $\rho_r = 1233$  kg/m<sup>3</sup> and  $\rho_2 = 3500$  kg/m<sup>3</sup>. Table 3.1 lists the comparisons of the natural frequencies obtained from the FEM and Ritz formulations with those obtained experimentally for the first three modes under different field intensities. A good agreement could be observed between the computed and measured frequencies, irrespective of the field intensity and the mode. Furthermore, the results obtained from the proposed finite element model are in close agreement with those derived from the Ritz method for the range of field intensities and modes considered.

Table 3.1. Comparison of natural frequencies of a partially treated cantilever MR-sandwich beam derived from the finite-element and Ritz formulations with the measured frequencies.

Field intensity (Gauss)	Mode	Natural Frequencies (Hz)				
		Measured	FEM		Ritz method	
			Results	% deviation	Results	% deviation
0	1	15	15.88	5.54	14.79	1.40
	2	85	80.96	4.75	83.13	2.20
	3	228	222.55	2.39	220.61	3.24
75	1	16	17.06	6.21	16.26	1.60
	2	87	82.26	5.45	85.88	1.29
	3	231	225.46	2.39	224.34	2.88
175	1	17	18.16	6.39	17.72	4.06
	2	90	83.68	7.02	88.52	1.64
	3	235	228.54	2.75	228.50	2.77
400	1	19	19.56	2.86	19.71	3.60
	2	94	85.81	8.71	93.19	0.86
	3	239	233.08	2.48	234.94	1.70
500	1	21	19.89	5.29	20.20	3.81
	2	95	86.37	9.08	94.33	0.71
	3	240	234.26	2.39	236.68	1.38

### 3.4 PARAMETRIC STUDIES

The properties of a partially treated MR-fluid sandwich beam are strongly influenced by many fluid and structure-related parameters such as field intensity, fluid layer thickness, complex shear modulus of the MR fluid, beam geometry and boundary conditions. Apart from these, the properties could also be identified by the number, size and location of the MR-fluid segments in case of a partially treated structure. Here in this study, the proposed finite element model is used to investigate the effects of variations in the location and length of the MR fluid segments of the beam on the natural frequencies and loss factor under different magnetic field intensities. The influence of length and location of such segments on the transverse vibration response are also investigated. For this purpose four different configurations of the localized MR damping treatments, denoted as 'A', 'B', 'C' and 'D' (Figure 3.4) , are considered together with different boundary conditions namely simply supported (SSB), clamped-free (CFB) and clamped clamped (CCB). The total length of the multi-layer beam is divided into 24 segments of equal length, while the MR fluid treatment is applied to selected segments or pockets of the structure. The remaining segments of the beam are considered to be of aluminum material. The total length of the MR fluid layer in all the configurations is assumed to be constant to facilitate relative property analyses. The simulation results are obtained by considering identical baseline thickness of 1mm of the elastic and fluid layers, while the material and all other properties of the layers are identical to those described in section 3.3.

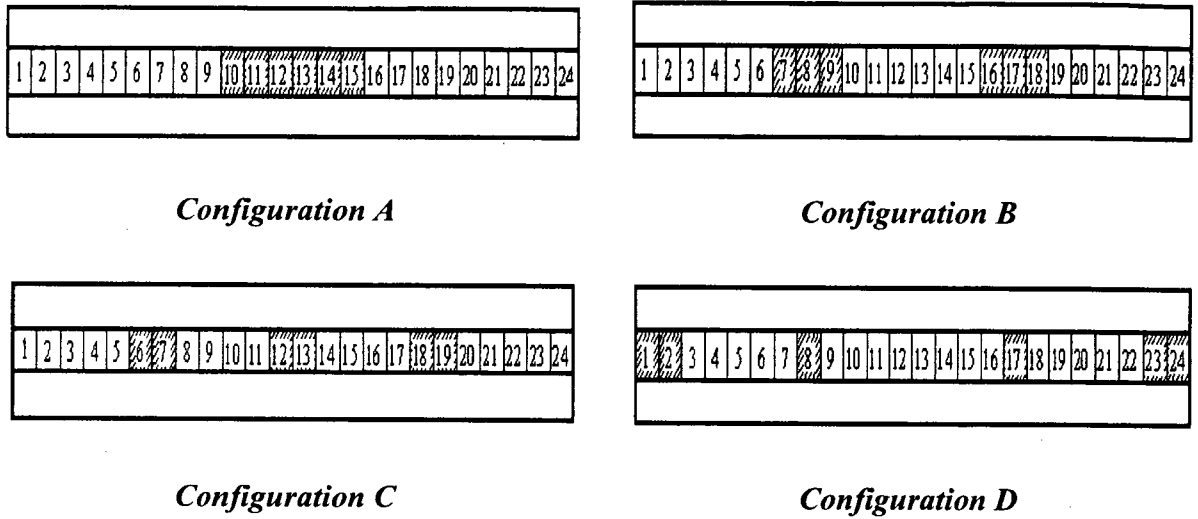


Figure 3.4. Various configurations of partially treated MR fluid sandwich beam

Table 3.2. Comparison of natural frequencies of a partially treated simply supported MR-sandwich beam derived from the finite-element and Ritz formulations at the magnetic field of 0 Gauss.

Configuration	Mode	Natural Frequencies (Hz)		
		FEM	Ritz method	% deviation
A	1	28.30	29.04	2.55
	2	198.14	201.65	1.74
	3	473.74	475.71	0.41
B	1	33.40	33.93	1.56
	2	113.58	114.95	1.19
	3	484.07	486.35	0.47
C	1	34.16	35.29	3.20
	2	126.21	125.29	0.73
	3	270.68	269.75	0.34
D	1	50.10	49.94	0.32
	2	163.94	164.70	0.46
	3	473.99	476.58	0.54

The validity of the developed finite element formulations for the four different configurations considered has been demonstrated by comparing the natural frequencies corresponding to the first three modes obtained from the FEM with Ritz formulations for the simply supported end conditions without any magnetic field. The results are presented

in Table 3.2. A good agreement exists between the natural frequencies computed through FEM and Ritz formulations.

#### **3.4.1. Influence of magnetic field intensity on natural frequencies**

The influence of variations in the magnetic field intensity on the natural frequencies for the different configurations of a partially treated MR sandwich beam is investigated under different end conditions. The results attained from the FEM in terms of natural frequencies corresponding to the first five modes are summarized in Tables 3.3 and 3.4 for the four configurations subject to three different field intensities (0, 250 and 500 Gauss). It can be seen from Table 3.3 that the natural frequencies corresponding to all the modes increase with increasing the magnetic field, irrespective of the configuration considered. The increase in the natural frequencies with increasing magnetic field can be attributed to increase in the complex shear modulus of the MR fluid and thus the structure stiffness under a higher magnetic field, which is evident from the element stiffness matrix presented in Appendix B. This confirms the potential of the MR fluid treatment to control the response of the structure. This trend of increasing natural frequency with the applied magnetic field intensity has also been represented in fewer studies on fully treated beams [Yalcintas and Dai, 1999; Yalcintas and Dai , 2004; Sun et al., 2003; Yeh and Shih, 2006].

Table 3.3. Influence of variations in the magnetic field intensity on the natural frequencies of different configurations of a partially treated simply supported MR sandwich beam.

Field intensity (Gauss)	Configuration	Mode number				
		1	2	3	4	5
0	A	28.30	198.14	473.74	694.21	1114.10
	B	33.40	113.58	484.07	742.85	1247.70
	C	34.16	126.21	270.68	906.34	1170.50
	D	50.10	163.94	473.99	605.89	965.40
250	A	29.86	206.33	479.52	700.13	1127.60
	B	35.61	116.02	493.07	751.09	1252.10
	C	36.63	129.05	273.94	915.50	1177.80
	D	54.20	168.26	484.31	616.8	970.44
500	A	30.68	210.47	482.73	703.46	1135.30
	B	36.77	117.38	498.14	755.59	1254.60
	C	37.95	130.62	275.82	920.79	1182.00
	D	56.37	170.64	490.24	623.16	973.41

Table 3.4. Influence of variations in the end conditions on the natural frequencies of the fully and partially treated MR sandwich beams at the magnetic field of 500 Gauss.

End conditions	Configuration	Mode number					
		1	2	3	4	5	
Simply supported	Fully treated beam	55.89	128.95	233.97	371.00	543.05	
	Partially treated beam	A	30.68	210.47	482.73	703.46	1135.30
		B	36.77	117.38	498.14	755.59	1254.60
		C	37.95	130.62	275.82	920.79	1182.00
		D	56.37	170.64	490.24	623.16	973.41
Clamped - free	Fully treated beam	16.23	82.20	180.78	302.78	458.30	
	Partially treated beam	A	20.36	88.31	285.59	655.09	934.52
		B	18.31	101.18	212.42	608.96	911.77
		C	18.07	97.42	239.26	383.43	1061.80
		D	13.27	94.73	227.70	690.62	988.36
Clamped - clamped	Fully treated beam	70.75	162.30	285.50	440.48	629.52	
	Partially treated beam	A	113.69	300.24	654.74	931.05	1320.60
		B	139.03	241.52	628.35	924.01	1525.00
		C	117.61	299.61	411.70	1076.80	1450.00
		D	74.87	201.83	649.90	903.64	1168.30

Tables 3.4 summarizes the influence of variations in different boundary conditions, including the simply-supported (SSB), clamped free (CFB) and clamped – clamped (CCB) conditions, on the natural frequencies of a partially treated MR-fluid sandwich beam structure at a magnetic field intensity of 500 Gauss. The results are presented for all the four configurations and compared with those of fully treated MR sandwich beams subject to the same magnetic field. It can be observed that the natural frequencies of the partially treated beam are generally greater than those of the fully treated beam, irrespective of the configuration, end conditions and modes of vibration. This is primarily attributed to the contributions of the aluminum segment replacing the MR fluid in the partially-treated configurations, which also yields lower mass compared to the fully treated beam.

The above trend, however, is not evident for the fundamental mode of the configurations A, B and C and second mode of configuration B, respectively with simply supported end conditions and fundamental mode of the configuration D with clamped-free end conditions, which can be related to the relative changes in the stiffness and mass corresponding to the fundamental mode. In other words, even though the mass of the beam has been decreased considerably in partially treated configurations compared to the fully treated beam, the decrease in stiffness would be relatively larger than that of mass corresponding to the fundamental mode. The results also show that depending on the mode of vibration, the natural frequency of a particular partially treated configuration may be considerably higher than those of the other configuration, irrespective of the end conditions, which can also be related to the relative changes in the stiffness and mass of the beam. Furthermore, as expected, the clamped-clamped and clamped-free end

conditions yield the highest and the lowest natural frequencies, respectively, for all modes considered, irrespective of the magnetic field intensity and the treatment configuration considered.

### **3.4.2. Influence of magnetic field intensity on loss factor**

The loss factor is computed as the ratio of the square of the imaginary component of the complex natural frequency to that of the real component [Yalcintas and Dai, 1999]. The influence of variations in the magnetic field intensity on the loss factor corresponding to the first five modes for the various configurations of a partially treated MR sandwich beam is investigated and compared with those of fully treated MR sandwich beam for different end conditions under magnetic field intensities of 0, 250 and 500 Gauss and the results are summarized in Table 3.5. The results generally show that the loss factor increases with increasing magnetic field intensity for all the configurations considered.

The loss factor is merely the ratio of energy dissipated per radian to the total strain energy, both of which increase with the magnetic field. Furthermore, the dissipated energy is directly related to the loss modulus, which increases with the field intensity as seen in Eq. (3.28). The relative increase in the loss modulus and thus the dissipated energy with increase in the magnetic field, however, is greater than that in the total strain energy, which leads to higher loss moduli under increasing magnetic field. This trend of increasing loss factor with the applied magnetic field intensity has also been represented in fewer studies on fully treated beams [Yalcintas and Dai, 1999; Yalcintas and Dai , 2004; Sun et al., 2003; Yeh and Shih, 2006].

The above trend, however, is not evident for the fundamental mode under simply supported and clamped-free end conditions and few higher modes such as mode 3, mode 5 and modes 2 and 3 for the configurations A, B and D, respectively, under clamped-free end conditions. It increases considerably under the application of the magnetic field of intensity up to 250 Gauss but decreases slightly with further increase in the field intensity. This can be attributed to the relative changes in the dissipated and strain energy corresponding to the fundamental mode. The increase in the total strain energy related to the corresponding mode with the magnetic field would be relatively smaller compared to that of energy dissipated resulting in increase in the loss factor until the magnetic field reaches a certain value. However, a further increase in magnetic field yields higher relative change in the total strain energy at the corresponding mode compared to that of the energy dissipated, which results in slightly lower loss factor.

Table 3.5. Influence of variations in the magnetic field intensity on the loss factor for the various configurations of a partially treated MR sandwich beam under different end conditions

End condition	Field intensity (Gauss)	Configuration	Mode number					
			1	2	3	4	5	
SSB	0	Fully treated beam	0.0999	0.0603	0.0384	0.0253	0.0176	
		Partially treated beam	A	0.0190	0.0147	0.0041	0.0029	0.0039
			B	0.0230	0.0072	0.0062	0.0038	0.0011
			C	0.0249	0.0076	0.0039	0.0033	0.0021
	D		0.0283	0.0089	0.0072	0.0059	0.0017	
	250	Fully treated beam	0.1077	0.0772	0.0559	0.0400	0.0292	
		Partially treated beam	A	0.0292	0.0210	0.0070	0.0049	0.0071
			B	0.0346	0.0122	0.0107	0.0063	0.0021
			C	0.0380	0.0127	0.0071	0.0059	0.0036
	D		0.0424	0.0148	0.0126	0.0106	0.0031	
	500	Fully treated beam	0.0941	0.0719	0.0545	0.0405	0.0304	
		Partially treated beam	A	0.0291	0.0215	0.0073	0.0052	0.0077
B			0.0342	0.0128	0.0112	0.0065	0.0023	

		beam	C	0.0377	0.0132	0.0076	0.0064	0.0039	
			D	0.0419	0.0153	0.0135	0.0114	0.0034	
		Fully treated beam		0.0581	0.0597	0.0483	0.0323	0.0224	
	0	Partially treated beam	A	0.0458	0.0082	0.0096	0.0044	0.0019	
			B	0.0485	0.0137	0.0033	0.0047	0.0034	
			C	0.0492	0.0154	0.0044	0.0020	0.0029	
			D	0.0436	0.0144	0.0055	0.0030	0.0042	
CFB	250	Fully treated beam		0.0518	0.0661	0.0615	0.0472	0.0353	
		Partially treated beam	A	0.0485	0.0133	0.0136	0.0076	0.0034	
			B	0.0520	0.0214	0.0059	0.0080	0.0051	
			C	0.0530	0.0240	0.0078	0.0036	0.0053	
	D		0.0493	0.0197	0.0081	0.0049	0.0066		
	500	Fully treated beam		0.0431	0.0588	0.0570	0.0462	0.0357	
		Partially treated beam	A	0.0414	0.0137	0.0132	0.0080	0.0036	
			B	0.0447	0.0216	0.0063	0.0085	0.0050	
			C	0.0456	0.0242	0.0084	0.0039	0.0057	
	D		0.0439	0.0189	0.0081	0.0051	0.0067		
	CCB	0	Fully treated beam		0.0566	0.0381	0.0262	0.0183	0.0133
			Partially treated beam	A	0.0039	0.0106	0.0045	0.0020	0.0029
B				0.0059	0.0024	0.0045	0.0038	0.0013	
C				0.0076	0.0028	0.0016	0.0029	0.0021	
D		0.0079		0.0027	0.0022	0.0022	0.0013		
250		Fully treated beam		0.0702	0.0536	0.0405	0.0301	0.0227	
		Partially treated beam	A	0.0066	0.0162	0.0077	0.0035	0.0054	
			B	0.0098	0.0043	0.0079	0.0063	0.0024	
			C	0.0130	0.0049	0.0030	0.0052	0.0037	
D			0.0137	0.0049	0.0040	0.0041	0.0023		
500		Fully treated beam		0.0640	0.0515	0.0406	0.0310	0.0239	
		Partially treated beam	A	0.0069	0.0161	0.0081	0.0038	0.0059	
	B		0.0101	0.0046	0.0084	0.0065	0.0026		
	C		0.0136	0.0053	0.0033	0.0056	0.0040		
D	0.0145		0.0053	0.0043	0.0044	0.0025			

It can also be observed that all the configurations with clamped-free and clamped-clamped end conditions yield the highest and lowest loss factor, respectively, among the end conditions considered at all levels of magnetic field. This can be related to the fact that the clamped-clamped and clamped-free end conditions have the highest and lowest strain energies, respectively, which result the corresponding lowest and highest loss factors.

Furthermore, the results show that the loss factor due to the fully treated MR sandwich beam is generally higher than those of the partially treated beams irrespective of the configurations and end conditions considered. This can be attributed to the relatively smaller length of the MR fluid layer in partially treated beams compared to that of the fully treated beam, which yields lower dissipated energy. The above trend, however, is not evident for the fundamental mode of the configurations B and C at magnetic field intensity of 250 Gauss and B, C and D with magnetic field intensity of 500 Gauss under clamped-free end conditions. This can be again related to the relative changes in the dissipated energy and the total strain energy at the lower mode. The increase in the strain energy of the partially-treated beam corresponding to the lower modes would be relatively smaller than that of the dissipated energy.

### **3.4.3. Influences of location of MR fluid**

The results presented in Tables 3.3 to 3.5 clearly illustrate the influence of location of the MR-fluid segments on both the natural frequencies and loss factors corresponding to the first five modes in which the total length of the MR fluid treatment is identical in all the configuration. The influence of location of the treatment is further investigated by considering the configuration A with simply supported and clamped - free end conditions. Four different locations of the partial treatment are considered for the analysis, as shown in Figure. 3.5. The 75 mm MR fluid treatment is applied over 6 different consecutive elements of the 24-element sandwich beam, which are denoted as A1, A2, A3 and A4 involving fluid treatments over 1-6, 7-12, 13-18 and 19-24 elements, respectively, as shown in Figure 3.6. The results obtained in terms of natural frequencies

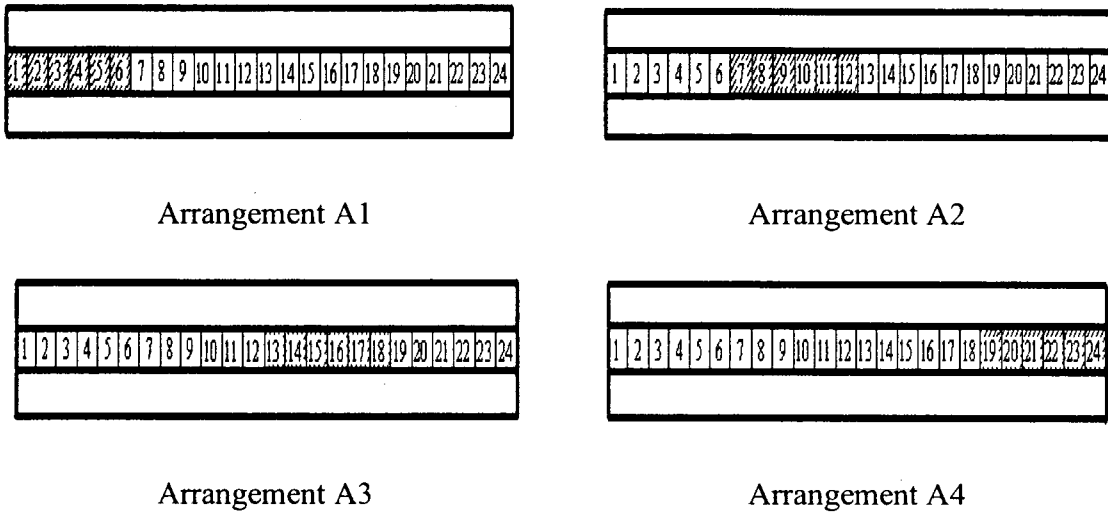


Figure 3.5. Different arrangements of configuration A of a partially treated MR sandwich beam.

and loss factor corresponding to the first five modes of the four arrangements are summarized in Tables 3.6 and 3.7, respectively, under a magnetic field of 500 Gauss. The tables also illustrate the results attained for configuration A, where the treatment is applied over elements 10-15. It can be observed that due to the nature of the symmetry of the simply supported end conditions, the natural frequencies and the loss factor for A1 & A4 and A2 & A3 arrangements are identical. The above trend, however, is not evident for the asymmetric clamped- free end conditions. It can also be seen that locating the MR-fluid segments at the boundary edges of the simply supported end conditions generally yields the higher loss factor except in the modes 2 and 5. For modes 2 and 5, locating the MR-fluids segments at the mid-span of the beam yields higher loss factor. It should be noted that such type variation could not be observed under clamped-free end conditions. However, the results generally show that the location of MR fluid pockets significantly affect the natural frequency and loss factor, irrespective of the end conditions and the mode of vibration.

Table 3.6. Influence of variations in the location of MR fluid on the natural frequency of configuration A of the partially treated MR sandwich beam at the magnetic field of 500 Gauss.

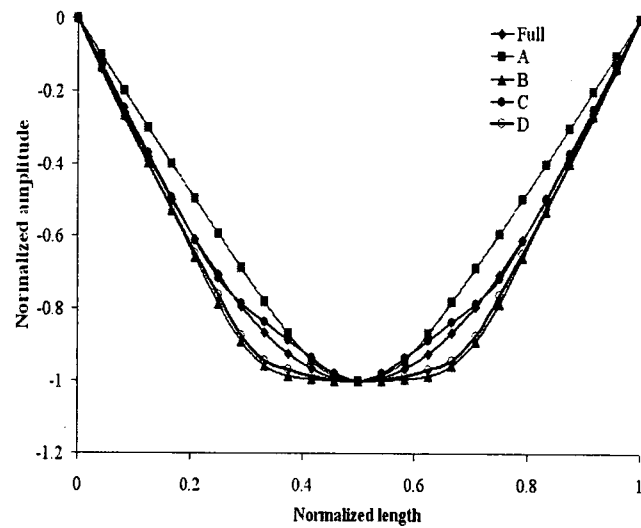
End conditions	Mode number	Natural frequency (Hz)				
		A (10-15)	A1 (1-6)	A2 (7-12)	A3 (13-18)	A4 (19-24)
Simply supported	1	30.68	68.51	33.62	33.62	68.51
	2	210.47	190.59	203.51	203.51	190.59
	3	482.73	470.71	412.89	412.89	470.71
	4	703.46	740.77	816.49	816.49	740.77
	5	1135.30	1190.90	1205.40	1205.40	1190.90
Clamped - free	1	20.36	10.49	16.38	24.76	28.48
	2	88.31	113.10	106.08	85.31	150.89
	3	285.59	282.45	319.09	278.21	297.29
	4	655.09	617.74	557.30	540.04	628.62
	5	934.52	937.36	980.27	972.65	952.46

Table 3.7. Influence of variations in the location of MR fluid on the loss factor of configuration A of the partially treated MR sandwich beam at the magnetic field of 500 Gauss.

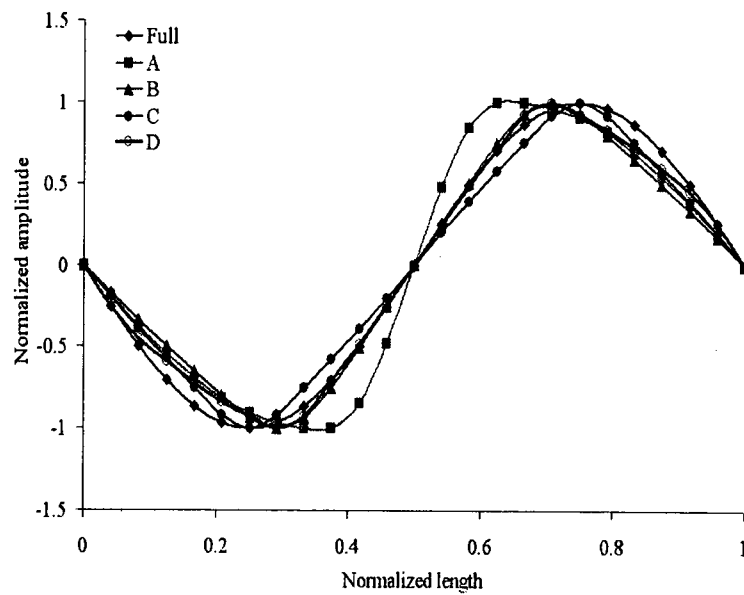
End conditions	Mode number	Loss factor				
		A (10-15)	A1 (1-6)	A2 (7-12)	A3 (13-18)	A4 (19-24)
Simply supported	1	0.02908	0.05066	0.03343	0.03343	0.05066
	2	0.02145	0.02005	0.01746	0.01746	0.02005
	3	0.00731	0.01081	0.00956	0.00956	0.01081
	4	0.00523	0.01082	0.00888	0.00888	0.01082
	5	0.00766	0.00361	0.00320	0.00320	0.00361
Clamped - free	1	0.04135	0.04952	0.04591	0.03042	0.01182
	2	0.01371	0.02164	0.01448	0.02241	0.01865
	3	0.01319	0.00887	0.00947	0.01303	0.01575
	4	0.00797	0.00567	0.00652	0.00585	0.01020
	5	0.00361	0.00733	0.00858	0.00872	0.01391

The effect of location of the MR-fluid treatment is further investigated by evaluating the deflection modes corresponding to the first four modes. For this purpose,

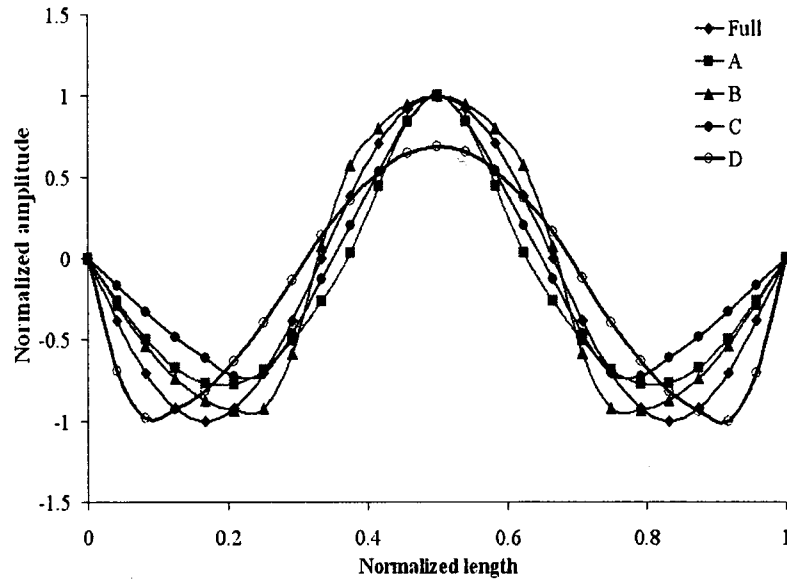
the mode shapes of the four configurations of the partially treated simply-supported beam are evaluated. Figure 3.6 illustrates the first four mode shapes of the partially treated MR



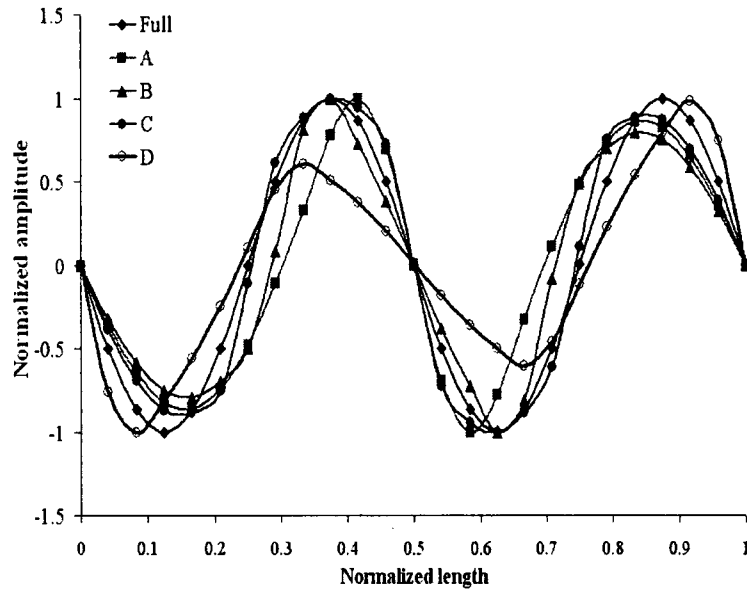
(a)



(b)



(c)



(d)

Figure 3.6. First four mode shapes of the fully and partially treated MR sandwich beam without applying magnetic field: (a) Mode 1. (b). Mode 2. (c) Mode 3. (d). Mode 4

sandwich beam. The results are attained in the absence of the magnetic field and compared with those of a fully-treated beam. The results suggest that the partial treatment

of the beam could alter the deflection mode, particularly the location of the peak normalized deflection. A fully-treated beam, owing to its symmetry consistently reveals harmonic deflection patterns. The above trend could not be observed in partially treated beams due to the partial location of MR-fluid segments. However, it can be observed that the configuration D yields the lowest peak deflection mode shape under modes 3 and 4. This can be attributed to the highest loss factor at the corresponding modes which is evident from Table 3.5. Although the configuration D yields higher loss factor even at the fundamental mode, such type of variation could not be observed. This can be related to the fact that the total strain energy dominates the dissipated energy as it can be realized from Table 3.3. This yields the higher natural frequency and hence the configuration D at mode 1 could not yield lower peak deflection mode shape.

#### **3.4.4. Influence of the length of MR fluid layer**

The influences of variation in the length of MR fluid treatment on the natural frequencies of a simply supported partially treated MR beam (Configuration A) is further investigated under the magnetic field of 500 Gauss. The simulations are performed by considering MR fluid treatments over 25%, 50%, 75% and 100% of the beam length. Figure 3.7 illustrates the variations in the natural frequencies of the configuration A with different lengths of the treatment corresponding to the first five modes. The results show significant effect of the fluid treatment length on the higher mode natural frequencies, while the effect is small on the lower modes. The results generally show a decrease in the higher modes natural frequencies with increasing length of the MR-fluid treatment, although the effect is highly non-linear. This can be attributed to relatively greater change in the beam mass than that in the stiffness corresponding to higher modes, when the

length of MR-fluid layer is increased. This trend, however, is not evident for the fundamental mode frequency, where the relative variation in the beam stiffness could be greater than that in the beam mass with increasing the fluid treatment length.

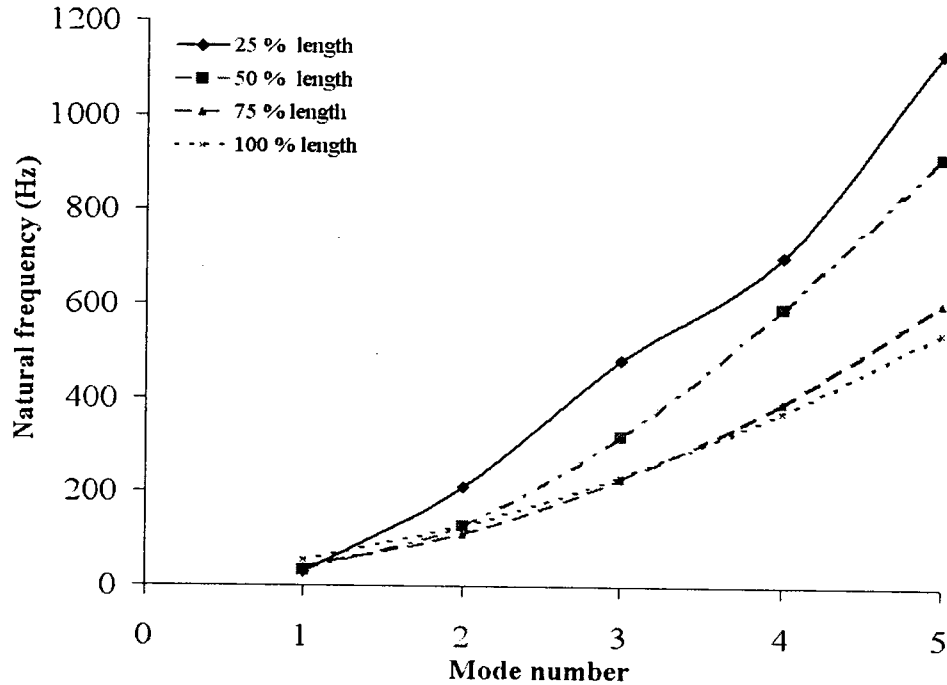


Figure 3.7. Influence of MR fluid layer length on the natural frequencies of a simply supported partially treated MR sandwich beam (Configuration A) under the magnetic field of 500 Gauss.

### 3.4.5. Transverse response of the partially treated MR sandwich beam

The influence of magnetic field on the transverse response of configuration D of a simply supported partially treated MR sandwich beam is investigated by considering sinusoidal excitation applied at a distance of 175 mm from the left support. The dynamic response characteristics of the beam were simulated under a 1N force excitation over the frequency range of 1-550 Hz for three different magnetic field intensities of 0, 250 and 500 Gauss.

The amplitude spectrum of the transverse displacement was evaluated at a distance of 187.5 mm from the left support and is illustrated in Figure 3.8. The results show increase in the natural frequencies (frequencies corresponding to response peaks) with increasing the magnetic field, as observed from the free vibration responses. The peak response magnitudes corresponding to all the modes also decrease with increasing the magnetic field, which may be attributed to higher loss factors under higher magnetic fields. The changes in the peak magnitudes, however, appear to be nonlinear functions of the magnetic field. An increase in the magnetic field from 0 to 250 Gauss yields substantial reduction in the peak amplitudes, which are approximately 11.6, 7.5 and 6.9 %, respectively, for the first 3 modes considered in the analysis.

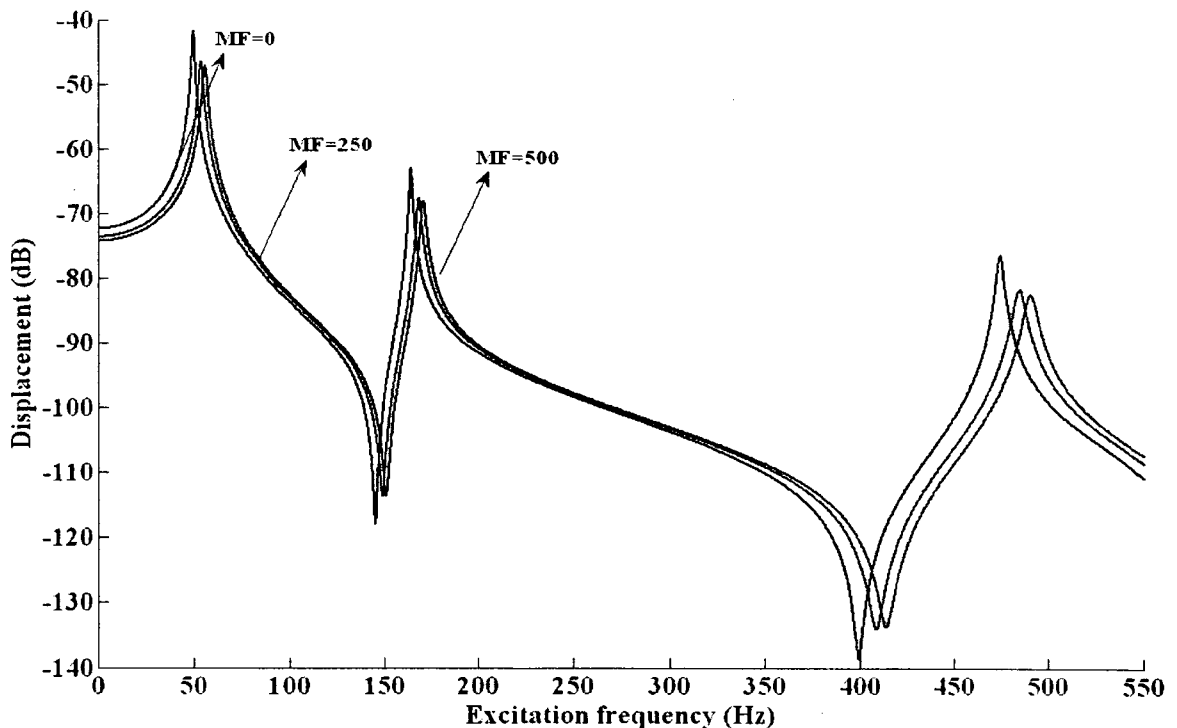


Figure 3.8. Influence of magnetic field on the transverse response of configuration D of a simply supported partially treated MR fluid sandwich beam.

The transverse response of various configurations of simply supported partially treated MR sandwich beams is also evaluated and compared with that of fully treated MR sandwich beam at a magnetic field of 250 Gauss by considering a sinusoidal excitation force of 1 N magnitude acting at a distance of 175 mm from the left support. Again, the transverse displacement is calculated at a distance of 187.5 mm from the left support over a frequency range of 1- 550 Hz and the results are shown in Figure 3.9. Furthermore, the magnitude and location (from the left end) of the maximum displacement of the beam under the magnetic field of 500 Gauss are evaluated at various excitation frequencies (30.23, 38.20 and 57.29 Hz) which are approximately equal to the first natural frequency of fully and various configurations of partially treated MR sandwich beam and compared with that of fully treated MR sandwich beam. The results are listed in Table 3.8. It can be observed that for the same excitation frequency, the location of the maximum displacement differs for the various configurations. Also the minimum magnitude of the maximum displacement occurs in the configuration D and is approximately equal to that of fully treated MR sandwich beam for the excitation frequencies considered in the analysis. This can be related to the higher loss factor for the fully treated and configuration D of the partially treated MR sandwich beam which is evident from Table 3.5. It can also be observed that the largest magnitude of maximum displacement occurs at the configuration A for all the excitation frequencies considered in the analysis. This is due to the fact that the configuration A has the lowest loss factor at the fundamental mode as evident from Table 3.5. This confirms that the MR fluid could be applied at any critical locations of the structure to suppress the vibration effectively.

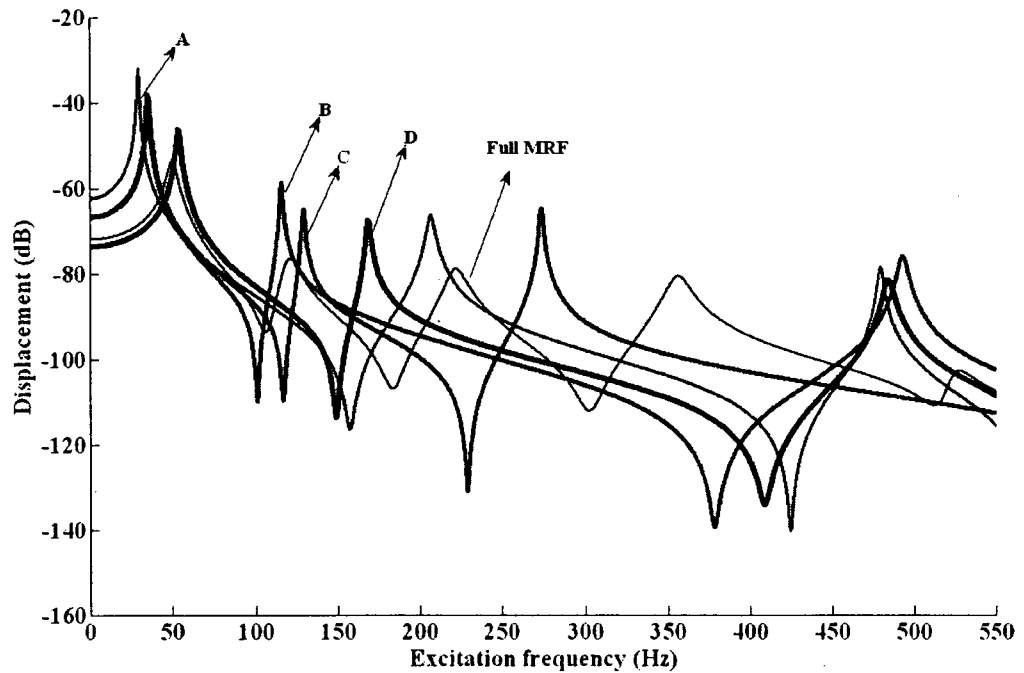


Figure 3.9. Transverse displacement of fully and partially treated MR sandwich beam at a magnetic field of 250 Gauss under simply supported end conditions.

Table 3.8. Location and magnitude of the maximum displacement of transverse displacement at magnetic field of 500 Gauss for simply supported end conditions.

Excitation frequency (Hz)	Configuration	Location of the maximum displacement from the left end (mm)	Magnitude of the maximum displacement (mm)
30.23	Fully treated	181	0.212
	A	168	0.748
	B	207	0.438
	C	168	0.441
	D	194	0.195
38.20	Fully treated	181	0.212
	A	168	0.752
	B	207	0.439
	C	168	0.442
	D	194	0.195
57.29	Fully treated	181	0.213
	A	168	0.767
	B	207	0.445
	C	168	0.448
	D	194	0.196

### 3.5 CONCLUSIONS

In this chapter, vibration response of a partially treated multi-layered beam with MR fluid as a sandwich layer between two layers of the continuous elastic structure has been analyzed. First, mathematical model of the partially treated MR composite beam was developed in finite element form and Ritz formulation to simulate the dynamic response of the system. The experimental study is then conducted to characterize the MR fluid behavior and to validate the developed formulations. Using the developed finite element formulation, different configurations of a partially treated MR sandwich beam has been studied and then various parametric studies have been conducted to demonstrate the controllable capabilities of the MR beam. It has been shown that the location and length of the MR fluid segments have significant effect on the natural frequencies and the loss factor of the partially treated MR sandwich structure in addition to the intensity of the magnetic field and the boundary conditions. It has been demonstrated that the MR fluid pockets should be located at a particular location depending on the boundary conditions and the mode of vibration to be controlled for the effective vibration suppression. Furthermore, the mode shape of the partially treated MR sandwich beam could be controlled by locating the MR fluid layers at the desired locations. It has also been shown that the natural frequency at the higher modes could be increased with decreasing the length of MR fluid layer. Transverse response of a partially treated MR sandwich beam also confirms that the amplitude of vibration could be considerably reduced using controllable MR fluids and conveniently applied them to partial or more critical components of a large structure to realize more efficient vibration control.

# **CHAPTER 4**

## **OPTIMUM DESIGN OF A MULTILAYER BEAM PARTIALLY TREATED WITH MAGNETORHEOLOGICAL FLUID**

### **4.1 INTRODUCTION**

In Chapter 2, the dynamic properties of a MR sandwich beam were investigated using finite element and Ritz formulations and compared the results with those obtained from the experimental investigations. Furthermore, the effectiveness of the MR fluids in controlling the vibration of fully treated MR fluid multilayer structures was demonstrated numerically and experimentally. It has also been demonstrated in Chapter 3 that a relatively simple design may be realized when the fluid is contained within a localized section or partially and the air cavity is replaced by the elastic material. This would also be beneficial in enhancing the natural frequencies.

In this chapter, the emphasis is placed on determining the optimal location of MR fluid segments in a partially treated MR sandwich beam to maximize the modal damping factors. The damping factor corresponding to each mode is evaluated by implementing the modal strain energy principle in the finite element model of the partially treated MR sandwich beam formulated in Chapter 3. An optimization problem is formulated and solved using the Genetic Algorithm (GA) to identify the optimum locations of the localized MR fluid treatments that would yield maximum modal damping factors corresponding to the first five modes, considered individually and simultaneously. The optimal distributions of the treatments are identified for different end conditions

including simply supported, clamped-free and clamped-clamped end conditions. Furthermore, the efficiency of GA to capture the global optimum solution is demonstrated by comparing the results with those obtained from the solution of the maximization problem using sequential quadratic programming (SQP) technique.

## **4.2 FINITE ELEMENT MODELING OF A PARTIALLY TREATED MULTI-LAYER BEAM**

The finite element formulation for a fully-treated three layer beam structure, reported in Chapter 2, is applied to model the structure with partial MR fluid segments. Consider a three-layer sandwich beam structure with multiple MR fluid segments within the mid-layer, as shown in figure 4.1(a). The beam section is modeled by treating each segment independently and then coupling with the adjacent segments to assure compatible deformation and continuous response of the sandwich beam. This is achieved by imposing compatibility conditions, which are identical displacements and the slopes at the boundaries of the two adjacent segments. The finite element formulation is derived upon consideration of a section of the beam comprising a fluid segment of length  $L_2$  constrained by the two elastic material segments of length  $L_1$  and  $L_3$ , as shown in Figure 4.1(b). A sealant material (Buna-N-rubber) is considered around the edges of each MR fluid pocket, as illustrated in the plan view of the beam segment with MR fluid in Figure 4.1(c). Considering that the Young's modulus of the MR-fluid is nearly negligible compared to that of the elastic layer, the normal stress developed in the fluid layer is considered negligible. Furthermore, the thickness of the individual elastic ( $h_A$  and  $h_B$ ), and fluid ( $h_C$ ) layers are very small compared to the length of the beam, and the slippage between the elastic and fluid layers is neglected. The shear strain and the damping in the

elastic layers are also assumed to be negligible and the transverse displacement  $w$  is considered to be uniform over a given cross-section.

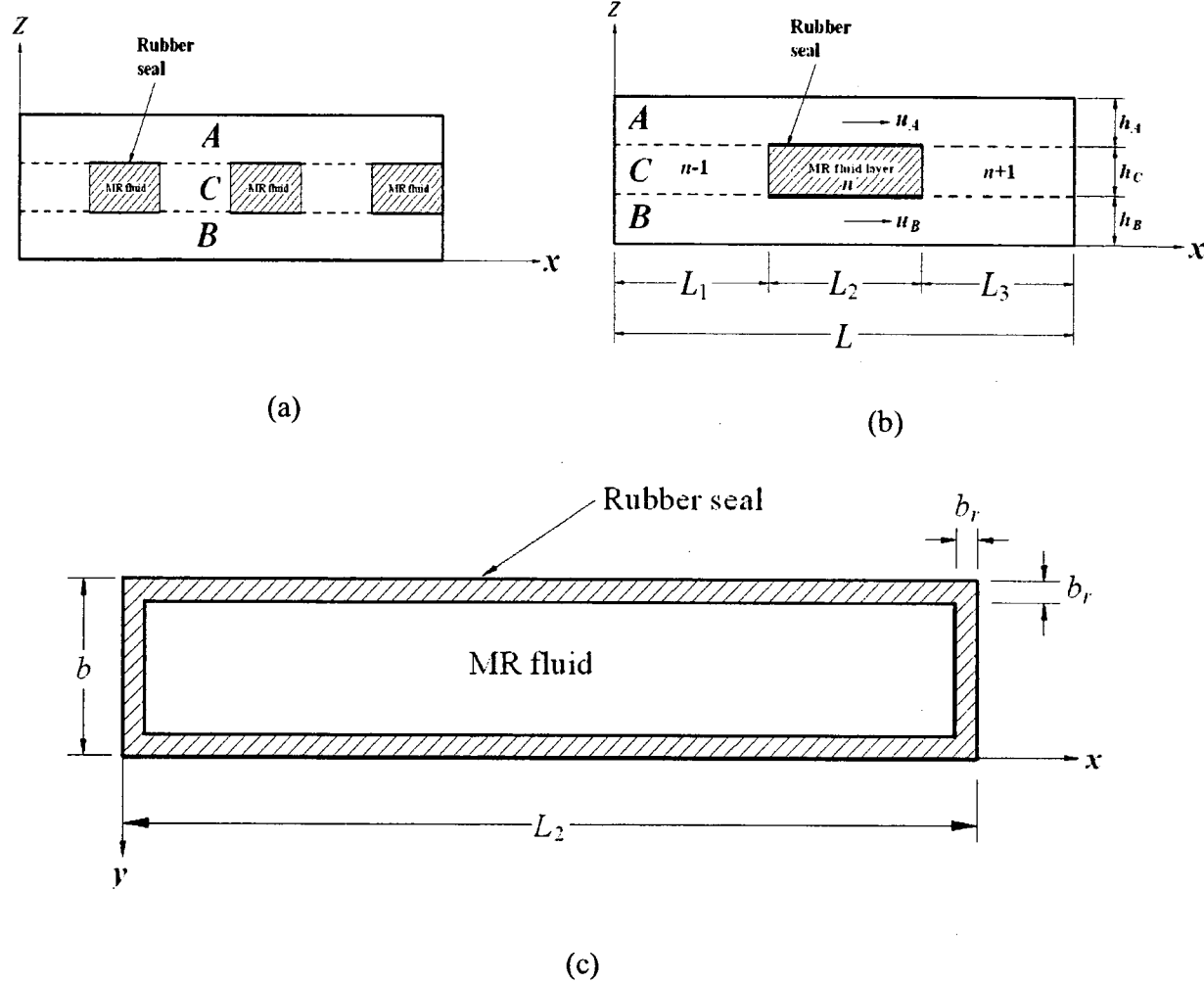


Figure 4.1: (a) Partially treated MR sandwich beam with multiple MR fluid segments. (b) Partially treated MR sandwich beam with single MR fluid segment (c) Plan view of mid-layer of the sandwich beam.

Each MR fluid segment comprising the fluid and the rubber seal is modeled as a homogeneous material layer with equivalent shear modulus,  $\bar{G}$ , expressed as:

$$\bar{G} = G_r \left( \frac{b_r}{b} \right) + G^* \left( 1 - \frac{b_r}{b} \right) \quad (4.1)$$

where  $b_r$  and  $b$  denote the widths of the rubber and the entire beam, respectively, as shown in Figure 4.1(c), and  $G_r$  and  $G^*$  are the shear moduli of the sealant material and the MR fluid, respectively.

The governing equations of motion for the partially treated MR sandwich beam are derived using the Lagrange's energy approach. The total strain energy  $V$  of the sandwich beam structure can be expressed as the sum of those due to the top (layer  $A$ ), bottom (layer  $B$ ) and middle (layer  $C$ ) layers, such that:

$$V = V_A + V_B + V_C \quad (4.2)$$

The strain energy due to elastic material layers ( $A$  and  $B$ ) of the sandwich beam,  $V_{A,B}$ , can be expressed as:

$$V_{A,B} = \frac{1}{2} \int_0^L (E_A A_A + E_B A_B e^2) \left( \frac{\partial u}{\partial x} \right)^2 dx + \frac{1}{2} \int_0^L (E_A I_A + E_B I_B) \left( \frac{\partial^2 w}{\partial x^2} \right)^2 dx \quad (4.3)$$

where  $I_A$  and  $I_B$  are the second moments of inertia at the centroid of the elastic layers  $A$  and  $B$ , respectively, and  $A_A$  and  $A_B$  are the respective cross sectional areas,  $E_A$  and  $E_B$  are the Young's moduli of layers  $A$  and  $B$ , respectively, and  $e = \frac{E_A A_A}{E_B A_B}$ . The longitudinal displacements of the mid-planes of the elastic layers in the  $x$ -direction are denoted by  $u$ .

The total strain energy of the mid-layer  $V_C$  is derived from sum of those associated with the partial elastic material and MR fluid layers together with the sealant material, such that:

$$\begin{aligned}
V_C = \frac{1}{2} \int_{L_1}^{L_1+L_2} G A_C \left[ \frac{D}{h_C} \frac{\partial w}{\partial x} - \frac{(1+e)u}{h_C} \right]^2 dx + \frac{1}{2} \int_0^{L_1} E_{Ce} A_C \left( \frac{\partial u}{\partial x} \right)^2 dx + \frac{1}{2} \int_0^{L_1} E_{Ce} I_{Ce} \left( \frac{\partial^2 w}{\partial x^2} \right)^2 dx \\
+ \frac{1}{2} \int_{L_1+L_2}^L E_{Ce} A_C \left( \frac{\partial u}{\partial x} \right)^2 dx + \frac{1}{2} \int_{L_1+L_2}^L E_{Ce} I_{Ce} \left( \frac{\partial^2 w}{\partial x^2} \right)^2 dx \quad (4.4)
\end{aligned}$$

where  $D = h_C + \frac{1}{2}(h_A + h_B)$  and  $A_C = b \cdot h_C$  is the cross sectional area of the layer C, and  $E_{Ce}$  and  $I_{Ce}$  are the Young's modulus and second moment of inertia, respectively, of the elastic material segments within the mid layer.

The kinetic energy of the sandwich beam structure is derived considering: (i) the transverse motion of the top and bottom elastic layers; (ii) the transverse motion of the middle layer comprising the elastic material and MR fluid segments together with the rubber material; (iii) the axial deformations of the top and bottom elastic layers; and (iv) the rotational deformation of the MR fluid segment due to shear strain displacement.

The total kinetic energy  $T$  of the sandwich beam is then obtained from:

$$T = T_1 + T_2 + T_3 \quad (4.5)$$

where  $T_1$  is the kinetic energy associated with the transverse motions of the top and bottom elastic layers and that due to transverse motion of the middle layer, expressed as:

$$\begin{aligned}
T_1 = \frac{1}{2} \int_0^L (\rho_A A_A + \rho_B A_B) \left( \frac{\partial w}{\partial t} \right)^2 dx + \frac{1}{2} \int_{L_1}^{L_1+L_2} (\rho_C A_C + \rho_r A_r) \left( \frac{\partial w}{\partial t} \right)^2 dx \\
+ \frac{1}{2} \int_0^{L_1} \rho_{Ce} A_C \left( \frac{\partial w}{\partial t} \right)^2 dx + \frac{1}{2} \int_{L_1+L_2}^L \rho_{Ce} A_C \left( \frac{\partial w}{\partial t} \right)^2 dx \quad (4.6)
\end{aligned}$$

where  $\rho_A$  and  $\rho_B$  are the mass densities of the top and bottom elastic layers, respectively and  $\rho_C$ ,  $\rho_{Ce}$  and  $\rho_r$  are the mass densities of the MR fluid, and elastic and the rubber materials segments, respectively, within the middle layer of the sandwich beam.  $A_r = b_r * h_C$  is the cross sectional area of the rubber sealant layer.

The kinetic energy associated with axial deformation of the top and bottom elastic layers,  $T_2$ , can be expressed as:

$$T_2 = \frac{1}{2} \int_0^L (\rho_A A_A + e^2 \rho_C A_C) \left( \frac{\partial u}{\partial t} \right)^2 dx \quad (4.7)$$

and the kinetic energy associated with the rotation due to shear strain of the MR-fluid layer,  $T_3$ , is expressed by:

$$T_3 = \frac{1}{2} \int_{L_1}^{L_1+L_2} I_C \rho_C \left[ \frac{-(1+e)}{h_C} \frac{\partial u}{\partial t} + \frac{D}{h_C} \frac{\partial^2 w}{\partial x \partial t} \right]^2 dx \quad (4.8)$$

where  $I_C$  is the second moment of inertia at the centroid of the MR-fluid layer.

It should be noted that apart from the strain and kinetic energies, the work done by the excitation force, if present, also needs to be considered in the formulation.

#### 4.2.1 Formulation of finite element matrices

The element matrices are formulated by considering a standard beam element with two end nodes with three Degrees-of-Freedom (DOF) for each node, namely, the transverse  $w$ , axial  $u$  and the angular  $\theta$  displacements. The transverse and axial displacement functions are derived from nodal displacement vector  $d(t) = \{u^1, w^1, \theta^1, u^2, w^2, \theta^2\}^T$ , and shape functions  $N_u(x)$  and  $N_w(x)$  such that [Rao, 1999]:

$$u(x,t) = N_u(x) \{d(t)\}$$

$$w(x,t) = N_w(x) \{d(t)\} \quad (4.9)$$

The axial and transverse displacement functions from Eq. (4.9) are substituted in the potential and kinetic energy expressions described in Eqs. (4.2) and (4.5), and the resultant energy functions are subsequently applied to the Lagrange's equations:

$$\frac{d}{dt} \left( \frac{\partial T}{\partial \dot{q}_i} \right) - \frac{\partial T}{\partial q_i} + \frac{\partial V}{\partial q_i} = Q_i, \quad i=1, 2, 3, n \quad (4.10)$$

where  $q_i$  and  $Q_i$  are the generalized coordinates and forces respectively.

The above equation resulted in the formulations of the governing equations of motion for the MR sandwich beam element, as:

$$[m^e] \{\ddot{d}\} + [k^e] \{d\} = \{f^e\} \quad (4.11)$$

where  $[m^e]$  and  $[k^e]$  are the element mass and stiffness matrices, respectively, and  $\{f^e\}$  is the element nodal force vector. The stiffness and mass matrices of the sandwich beam element containing the MR fluid can be found in the appendix B. The global governing equations of motion of the MR sandwich beam are subsequently obtained by assembling the mass and the stiffness matrices, and the force vector for all the elements, which can be expressed in finite element form as:

$$[M] \{\ddot{d}_g\} + [K] \{d_g\} = \{F\} \quad (4.12)$$

where  $[M]$ ,  $[K]$  and  $\{F\}$  are the global mass and stiffness matrices, and force vector, respectively.

For the partially-treated sandwich beam, the matrices  $[M]$  and  $[K]$  are formulated by imposing compatibility conditions, which impose identical transverse and axial displacements and slopes at the interfaces of the elastic material and MR-fluid segments within the mid-layer of the beam.

### 4.3 MODAL DAMPING FACTOR

The shear modulus of the MR fluid has been described in a number of studies on the basis of measured shear stress-shear strain properties, which have been characterized by two distinguished regions, referred to as ‘pre-yield’ and ‘post-yield’ regions [Li *et al.*, 1999; Choi *et al.*, 2005]. As the MR material demonstrates viscoelastic behavior in the pre-yield regime [Yalcintas and Dai, 1999; Yalcintas and Dai, 2004; Sun *et al.*, 2003], the modal damping factor corresponding to each mode of the partially treated MR sandwich beam could be calculated by implementing the principle of modal strain energy method for viscoelastic materials using the finite element model developed in the previous section. Assuming that the energy dissipation of a partially treated MR sandwich beam is mostly attributed to the properties of the MR fluid, the modal damping factor  $\eta_r$  for each mode  $\Phi^{(r)}$  of the beam can be expressed as the ratio of the elastic strain energy due to MR fluid to the total strain energy of the sandwich beam corresponding to each deflection mode, such that [Nashif *et al.*, 1985]:

$$\eta_r = \eta_d \frac{\sum_{e=1}^n \phi_e^{(r)} k_e \phi_e^{(r)}}{\phi^{(r)T} K \phi^{(r)}} \quad (4.13)$$

where  $\phi^{(r)}$  is the  $r^{\text{th}}$  mode shape vector,  $\phi_e^{(r)}$  is the vector extracted from  $\phi^{(r)}$  corresponding to motion of the nodes of the  $e^{\text{th}}$  MR fluid element,  $\eta_d$  is the loss factor of MR fluid,  $k_e$  is the element stiffness matrix of the  $e^{\text{th}}$  MR fluid element,  $K$  is the global stiffness matrix of the sandwich beam and  $n$  is the number of MR fluid elements considered in the structure model.

#### **4.3.1. Influence of location of MR fluid segments on the modal damping factor and natural frequency**

The properties of a partially treated MR-fluid sandwich beam are influenced by many fluid and structure-related parameters such as field intensity, fluid layer thickness, complex shear modulus of the MR fluid, beam geometry and boundary conditions. Apart from these, the dynamic characteristics of the partially treated MR-fluid structure are strongly influenced by the size and location of the MR fluid segments. Here in this section, the proposed finite element model is used to investigate the effects of variations in the location of the MR fluid segment of the beam on the modal damping factor and natural frequency under different end conditions including simply supported (SSB), clamped-free (CFB) and clamped-clamped (CCB). For this purpose, two different configurations, referred to as configurations A and B, of the partially treated MR

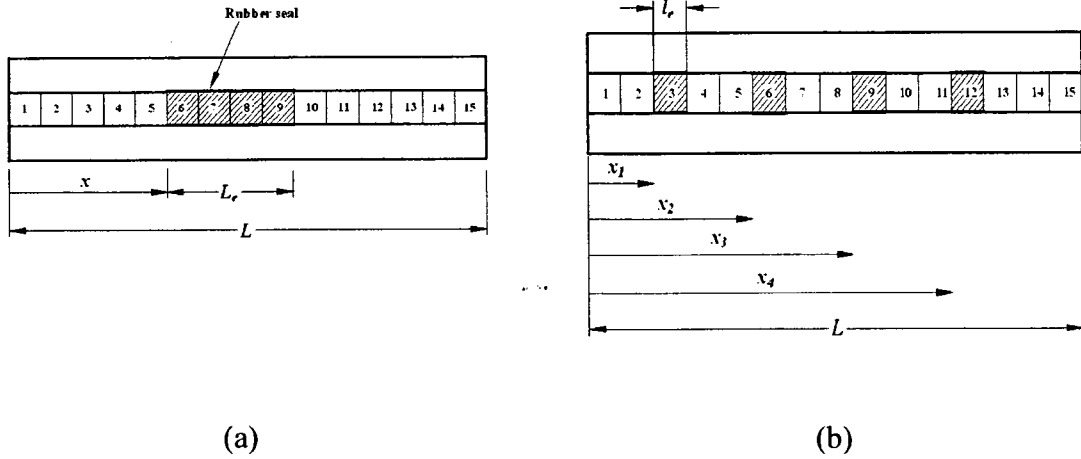


Figure 4.2: Two different configurations of a partially treated MR fluid sandwich beam.

a) Configuration A b) Configuration B

sandwich beam are considered for the analyses, as shown in Figure 4.2. The total length of the multi-layer beam is divided into 15 segments of equal length, while the MR fluid treatment is applied to selected segments or pockets of the structure. The remaining segments of the beam are considered to be of aluminum material. The configuration A is formulated by combining four MR fluid pockets together as a single segment (80 mm long), while configuration B considers localized treatments of four individual MR fluid pockets along the span. The total length of the MR fluid layer in both configurations is assumed to be identical to facilitate the relative property analyses. The simulation results are obtained by considering identical baseline thickness of 1mm of the elastic and fluid layers, while the length and width of the beam are taken as 300 mm (element length of 20 mm) and 30 mm, respectively. The material properties considered are as:  $\rho_A = \rho_B = 2700 \text{ kg/m}^3$ ;  $E_A = E_B = 68 \text{ Gpa}$ ;  $\rho_r = 1233 \text{ kg/m}^3$  and  $\rho_C = 3500 \text{ kg/m}^3$ . Experiments were performed to measure the free vibration response of a fully-treated MR sandwich beam in order to obtain an estimate of the complex shear modulus of the MR-fluid, as

reported in Section 2.3.1. The photograph of the experimental set-up has been provided in Figure 4.3. The relationship between the magnetic field induction and the complex shear modulus of MR fluid is considered as:

$$G^* = G' + iG'' \quad (4.14)$$

where  $G'$  and  $G''$  are storage and loss moduli, respectively, expressed as a polynomial functions of the magnetic field intensity  $B$  (in Gauss), as :

$$\begin{aligned} G' &= -3.3691B^2 + 4.9975 \times 10^3 B + 0.873 \times 10^6; \\ G'' &= -0.9B^2 + 0.8124 \times 10^3 B + 0.1855 \times 10^6 \end{aligned} \quad (4.15)$$

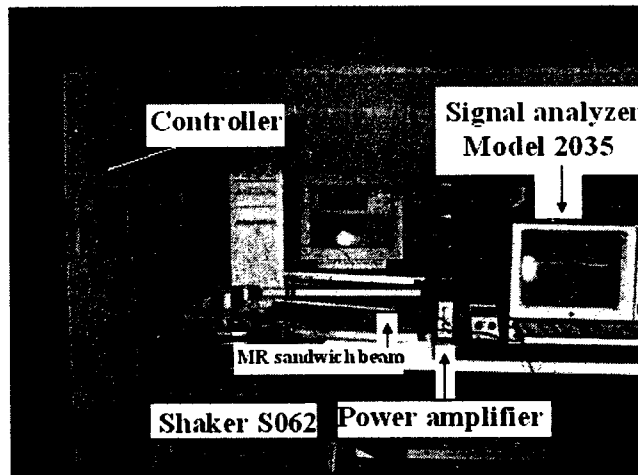
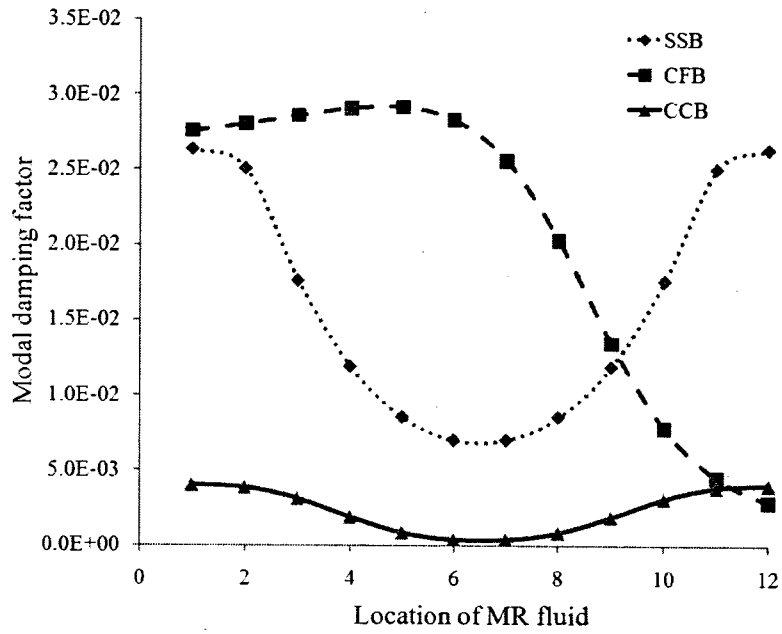


Figure 4.3. Photograph of the experimental set-up of the fully treated MR sandwich beam to evaluate the complex shear modulus of the MR fluid.

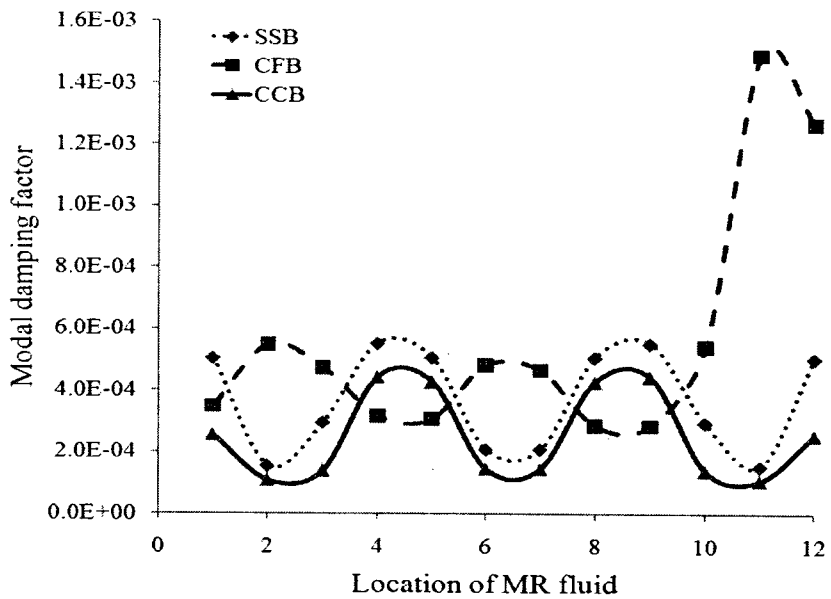
Figures 4.4 and 4.5 show the influence of location of the MR fluid segments along the span on the modal damping factors and natural frequencies, respectively, corresponding to modes 1 and 4 of configuration A comprising four MR fluid segments of total length of 80 mm. The abscissa in the figures shows the element number of the

first MR fluid segment, while the total number of MR fluid segments is limited to 4. The results are obtained under the application of the magnetic field of 250 Gauss, while considering three different end conditions: simply supported (SSB), clamped-free (CFB) and clamped-clamped (CCB). The results generally show that both the modal damping factors and natural frequencies are strongly influenced by the location of MR fluid segments, irrespective of the end condition. It can also be observed that the symmetry of the simply supported and clamped-clamped end conditions yields symmetric variation in the modal damping ratios and natural frequencies. The modal damping ratios and natural frequencies for the MR fluid segments located from positions 1 to 6 are identical to those obtained for the segments starting from positions 7 to 12. The above trend, however, is not evident for the asymmetric clamped- free end conditions.

It can also be seen that locating the MR fluid segments near the boundaries of the simply supported beam yields the highest modal damping factors and natural frequency corresponding to mode 1. The clamped-clamped beam also yields highest fundamental modal damping factor with MR fluid treatments near the supports, but this trend was not observed for the natural frequency. The variation in both the modal damping factor and natural frequency in this case, however, considerably smaller compared to the SSB condition. This is attributable to high strain energy associated with the CCB condition. The simply supported beam also yields highest modal damping and natural frequency corresponds to mode 4, when MR fluid is applied from 60 mm or 160 from left support (element #4 or #9). This location also appears to be optimal in view of the damping factor

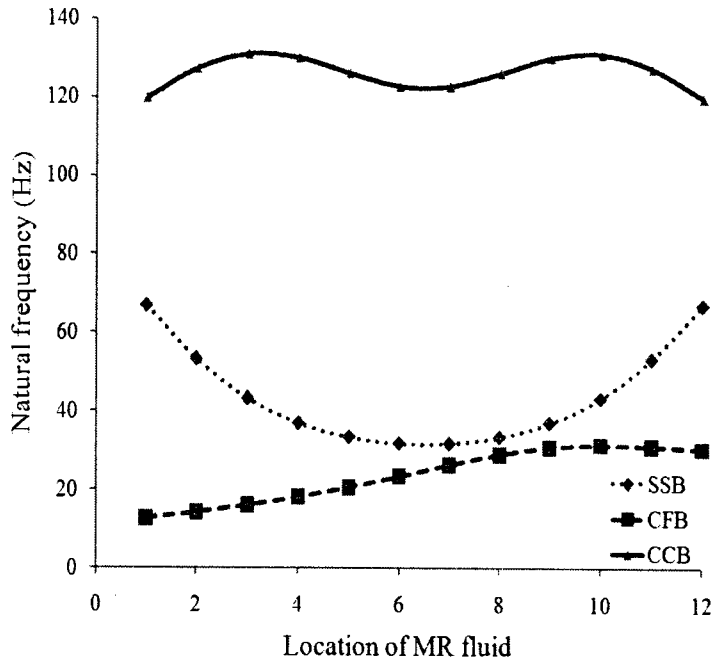


(a)

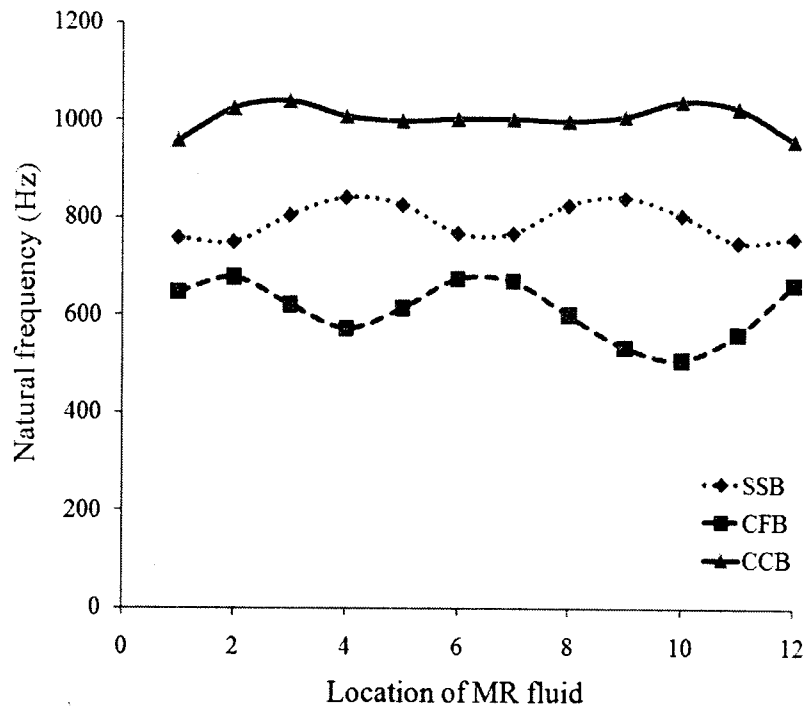


(b)

Figure 4.4. Influence of the location of a single MR fluid (80 mm long) segment on the modal damping factors of a partially treated MR sandwich beam with different end conditions subject to a magnetic field of 250 Gauss: (a) Mode 1; and (b) Mode 4.



(a)



(b)

Figure 4.5. Influence of the location of a single MR fluid (80 mm long) segment on the natural frequencies of a partially treated MR sandwich beam with different end conditions subject to a magnetic field of 250 Gauss: (a) Mode 1; and (b) Mode 4.

for the clamped-clamped end condition. On the other hand, the best locations for the highest modal damping factor under the clamped-free end conditions appear to be at distances of 80 mm and 200 mm from the fixed end corresponding to modes 1 and 4, respectively. The highest natural frequencies for the respective modes are obtained when the MR fluid is applied starting from 160 mm and 20 mm from the support. While the most appropriate location of a single MR fluid segment, for configuration A, could be identified in a straight forward manner, the identification of the distributed MR fluid segments, as in the case of configuration B would be quite complex to achieve maximum damping factors. The locations of distributed MR fluid segments are thus identified through formulation and solution of an optimization problem presented in the following section.

#### **4.4 FORMULATION OF THE OPTIMIZATION PROBLEM**

In order to design a partially treated MR sandwich beam, it is necessary to obtain an appropriate layout of a structure so that it yields the maximum shear energy distribution resulting in maximum modal damping factor. Although the distribution of MR fluid segments also affect the natural frequencies (Figure 4.5), in this study an optimization problem is formulated for the partially treated MR sandwich beam with multiple MR fluid pockets (configuration B shown in Figure 4.2(b)) to achieve maximum modal damping factor corresponding to selected modes. The problem is formulated for three different end conditions (SSB, CCB and CFB), while the magnetic field intensity is held constant at 250 Gauss. The optimal locations of the MR fluid pockets are sought for three different cases. In case 1, the objective function is formulated to seek the optimal locations of the MR fluid segments to achieve maximum modal damping factors

corresponding to the first five modes of flexural vibration, individually. In cases 2 and 3, the optimal locations of the MR fluid segments are identified to maximize the modal damping factor of the first five modes of flexural vibration simultaneously. The optimization problems for cases 2 and 3 are multi-objective optimization problems in which a single composite objective function is defined by considering both linear and logarithmic weighted summation of the modal damping factors for the first five modes, respectively. As the first few modes play an important role in structural vibration, the first five modes are considered in the optimization problem. The optimization functions formulated for each case are described below.

Case 1: The objective is to maximize the modal damping factor,  $\eta_r$ , corresponding to individual modes, while considering the first five modes, such that:

$$\text{Maximize } \eta_r = f(X) = \eta_d \frac{\sum_{e=1}^n \phi_e^{(r)} k_e \phi_e^{(r)}}{\phi^{(r)T} K \phi^{(r)}}, \quad r = 1, 2, \dots, 5 \quad (4.16)$$

Subject to:  $0 < X \leq N$

where  $n$  is the number of MR fluid segments considered, which is limited to 4, as illustrated for configuration B, and  $N$  is the number of finite elements of the sandwich beam. The vector  $X$  defines the locations of the MR-fluid pockets along the beam length based on element number segments,  $X = \{x_1, x_2, x_3, x_4\}$ .

Case 2: The objective in this case is to maximize the modal damping factor corresponding to the first five modes, considered simultaneously. The maximization

function is formulated upon linear combinations of the modal damping factors correspond to the first five modes, such that:

$$\text{Maximize } \eta_2 = f(X) = \sum_{r=1}^5 \eta_r = \sum_{r=1}^5 \left\{ \eta_d \frac{\sum_{e=1}^n \phi_e^{(r)} k_e \phi_e^{(r)}}{\phi^{(r)T} K \phi^{(r)}} \right\} \quad (4.17)$$

Subject to:  $0 < X \leq N$

where  $\eta_2$  is the linear sum of modal damping factors corresponds to the first five mode.

Case 3: A linear summation of the modal damping factors would be expected to yield a greater weighting of the first mode. Consequently, an alternate optimization function is formulated by considering the sum of logarithmic of the damping factors corresponds to the first five modes, such that:

$$\text{Maximize } \eta_3 = f(X) = \sum_{r=1}^5 \ln(\eta_r) = \sum_{r=1}^5 \ln \left\{ \eta_d \frac{\sum_{e=1}^n \phi_e^{(r)} k_e \phi_e^{(r)}}{\phi^{(r)T} K \phi^{(r)}} \right\} \quad (4.18)$$

Subject to:  $0 < X \leq N$

where  $\eta_3$  is the sum of logarithmic modal damping factors corresponds to the first five mode.

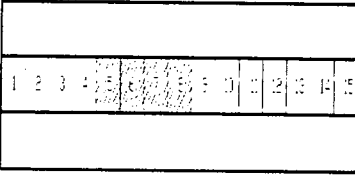
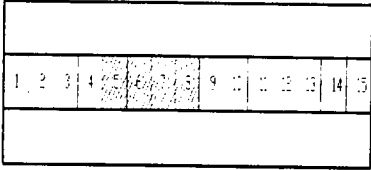
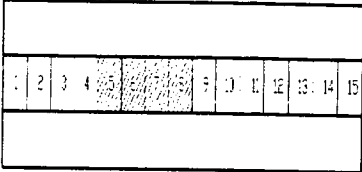
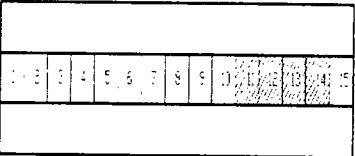
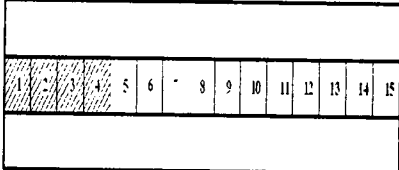
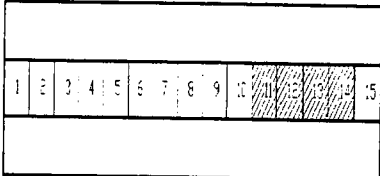
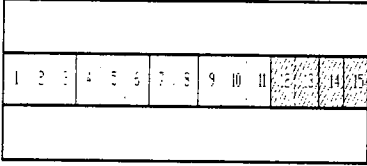
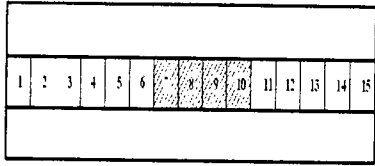
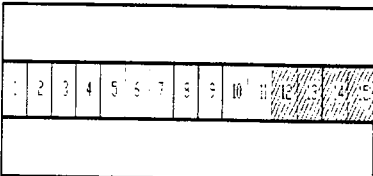
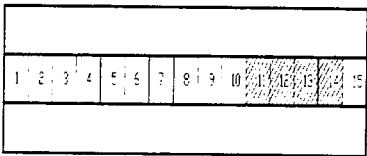
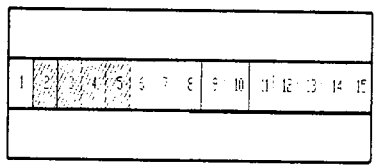
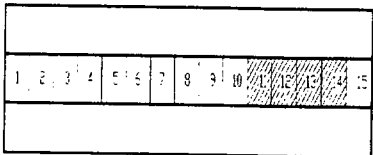
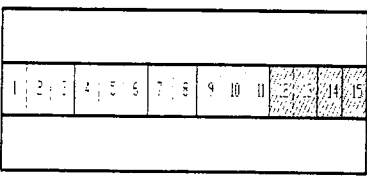
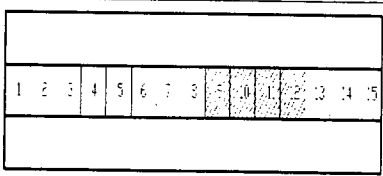
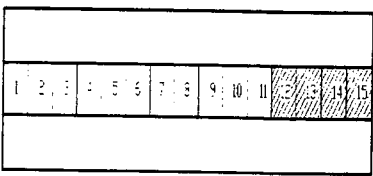
#### 4.4.1. Optimization methods and validation

The optimization problems defined for the three cases are solved to identify the global optimum locations within the feasible design domain ( $0 < x < L$ ). A number of optimization

algorithms are available to seek solutions of such types of problem. The vast majority of the gradient-based optimization algorithms tend to easily converge to local optima. The global optimum solution is generally identified from multiple solutions attained with random starting vectors or through perturbation analyses [Rao, 1996; Bonnans and Shapiro, 2000]. Alternatively, non-gradient stochastic search algorithms such as Genetic Algorithms (GAs) or Simulated Annealing (SA) may be used to locate the global optimum point with reasonable accuracy in a more efficient manner [Muc and Gurba, 2001; Zeng *et al.*, 2006; Al-Ajmi and Bourisli, 2008].

The optimization problems were initially solved using both the GA and SQP technique available in the MATLAB optimization toolbox. The optimal solutions were initially attained for configuration A of the partially treated beam, where an optimum location of the cluster of MR-fluid pockets could be conveniently verified using the results in Figure 4.4. The results attained from the GA and SQP methods could also be compared to assess their relative effectiveness in converging towards global optima. Table 4.1, as an example, compares the optimal solutions attained from the two methods for the partially-treated clamped-free beam corresponds to the first five modes. The table illustrates the optimal locations of the MR-fluid segments together with the optimal modal damping factors ( $\eta_r^*$ ) derived from the GA and SQP techniques. The influence of the fluid segments locations on the modal damping factors for all the five modes were

Table 4.1. Comparisons of optimum locations of the MR fluid segments and modal damping factors of configuration A of a partially treated MR sandwich beam with clamped-free end conditions computed using GA and SQP with those identified from Figure 4.4.

Mode	Optimum location and values ( $\eta_r^*$ ) of the modal damping factors		
	Genetic algorithm	SQP	Global location
1	 $\eta_r^* = 2.915 \times 10^{-2}$	 $\eta_r^* = 2.915 \times 10^{-2}$	 $\eta_r^* = 2.915 \times 10^{-2}$
2	 $\eta_r^* = 1.443 \times 10^{-2}$	 $\eta_r^* = 4.374 \times 10^{-3}$	 $\eta_r^* = 1.443 \times 10^{-2}$
3	 $\eta_r^* = 2.485 \times 10^{-3}$	 $\eta_r^* = 1.872 \times 10^{-3}$	 $\eta_r^* = 2.485 \times 10^{-3}$
4	 $\eta_r^* = 1.492 \times 10^{-3}$	 $\eta_r^* = 5.482 \times 10^{-4}$	 $\eta_r^* = 1.492 \times 10^{-3}$
5	 $\eta_r^* = 9.312 \times 10^{-4}$	 $\eta_r^* = 4.878 \times 10^{-4}$	 $\eta_r^* = 9.312 \times 10^{-4}$

also investigated to identify the optimal locations (e.g. Figure 4.4), which are also presented in Table 1, denoted as “Global locations”. The comparisons show that the GA converges to optimal locations for all the five modes. The similar trend, however, could be observed in the SQP solutions only for the first mode. The results attained for the higher modes, however, differ from the global locations, which is attributable to the presence of many local optima values at higher modes. Depending on the selection of initial starting design vector, the SQP may converge to a global or one of the local optimum values. Similar trend were also observed for the other end conditions considered in the study. The subsequent analysis involving optimal solutions for configuration B of the partially treated beams were thus performed using GA.

## **4.5. RESULTS AND DISCUSSION**

### **4.5.1. Optimal locations based on individual modes (Case 1)**

The optimization problems defined in Eqs. (4.16) to (4.18) were solved for configuration B of the partially treated beams with three different end conditions. Tables 4.2 to 4.4 present the optimal solutions corresponding to the first five flexural modes of the partially treated beams (Case 1) with simply- supported, clamped-free and clamped-clamped end conditions, respectively. The tables show the optimal locations of the MR fluid segments, the modal damping factors ( $\eta_r^*$ ) and the mode shapes corresponds to each of the five modes. The mode shapes are also compared with those of the beam without the MR fluid treatment. The ordinates are normalized with respect to the maximum value of the modal vector of the corresponding beam, while the abscissa is indicated by the element number. The results suggest that the optimum locations of the MR fluid

segments are strongly dependent upon the mode of vibration, irrespective of the boundary conditions. Furthermore, the results generally show that the optimal modal damping factor decreases with increasing mode number. This can be related to the increase in the total strain energy of the structure for higher flexural modes of vibration, which results in reduction in the modal damping factor, as it is evident from Eq. (4.16). It can also be observed that the clamped-free end condition yields the highest optimal modal damping factor, while clamped-clamped end condition yields the lowest optimal modal damping factor corresponding to all of the modes considered. This is due to the fact that the structures with the clamped-free and clamped-clamped end conditions have the lowest and highest strain energy, respectively. Furthermore, a comparison of the results in Tables 4.1 and 4.3 for the clamped-free end condition suggest that the distributed MR fluid treatments (configuration B) would generally yield considerably higher optimal modal damping factors than the treatment involving a cluster of fluid segments (configuration A). This trend was also evident for the beams with SSB and CCB conditions.

The results also suggest that the partial treatment of the beam could significantly alter the deflection modes. In particular, the locations of the peak normalized deflection and the nodes are strongly affected when compared to those of the beams without the MR fluid treatments. The deflection modes generally exhibit peaks in the vicinity of the MR fluid treatments, irrespective of the end condition. The locations of the peak deflection generally differ from those of the untreated beams. This can be associated with greater concentration of the mass in the vicinity of the treatments since the mass density of the fluid is considerably larger than that of the aluminum ( $\rho_C > \rho_A$ ). The deflection modes

of the beams with MR fluid treatments thus consistently show considerable shifts in the locations of the nodes, particularly at higher modes. A higher concentration of the MR fluid at a particular location thus yields larger normalized deflection near the same location for all the end conditions considered in this study. A few exceptions, however, are observed in case of the CCB condition, where the solutions of the optimization problem converged towards relatively greater clustering of the fluid segments. The higher deflections in the vicinity of the fluid treatments would yield higher strain energy associated with fluid shear and thus the higher modal damping factors.

The results generally suggest that the MR fluid treatments near the supports would yield higher modal damping factors corresponding to all the modes considered in this study for the simply supported and clamped-clamped condition. The deflection modes 2 and 4 for the clamped-clamped end condition, however, form exception, where the maximum deflections occur near the mid-span (elements #6 and #10) and one-quarter span (elements #3 and #5), respectively. The treatments near these locations thus resulted in highest modal damping factors corresponding to modes 2 and 4. It is interesting to note that the solutions for the CCB conditions converge towards relatively greater clustering of the MR fluid segments (60 to 80 mm long) compared to the SSB and CFB conditions. This can be associated with the greatest strain energy of the structure with CCB condition, which would require larger concentration of the MR fluid treatment in order to realize larger modal damping, as seen in (4.16). The optimal treatment locations for the CFB condition, however, appear near the free end, where the greater mass concentration contributes to larger deflection and thus the damping energy.

Table 4.2. Optimum location of MR fluid segments of the partially treated (configuration B) simply-supported beam, and the modal damping factors and deflection modes corresponding to the first five modes (Magnetic field = 250 Gauss; — With MR fluid treatment; - - - - - Without MR fluid treatment)

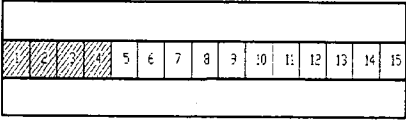
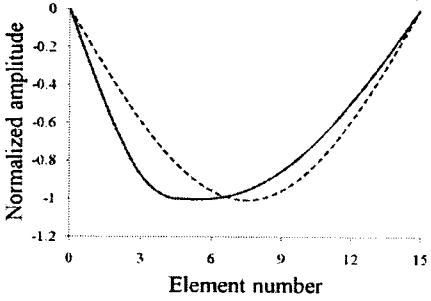
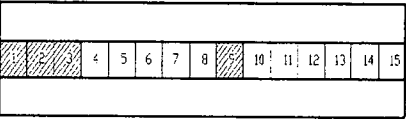
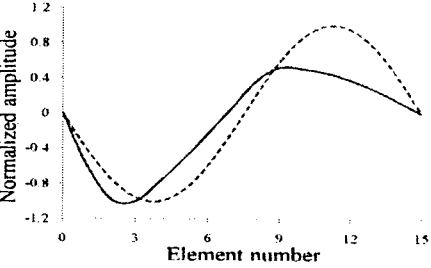
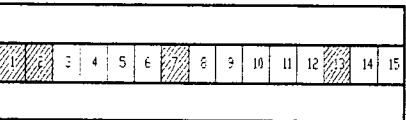
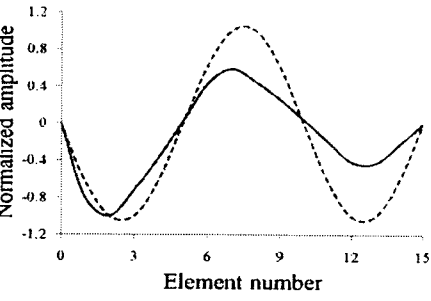
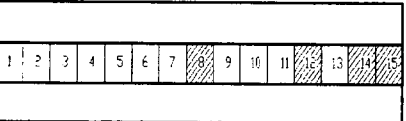
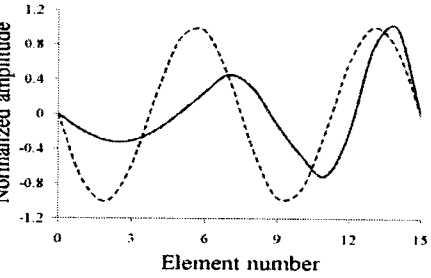
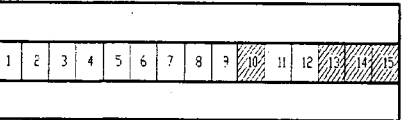
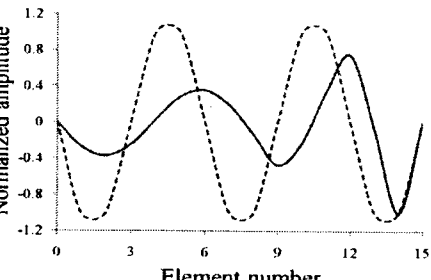
Mode	Optimum location	Mode shape
1	 $\eta_r^* = 2.636 \times 10^{-2}$	
2	 $\eta_r^* = 8.057 \times 10^{-3}$	
3	 $\eta_r^* = 2.331 \times 10^{-3}$	
4	 $\eta_r^* = 8.167 \times 10^{-4}$	
5	 $\eta_r^* = 4.857 \times 10^{-4}$	

Table 4.3. Optimum location of MR fluid segments of the partially treated (configuration B) clamped-free beam, and the modal damping factors and deflection modes corresponding to the first five modes (Magnetic field = 250 Gauss; — with MR fluid treatment; - - - - - without MR fluid treatment)

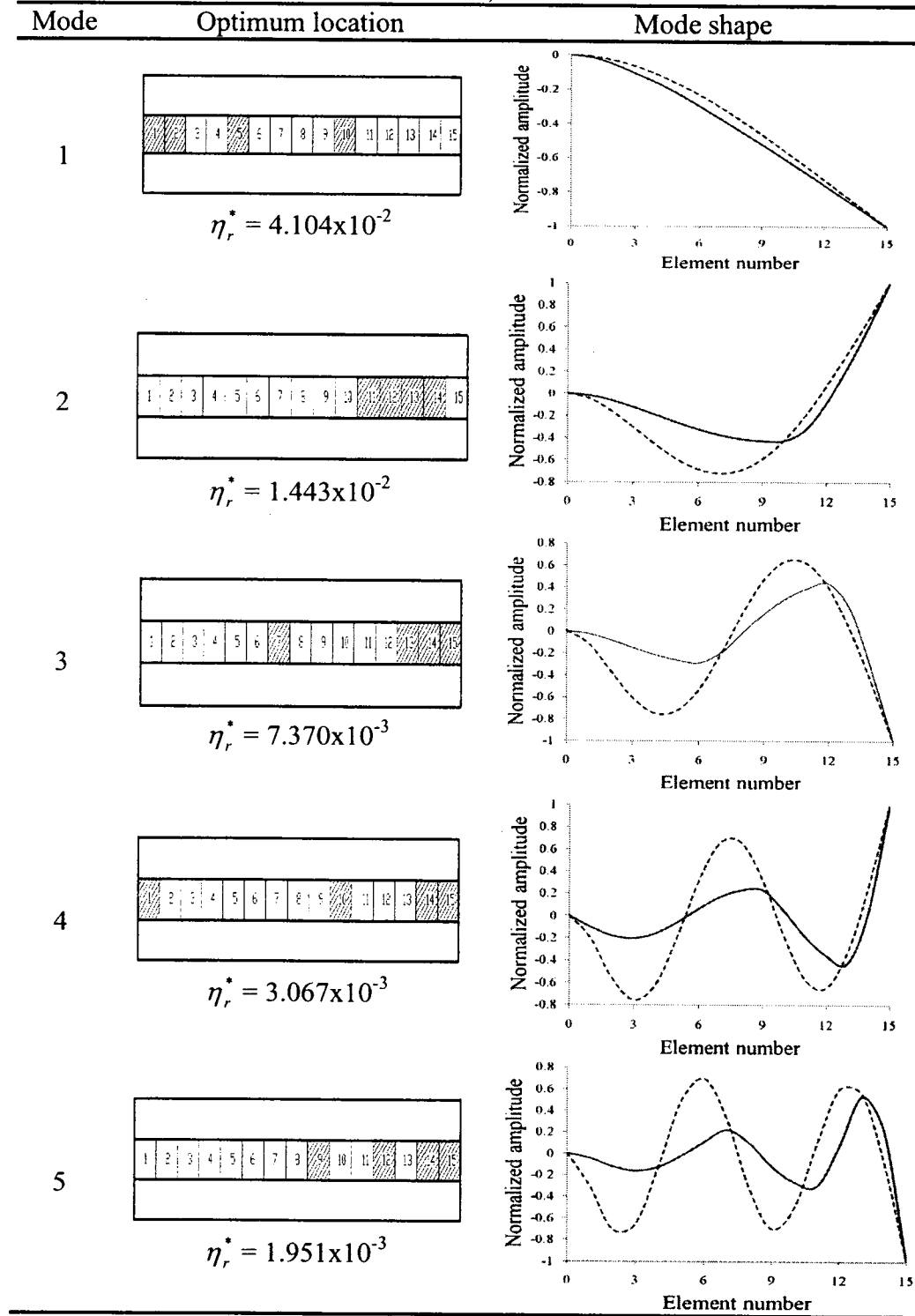
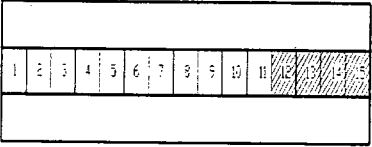
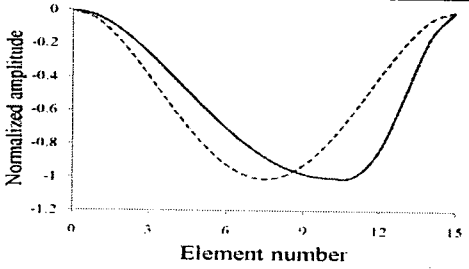
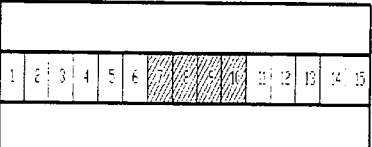
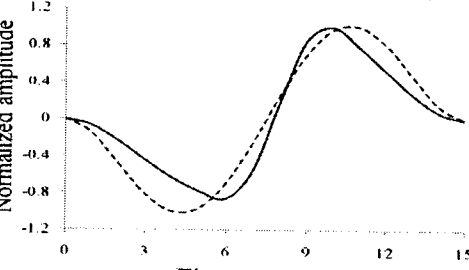
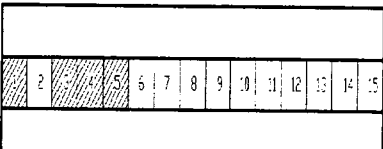
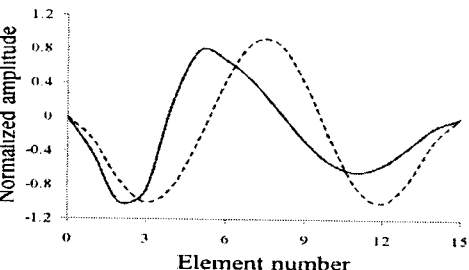
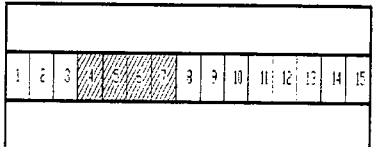
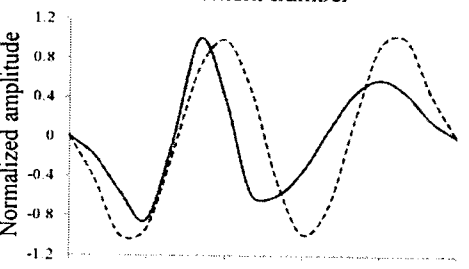
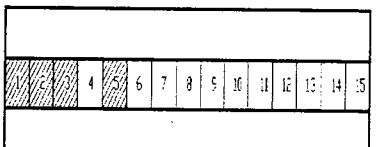
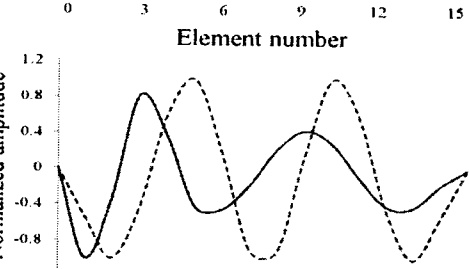


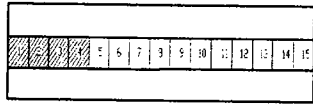
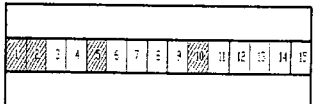
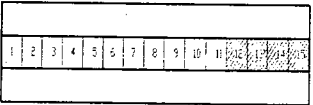
Table 4.4. Optimum location of MR fluid segments of the partially treated (configuration B) clamped-clamped beam, and the modal damping factors and deflection modes corresponding to the first five modes (Magnetic field = 250 Gauss; — with MR fluid treatment; - - - - without MR fluid treatment)

Mode	Optimum location	Mode shape
1	 $\eta_r^* = 4.014 \times 10^{-3}$	
2	 $\eta_r^* = 2.054 \times 10^{-3}$	
3	 $\eta_r^* = 7.207 \times 10^{-4}$	
4	 $\eta_r^* = 4.445 \times 10^{-4}$	
5	 $\eta_r^* = 2.051 \times 10^{-4}$	

#### **4.5.2. Optimal locations based on linear combination of the modal damping factors (Case 2)**

Table 4.5 presents the optimal locations of the MR fluid treatment identified from maximization of linear summation of modal damping factors corresponding to the first five modes, as described in (4.17). The table presents the optimal values of the modal damping factors corresponding to each of the five modes. The optimal modal damping factors are also compared with those derived from the optimal locations of MR fluid segments derived from case 1. The changes in the optimal damping factors relative to those derived in case 1 are indicated by percent increase (+) and decrease (-). The results consistently show that the optimal locations of MR fluid segments derived from consideration of the linear combination of the first five modes are identical to those obtained for the first mode alone, irrespective of the end conditions, as seen in Tables 4.2 to 4.4. This suggests that the solution converges to the fundamental mode damping factor that is significantly higher than those of the higher modes. This is evident from the percent changes summarized in table 4.5, which confirm the convergence to the first mode damping factor due to its greater weighting in the linear summation. The modal damping factors corresponds to the higher modes thus tend to be significantly lower than those identified through optimization for the individual modes. It is thus concluded that maximization of the linear summation of damping factors for the first five modes would yield the optimal value for the first mode alone.

Table 4.5. Optimum locations of the MR fluid segments of the partially treated MR sandwich beams identified through the linear combination of the first five modes (Case 2).

End condition	Optimum locations	Mode	Modal damping factor (Case 2)	Modal damping factor (Case 1)	% change
Simply supported		1	$2.636 \times 10^{-2}$	$2.636 \times 10^{-2}$	0
		2	$2.165 \times 10^{-3}$	$8.057 \times 10^{-3}$	-73.1
		3	$1.174 \times 10^{-3}$	$2.331 \times 10^{-3}$	-49.6
		4	$5.046 \times 10^{-4}$	$8.167 \times 10^{-4}$	-38.2
		5	$1.073 \times 10^{-4}$	$4.857 \times 10^{-4}$	-77.9
Clamped-free		1	$4.104 \times 10^{-2}$	$4.104 \times 10^{-2}$	0
		2	$2.954 \times 10^{-3}$	$1.443 \times 10^{-2}$	-79.5
		3	$4.110 \times 10^{-4}$	$7.370 \times 10^{-3}$	-94.4
		4	$4.637 \times 10^{-4}$	$3.067 \times 10^{-3}$	-84.9
		5	$4.713 \times 10^{-5}$	$1.951 \times 10^{-3}$	-97.6
Clamped-clamped		1	$4.014 \times 10^{-3}$	$4.014 \times 10^{-3}$	0
		2	$4.367 \times 10^{-4}$	$2.054 \times 10^{-3}$	-78.7
		3	$3.567 \times 10^{-4}$	$7.207 \times 10^{-4}$	-50.5
		4	$2.563 \times 10^{-4}$	$4.445 \times 10^{-4}$	-42.3
		5	$4.858 \times 10^{-5}$	$2.051 \times 10^{-4}$	-76.3

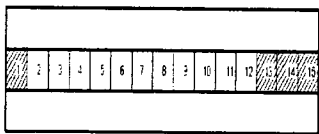
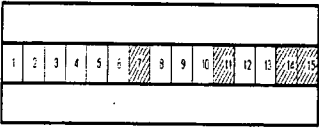
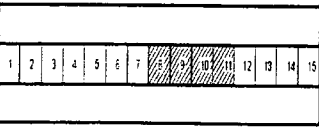
#### 4.5.3. Optimal locations based on logarithmic combination of the modal damping factors (Case 3)

The optimal locations of the MR fluid segments and the modal damping factors for the first five modes, derived from maximization of the logarithmic combination of modal damping factors corresponding to the five modes are presented in Table 4.6. The table also shows the comparisons of the resulting modal damping factors corresponding to the five modes with those derived upon consideration of the individual modes (Case1) together with the percent change. Unlike the case 2 based on linear combination of individual model damping factor, the consideration of the logarithmic combination yields reduction in the modal damping factors corresponding to all of the modes, when compared to those derived for the individual modes (Case 1). The resulting solution could

thus be considered as a compromise leading to optimal damping factors corresponding to all of the five modes.

A comparison of the identified optimal locations of the MR fluid segments with those presented in Table 4.2 to 4.4 suggest that the solutions are different from those derived for the individual modes, irrespective of the end conditions. The solution for the CCB condition appears to be closer to that obtained for mode 2 alone (Case 1), while those for the CFB and SSB conditions are somewhat closer to those of modes 4 and 5 alone respectively. The relative reductions in the damping factors corresponding to the above-mentioned modes are thus lower. The relative reductions in the modal damping factors, however, are considerably smaller than those observed for the linear combination case (Table 4.5), with the exception of the fundamental mode damping factor.

Table 4.6. Optimum locations of the MR fluid segments of the partially treated MR sandwich beams identified through the logarithmic combination of the first five modes (Case 3)

End condition	Optimum locations	Mode	Modal damping factor (Case 3)	Modal damping factor (Case 1)	% change
Simply supported		1	$1.733 \times 10^{-2}$	$2.636 \times 10^{-2}$	-34.1
		2	$3.844 \times 10^{-3}$	$8.057 \times 10^{-3}$	-52.3
		3	$5.684 \times 10^{-4}$	$2.331 \times 10^{-3}$	-75.6
		4	$4.807 \times 10^{-4}$	$8.167 \times 10^{-4}$	-41.1
		5	$3.204 \times 10^{-4}$	$4.857 \times 10^{-4}$	-34.1
Clamped-free		1	$1.346 \times 10^{-2}$	$4.104 \times 10^{-2}$	-67.2
		2	$3.582 \times 10^{-3}$	$1.443 \times 10^{-2}$	-75.2
		3	$1.680 \times 10^{-3}$	$7.370 \times 10^{-3}$	-77.2
		4	$1.540 \times 10^{-3}$	$3.067 \times 10^{-3}$	-49.8
		5	$5.306 \times 10^{-4}$	$1.951 \times 10^{-3}$	-72.8
Clamped-clamped		1	$8.432 \times 10^{-4}$	$4.014 \times 10^{-3}$	-79.0
		2	$1.381 \times 10^{-3}$	$2.054 \times 10^{-3}$	-32.8
		3	$3.172 \times 10^{-4}$	$7.207 \times 10^{-4}$	-56.0
		4	$4.292 \times 10^{-4}$	$4.445 \times 10^{-4}$	-3.40
		5	$9.354 \times 10^{-5}$	$2.051 \times 10^{-4}$	-54.4

#### 4.5.4. Transverse vibration response

The transverse vibration responses of the beams were also investigated to assess the beneficial effects of optimal distributions of the MR fluid segments. As an example, the vibration responses of the clamped-free beam with optimally distributed MR fluid segments (Case 2 and Case 3) are presented under the application of a 1 N harmonic force (frequency range: 1 to 2500 Hz) at a distance of 200 mm from the support. The frequency responses in tip deflection of the beams are presented in figure 4.6 together with that of an untreated aluminum beam with identical end conditions. The frequency responses are presented in the 10-1600 Hz, which included the responses over the first five modes. The results clearly show significant effects of MR fluid treatments on both the magnitudes of deflection peaks and the corresponding frequencies, which are attributable to changes in mass distributions and the damping factors due to the fluid segments.

The MR fluid treated beams (Case 2 and Case 3) consistently show considerably lower magnitude peaks compared to those of the untreated beam. The frequencies corresponding to the magnitude peaks, considered as the resonance frequencies, of the treated beams also tend to be lower than those of the untreated beam. The beams with MR fluid segments locations identified on the basis of the linear summation of modal damping factors (Case 2) reveals significantly lower resonant frequencies corresponding to all the modes. The reduction in the resonant frequencies of the beams configured on the basis of the logarithmic summation of the damping factors (Case 3), however, are relatively smaller, except for the frequency corresponding to mode 5. The lower peak deflections of the beams with distributed MR fluid segments are due to their higher

modal damping factors. The magnitudes of the displacements peaks in the response of the beam configured using Case 3 are generally much smaller than those of the beam realized using the results of Case 2. This again is attributable to relatively higher modal damping factors and the resonance frequencies of the beams realized in Case 3.

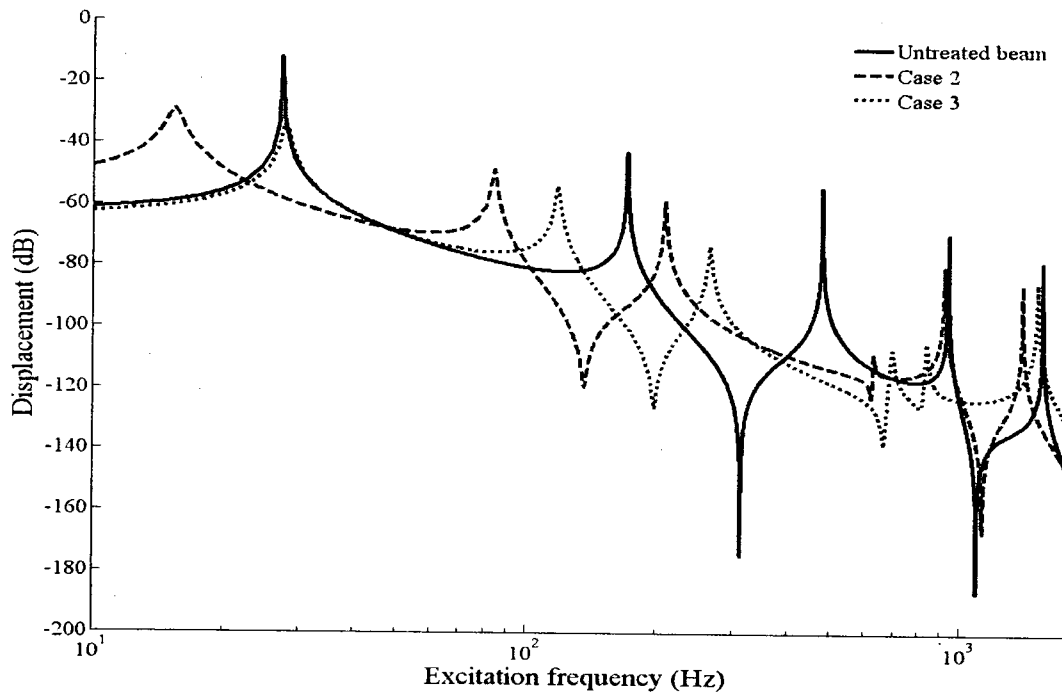


Figure 4.6. Comparison of the transverse response of the clamped-free untreated beam and partially treated MR sandwich beams with optimum configurations of cases 2 and 3.

Although the modal damping factor corresponding to mode 1 of the sandwich beam identified in Case 3 is approximately 67% lower than that of the beam obtained from Case 2, the magnitude of the first deflection peak in Case 3 is considerably lower. This is due to its higher natural frequency that yields higher stiffness and thus the lower peak displacements. Substantial reductions in the peak magnitudes can be noted in the

responses corresponding to the first three modes and the fifth mode of the sandwich beam identified with Case 3, which are approximately 18%, 12%, 25% and 31%, respectively lower than those of the beam realized from Case 2. On the other hand, the peak displacement of the sandwich beam corresponding to mode 4 obtained with case 3 is approximately 2% higher than that of the beam identified with case 2. The vibration responses of the clamped-free beams confirm that the optimal location of MR fluid segments identified through consideration of the logarithmic sum of the modal damping factor would be more beneficial in attenuating the vibration corresponding to the modes considered. The resulting distribution of the MR fluid segments would yield greater and more uniform shear energy distribution compared to that attained by considering individual modes or a linear summation of the individual modes.

#### **4.6 CONCLUSIONS**

In this study, the damping performance of a partially treated MR multilayer beam was studied in terms of the modal damping factors. First, the modal damping factor corresponding to each mode of the partially treated MR sandwich beam have been evaluated by implementing the principle of modal strain energy method for viscoelastic materials using the finite element model developed for a partially treated MR sandwich beam. The influence of location of the MR fluid segments of a partially treated MR sandwich beam on modal damping factors in each mode is demonstrated under various end conditions. It was shown that the location of the MR fluid segments play an important role on the variation of the modal damping factor irrespective of the end conditions. It was also concluded that the clamped-free and clamped-clamped end conditions yield the highest and lowest modal damping factors respectively among the

end conditions considered irrespective of the mode of vibration. Then a design optimization methodology to maximize the modal damping factor of each mode individually and simultaneously has been formulated by combining the developed finite element analysis and optimization algorithms based on GA and SQP. Different optimization problems including maximization of the modal damping factor of the first five modes individually and linear and logarithmic combination of the modal damping factors of the first five modes have been studied. It has been demonstrated that GA yields better optimal results compared to SQP in terms of location of the MR fluid segments and the optimal modal damping factor. It was concluded that optimal locations of MR fluid segments for the linear combination of the first five modes are identical to those obtained for the first mode irrespective of the end conditions. Also, it was suggested that the modal damping factor could be distributed uniformly at all the modes, if the optimization is performed based on the logarithmic combination of the first five modes. It was also shown that the modal damping factor under clamped-free end conditions at all the modes is increased except in the first mode. The advantage of distribution of modal damping factor at all the modes has been demonstrated by investigating the transverse response of the MR sandwich beam and comparing with that of plain beam under clamped-free end conditions. It was shown that the optimization of location based on the logarithmic combination of the first five modes yields higher peak displacement reduction compared to that of based on linear combination of the first five modes. Hence it was concluded that optimization performed by considering the logarithmic summation of the modes provides the efficient layout of a partially treated MR sandwich beam.

## CHAPTER 5

# OPTIMAL VIBRATION CONTROL OF BEAMS WITH TOTAL AND PARTIAL MR-FLUID TREATMENTS

### 5.1 INTRODUCTION

The vibration properties of MR/ER-fluid treated beams have been mostly investigated under various fixed intensities of the applied field in an open-loop manner. The efforts in deriving semi-active and active control synthesis have been mostly limited to simple single- of-two-degree of freedom lumped parameters models, where the stiffness and/or damping properties of ER/MR fluids are described as a function of the applied field [Leitmann and Reithmeier, 1993; Leitmann, 1994]. Only limited efforts have been made towards synthesis of semi-active and active controllers for the ER/MR-fluid treated sandwich beams, although the controller design for structures employing piezoelectric actuators have been widely reported [eg., Sadri *et al.*, 1999; Hu and Ma, 2005; Baillargeon and Vel, 2005]. Shaw (2000) proposed a two-stage controller to reduce the vibration of a ER-fluid beam subjected to harmonic excitations and investigated the performance characteristics through laboratory experiments. The study employed two independent controllers: a fuzzy logic- based semi-active controller to tune the resonance frequencies; and an active force control for cancelling the external disturbance.

In Chapter 2, the effectiveness of the MR fluids in controlling the vibration of fully treated MR fluid multilayer structures was demonstrated numerically and experimentally. It has also been demonstrated in chapter 3 that a relatively simple design may be realized when the fluid is contained within a localized section or partially and the

air cavity is replaced by the elastic material. This would also be beneficial in enhancing the natural frequencies. In chapter 4, the optimal locations of MR fluid segments in a partially treated MR sandwich beam were determined to maximize the modal damping factors.

This chapter presents synthesis of full-state and limited state flexible mode shape (FMS)- based controllers for suppression of free- and forced vibration of a cantilever beam fully and partially treated with the magneto-rheological (MR) fluid. The governing equations of motion of the three layer MR sandwich beam are expressed in the state variable form comprising a function of the control magnetic field. An optimal control strategy based on the linear quadratic regulator (LQR) and a full-state dynamic observer is formulated to suppress the vibration of the beam under a limited magnetic field intensity. The lower flexural mode shapes of the passive beam are used to obtain the estimates of the deflection states so as to formulate a limited state LQR control synthesis. The free-and forced vibration control performances of both the full-state observer-based and limited state FMS based LQR control strategies are evaluated for the fully as well as partially treated MR-fluid sandwich beams.

## **5.2. FINITE ELEMENT FORMULATION OF MR SANDWICH BEAM**

The finite element formulations for the fully and a partially treated three layer beam structures containing MR fluid as the core in between the two elastic layers , as shown in Figure 5.1 have been reported in chapter 2 and chapter 3, respectively. These formulations are considered here for synthesis of a semi-active vibration control of the multilayer beam. The governing equations of motion in the finite element form for the fully and partially treated MR sandwich beam were derived using Lagrange's energy

approach upon by considering a two-node beam element with three degrees of freedom (transverse  $w$ , axial  $u$  and rotational  $\theta$  displacements of the beam) at each node. Energy expressions for a fully treated MR sandwich beam have been derived as follows:

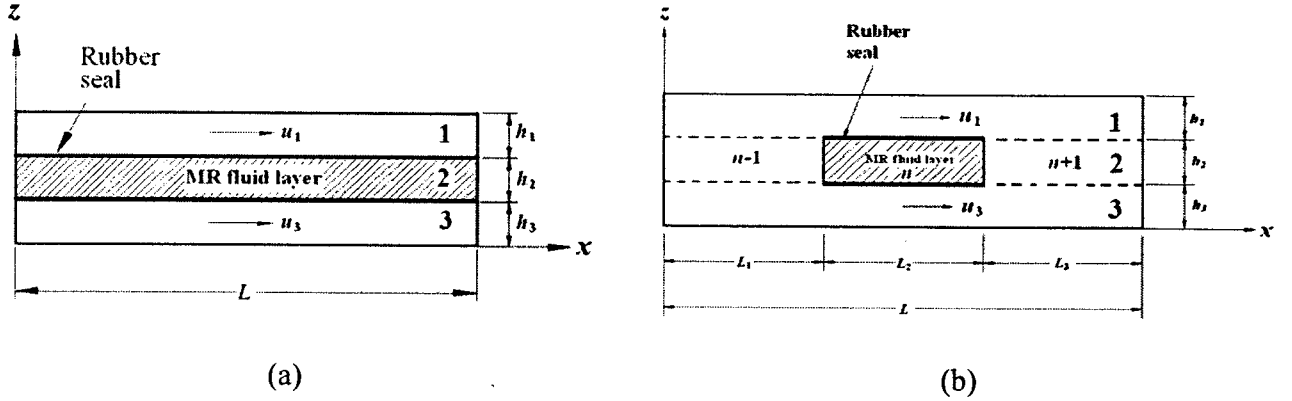


Figure. 5.1. (a) Fully treated MR sandwich beam. (b) Partially treated MR sandwich beam

The total kinetic energy  $T$  for a fully-treated MR sandwich beam has been derived as :

$$\begin{aligned}
 T = & \frac{1}{2} \int_0^L (\rho_1 A_1 + \rho_2 A_2 + \rho_r A_r + \rho_3 A_3) \left( \frac{\partial w}{\partial t} \right)^2 dx \\
 & + \frac{1}{2} \int_0^L (\rho_1 A_1 + e^2 \rho_3 A_3) \left( \frac{\partial u}{\partial t} \right)^2 dx + \frac{1}{2} \int_0^L I_2 \rho_2 \left[ \frac{-(1+e) \partial u}{h_2 \partial t} + \frac{D \partial^2 w}{h_2 \partial x \partial t} \right]^2 dx
 \end{aligned} \quad (5.1)$$

The total potential energy is the sum of energies associated with the three layers, such

that:

$$V = V_1 + V_2 + V_3 \quad (5.2)$$

where the energy associated with the elastic layers ( $V_1, V_3$ ) and MR fluid layer ( $V_2$ ) are

given by:

$$V_{1,3} = \frac{1}{2} \int_0^L (E_1 A_1 + E_3 A_3 e^2) \left( \frac{\partial u}{\partial x} \right)^2 dx + \frac{1}{2} \int_0^L (E_1 I_1 + E_3 I_3) \left( \frac{\partial^2 w}{\partial x^2} \right)^2 dx$$

and

$$V_2 = \frac{1}{2} \int_0^L \bar{G} A_2 \left[ \frac{D}{h_2} \frac{\partial w}{\partial x} - \frac{(1+e)u}{h_2} \right]^2 dx$$

In the above equations,  $I_1$ ,  $I_3$  and  $I_2$  are the second moments of inertia at the centroid of the elastic layers 1 and 3, and the MR fluid layer 2, respectively (Fig.5.1(a)),  $\rho_1$  and  $\rho_3$  are mass densities of the elastic layers, and  $\rho_2$  and  $\rho_r$  are the mass densities of the fluid and the sealant rubber material, respectively.  $A_1$ ,  $A_2$ ,  $A_3$  and  $A_r$  are the cross section areas of layers 1, 2 and 3, and the rubber material, respectively, and  $E_1$  and  $E_3$  are Young's moduli of the elastic layers 1 and 3, respectively.  $h_1$ ,  $h_2$  and  $h_3$  are the thickness of layers 1, 2 and 3, respectively, and  $\bar{G} = G_r \left( \frac{b_r}{b} \right) + G^* \left( 1 - \frac{b_r}{b} \right)$ , is the equivalent shear modulus of the homogeneous layer in which  $b_r$  and  $b$  are the widths of the sealant rubber and the entire beam, respectively,  $G_r$  and  $G^*$  are the shear moduli of the rubber and the MR fluid, respectively, and  $D = h_2 + \frac{1}{2}(h_1 + h_3)$  and  $e = \frac{E_1 A_1}{E_3 A_3}$ .

Energy expressions for a partially treated MR sandwich beam have been derived in a similar manner as in chapter 3, as follows:

The total kinetic energy  $T_P$  for a partially-treated MR sandwich beam is given as:

$$T_P = \frac{1}{2} \int_0^L (\rho_1 A_1 + \rho_3 A_3) \left( \frac{\partial w}{\partial t} \right)^2 dx + \frac{1}{2} \int_{L_1}^{L_1+L_2} (\rho_2 A_2 + \rho_r A_r) \left( \frac{\partial w}{\partial t} \right)^2 dx$$

$$+ \frac{1}{2} \int_0^{L_1} \rho_{2e} A_{2e} \left( \frac{\partial w}{\partial t} \right)^2 dx + \frac{1}{2} \int_{L_1+L_2}^L \rho_2 A_{2e} \left( \frac{\partial w}{\partial t} \right)^2 dx + \frac{1}{2} \int_0^L (\rho_1 A_1 + e^2 \rho_3 A_3) \left( \frac{\partial u}{\partial t} \right)^2 dx$$

$$+ \frac{1}{2} \int_{L_1}^{L_1+L_2} I_2 \rho_2 \left[ \frac{-(1+e)}{h_2} \frac{\partial u}{\partial t} + \frac{D}{h_2} \frac{\partial^2 w}{\partial x \partial t} \right]^2 dx \quad (5.3)$$

and the total potential energy for a partially-treated MR sandwich beam has been expressed as:

$$V = V_{1p} + V_{2p} + V_{3p} \quad (5.4)$$

$$\text{where } V_{1p,3p} = \frac{1}{2} \int_0^L (E_1 A_1 + E_3 A_3 e^2) \left( \frac{\partial u}{\partial x} \right)^2 dx + \frac{1}{2} \int_0^L (E_1 I_1 + E_3 I_3) \left( \frac{\partial^2 w}{\partial x^2} \right)^2 dx$$

$$\text{and } V_{2p} = \frac{1}{2} \int_{L_1}^{L_1+L_2} G b h_2 \left[ \frac{D}{h_2} \frac{\partial w}{\partial x} - \frac{(1+e)u}{h_2} \right]^2 dx$$

$$+ \frac{1}{2} \int_0^{L_1} E_{2e} A_{2e} \left( \frac{\partial u}{\partial x} \right)^2 dx + \frac{1}{2} \int_0^{L_1} E_{2e} I_{2e} \left( \frac{\partial^2 w}{\partial x^2} \right)^2 dx$$

$$+ \frac{1}{2} \int_{L_1+L_2}^L E_{2e} A_{2e} \left( \frac{\partial u}{\partial x} \right)^2 dx + \frac{1}{2} \int_{L_1+L_2}^L E_{2e} I_{2e} \left( \frac{\partial^2 w}{\partial x^2} \right)^2 dx$$

where  $V_{1p}$ ,  $V_{2p}$  and  $V_{3p}$  refer to the potential energy due to three layer of the partially treated beam,  $L_1$  and  $L_2$  define the lengths of elastic and fluid segments, as seen in Fig. 5.1(b),  $E_{2e}$  and  $I_{2e}$  are the Young's modulus and second moments of inertia of the elastic layers, respectively, located at the mid-layer of the sandwich beam.

Considering the relations between the displacement functions and nodal displacement vectors and substituting into the energy expressions, the governing equations of motion for the undamped partially or fully-treated MR sandwich beam element in the finite element form could be obtained from the Lagrange's equations:

$$[m^e]\{\ddot{d}\} + [k^e]\{d\} = \{f^e\} \quad (5.5)$$

where  $[m^e]$  and  $[k^e]$  are the element mass and stiffness matrices, respectively, and  $\{f^e\}$  is the element force vector and  $\{d\}$  is the displacement vector. Assembling the mass and stiffness matrices and the force vector for all the elements yields the system governing equations of motion of the MR sandwich beam in the following form:

$$[M]\{\ddot{d}_g\} + [K]\{d_g\} = \{F\} \quad (5.6)$$

where  $[M]$ ,  $[K]$  and  $\{F\}$  are the system mass and stiffness matrices, and the force vector, respectively.

### 5.3. DESIGN OF AN OPTIMAL CONTROLLER

Control of vibration in a structure is generally concerned with specific modes of flexural vibration. It may thus be appropriate to express Eq. (5.6) in the modal form using the modal coordinates, which would yield uncoupled governing equations of motion for the MR sandwich beam. Assuming proportional damping, Eq. (5.6) can be written in the following form:

$$\{\ddot{\eta}_i\} + [2\xi_i\omega_i]\{\dot{\eta}_i\} + [\omega_i^2]\{\eta_i\} = \{f_i\}, \quad i = 1, 2, \dots, n \quad (5.7)$$

where  $\{\eta\}$  is the modal coordinate vector, which is related to the modal matrix  $[q]$  such that  $\{d\} = [q]\{\eta\}$ ,  $\xi_i$  is the modal damping ratio for the  $i^{\text{th}}$  normal mode,  $\omega_i$  is the corresponding natural frequency of the system without considering the structural damping, and  $f_i = [q]^T\{F\}$ . Both the damping factor and natural frequencies of the beam would vary with the applied magnetic field; Eq. (5.7) may thus be expressed as a function of the controlled magnetic field  $u_i$ :

$$\{\ddot{\eta}_i\} + C'(u_i)\{\dot{\eta}_i\} + K'(u_i)\{\eta_i\} = \{f_i\}, \quad i = 1, 2, \dots, n \quad (5.8)$$

where  $K'(u_i) = [\omega_i^2]$  and  $C'(u_i) = [2\xi_i\omega_i]$  are assumed to be linear functions of the applied magnetic field  $u_i$  such that:

$$K'(u_i) = \alpha_{ki} + \beta_{ki}u_i, \quad 0 \leq u_i \leq u_{\max}; \quad C'(u_i) = \alpha_{ci} + \beta_{ci}u_i, \quad 0 \leq u_i \leq u_{\max} \quad (5.9)$$

where  $u_{\max}$  refers to the maximum magnetic field that could be applied, which may be limited due to the practical limitations of the electromagnet, power requirement and/or the saturation limit of the MR fluid used. The coefficients  $\alpha_{ki}, \beta_{ki}$  and  $\alpha_{ci}, \beta_{ci}$  are functions of the applied magnetic field corresponding to each mode,  $u_i$ .

A linear quadratic regulator (LQR) based controller synthesis is realized here using the full state feedback. The finite element models of the fully- and partially- treated beams are thus expressed in the state-space form, as:

$$\{\dot{x}_S\} = [A]\{x_S\} + [B]\gamma + \{f\} \text{ and } \{y_S\} = [C]\{x_S\} \quad (5.10)$$

where  $[A] = \begin{bmatrix} [0] & [I] \\ [-\alpha_{ki}] & [-\alpha_{ci}] \end{bmatrix}$ ;  $[B] = \begin{bmatrix} [0] & [0] \\ [-\beta_{ki}] & [-\beta_{ci}] \end{bmatrix}$ ;  $[C] = \begin{bmatrix} I & 0 \\ 0 & 0 \end{bmatrix}$ ;  $\{\gamma\} = [U]\{x_S\}$

$[U] = \begin{bmatrix} [u_i] & [0] \\ [0] & [u_i] \end{bmatrix}$  is the control input matrix;  $\{f\} = \begin{bmatrix} [0] \\ [f_i] \end{bmatrix}$ ; and  $\{x_S\} = \{\{\eta\}, \{\dot{\eta}\}\}^T$  is the

state vector; and  $\{y_S\}$  is the response vector.

In Equation (5.10), the generalized excitation force vector  $\{f\}$  and the matrix  $[U]$  define the inputs, while  $\{y_S\}$  is the output vector. In the closed-loop configuration, the control input vector  $\{\gamma\}$  in Equation (10) is related to the state feedback vector, as:

$$\{\gamma\} = -[U]\{x_S\} \quad (5.11)$$

where the magnetic field matrix  $[U]$  serves as the control gain matrix, which is evaluated according to the desired control law, while negative sign indicates externally applied

control magnetic field. Upon substituting for  $\{\gamma\}$  in Equation (10), the closed loop system can be expressed in the state space form, as:

$$\{\dot{x}_S\} = ([A] - [B][U])\{x_S\} + \{f\} \quad (5.12)$$

From Equation (5.9), it can be stated that the control gain matrix  $[U]$  directly relates to the system damping,  $C'(u_i)$ , and stiffness,  $K'(u_i)$ , properties. An optimal control is synthesized through minimization of a cost function that is proportional to a measure of the system's response and the desired control inputs using the linear quadratic regulator (LQR) approach [Sethi and Song, 2005; Burl, 1999], such that:

$$J = \frac{1}{2} \int_0^{\infty} (\{x_S\}^T [Q] \{x_S\} + \{\gamma\}^T [R] \{\gamma\}) dt \quad (5.13)$$

where  $[Q]$  and  $[R]$  are the symmetric semi-definite and positive-definite weighting matrices, respectively. The relative magnitudes of  $[Q]$  and  $[R]$  are selected so as to achieve an optimal trade off between the vibration response and the intensity of the control magnetic field. While  $[Q]$  defines the relative weight of each state variable,  $[R]$  defines the relative weight of control magnetic field.

Minimization of Eq. (5.13) yields a linear full-state feedback control law,  $\{\gamma\} = -[U]\{x_S\}$ , where the control gain matrix,  $[U] = [R]^{-1}[B]^T [P]$  is evaluated by solving for  $[P]$  from the following algebraic Ricatti equation [38]:

$$[A]^T [P] + [P][A] + [Q] - [P][B][R]^{-1}[B]^T [P] = 0 \quad (5.14)$$

### 5.3.1 Observer based optimal controller

The LQR controller based on the full state dynamic observer is formulated to derive the control gain matrix [Burl, 1999; Mutambara, 1999]. The dynamic state observer can be given by:

$$\dot{\{\hat{x}_S\}} = [A]\{\hat{x}_S\} + [B]\{\gamma\} + [L](\{y_S\} - \{\hat{y}_S\}) + \{f\}; \text{ and } \{\hat{y}_S\} = [C]\{\hat{x}_S\} \quad (5.15)$$

where  $\{\hat{x}_S\}$  is the estimated state vector and  $[L]$  is the observer gain that determines the convergence of  $\{x_S\} \rightarrow \{\hat{x}_S\}$ , and  $\{\hat{y}_S\}$  is the output vector evaluated from  $\{\hat{x}_S\}$ .

The control input vector can also be expressed as a function of  $\{\hat{x}_S\}$  such that:

$\{\gamma\} = -[U]\{\hat{x}_S\}$ . Eqs. (10) and (15) may be written in terms of the estimated state, as:

$$\dot{\{x_S\}} = [A]\{x_S\} - [B][U]\{\hat{x}_S\} + \{f\} \quad (5.16)$$

$$\dot{\{\hat{x}_S\}} = ([A] - [B][U] - [L][C])\{\hat{x}_S\} + [L]\{y_S\} + \{f\} \quad (5.17)$$

Upon substituting for  $\{y_S\} = [C]\{x_S\}$  in Eq. (17) and rearranging, the closed loop system with observer yields:

$$\begin{Bmatrix} \dot{\{x_S\}} \\ \dot{\{\hat{x}_S\}} \end{Bmatrix} = \begin{bmatrix} [A] & -[B][U] \\ [L][C] & [A] - [B][U] - [L][C] \end{bmatrix} \begin{Bmatrix} \{x_S\} \\ \{\hat{x}_S\} \end{Bmatrix} + \begin{Bmatrix} \{f\} \\ \{f\} \end{Bmatrix} \quad (5.18)$$

Equation (16) can also be rewritten in terms of the observer error  $\varepsilon$  between the measured and estimated state vector, as:

$$\dot{\{x_S\}} = ([A] - [B][U])\{x_S\} + [B][U]\varepsilon + \{f\} \quad (5.19)$$

where  $\varepsilon = \{x_S\} - \{\hat{x}_S\}$ , which can be derived from Eqs. (5.17) and (5.12), as:

$$\dot{\varepsilon} = ([A] - [B][U] - [L][C])\varepsilon + \{f\} \quad (5.20)$$

The closed loop system with the observed state vector feedback control system can be expressed using the above two equations, as:

$$\begin{Bmatrix} \dot{\{x_S\}} \\ \dot{\varepsilon} \end{Bmatrix} = \begin{bmatrix} [A] - [B][U] & [B][U] \\ 0 & [A] - [B][U] - [L][C] \end{bmatrix} \begin{Bmatrix} \{x_S\} \\ \varepsilon \end{Bmatrix} + \begin{Bmatrix} \{f\} \\ \{f\} \end{Bmatrix} \quad (5.21)$$

The above closed-loop system with observer based LQR controller is known to be inherently stable, while the observability and controllability of the system have also been

evaluated through solution of the Lyapunov equations for controllability gramian  $[W_C]$  and observability gramian  $[W_O]$ , given by [Ogata, 2008]:

$$[A][W_C]+[W_C][A^T]+[B][B^T]=0; \text{ and } [A^T][W_O]+[W_O][A]+[C^T][C]=0 \quad (5.22)$$

The system is said to be controllable and observable if  $[W_C]$  and  $[W_O]$  are of full rank.

### 5.3.2. Flexural mode shape (FMS) based optimal controller

Unlike the full-state LQR control, a limited state control synthesis could be realized using the mode shapes of the flexible beam. This approach could considerably reduce the number of feedback variables and facilitate hardware implementation by limiting the number of sensors. The known flexural mode shapes of the beam could be applied to obtain estimates of the state vector on the basis of measurements of only a few state variables. The flexural mode shape (FMS) based controller design can be further simplified, when the vibration control is sought for only a few selected modes. Using the mode summation method, the displacement response vector of the beam can be estimated from the flexural mode shapes, as:

$$\{d_e(x, t)\} = \sum_{i=1}^n \{\phi_i(x)\}q_i(t) \quad (5.23)$$

where  $\{d_e(x, t)\}$  is the estimated displacement vector of the beam,  $\{\phi_i(x)\}$  is the mode shape vector corresponding to the normal mode  $i$  and  $q_i$  is the generalized  $i^{\text{th}}$  coordinate. Considering that the vibration response of a beam is generally dominated by a few lower modes, the limited state controller synthesis is formulated by considering only the first two modes. The estimation of the generalized coordinate vectors corresponding to the first two modes,  $\{q_1(t)\}$  and  $\{q_2(t)\}$ , would require measurements of the state at a minimum of two locations. Initially the mode shape vector corresponds to the two modes,

$\phi_1$  and  $\phi_2$ , could be obtained for the open-loop structure in the absence of a magnetic field. Considering the measurements of deflections,  $d_m(l/2)$  and  $d_m(l)$  at  $x = l/2$  and  $x=l$ , respectively, the generalized coordinates may be estimated from:

$$\begin{Bmatrix} q_1(t) \\ q_2(t) \end{Bmatrix} = \begin{bmatrix} \phi_1(l) & \phi_2(l) \\ \phi_1(l/2) & \phi_2(l/2) \end{bmatrix}^{-1} \begin{Bmatrix} d_m(l,t) \\ d_m(l/2,t) \end{Bmatrix} \quad (5.24)$$

Eq. (5.23) yields the estimated displacement vector  $\{d_e(x,t)\}$  on the basis of two measured deflections, which is subsequently used to evaluate the control vector,  $\{\gamma\} = -[U]\{x_e(x,t)\}$ , where the estimated state vector  $\{x_e(x,t)\}$  consists of  $\{d_e(x,t)\}$  and their derivatives. The equation for the closed loop system based on FMS optimal controller can thus be written as:

$$\{\dot{x}_s\} = ([A] - [B][U])\{x_e(x,t)\} + \{f\} \quad (5.25)$$

#### 5.4. RESULTS AND DISCUSSION

Simulations were performed to evaluate the effectiveness of the full-and limited-state optimal LQR controllers in suppressing the vibration of fully-and partially-treated MR sandwich beams with clamped-free boundary conditions under a unit impulse load and a white noise force disturbance applied at the tip of the beam. The white noise force signal was synthesized to yield nearly constant auto spectral density up to 500 Hz. The simulation results were obtained by considering identical baseline thickness (1mm) of each of the elastic and fluid layers, while the length and width of the fully-and partially-treated beams were taken as 300 mm and 30 mm, respectively. The material properties were considered as:  $\rho_1 = \rho_3 = 2700 \text{ kg/m}^3$ ;  $E_1 = E_3 = 68 \text{ GPa}$ ;  $\rho_r = 1233 \text{ kg/m}^3$  and  $\rho_2 =$

3500 kg/m<sup>3</sup>. Two different partially-treated MR sandwich beams were configured with four localized MR fluid segments, each having 20 mm length. The locations of the fluid segments were chosen on the basis of an earlier study , and denoted as configurations A and configuration B, as shown in Figures 5.2(a) and 5.2(b), respectively. The configurations A and B were shown to yield maximum damping factors corresponding to the first five modes, when subjected to a constant magnetic field. Furthermore, the complex shear modulus of the MR fluid was considered to be a function of the storage and loss moduli, as:

$$G^*(B) = G'(B) + iG''(B) \quad (5.26)$$

where  $G'$  and  $G''$  are storage and loss moduli, respectively, expressed as the nonlinear functions of the magnetic field intensity  $B$ .

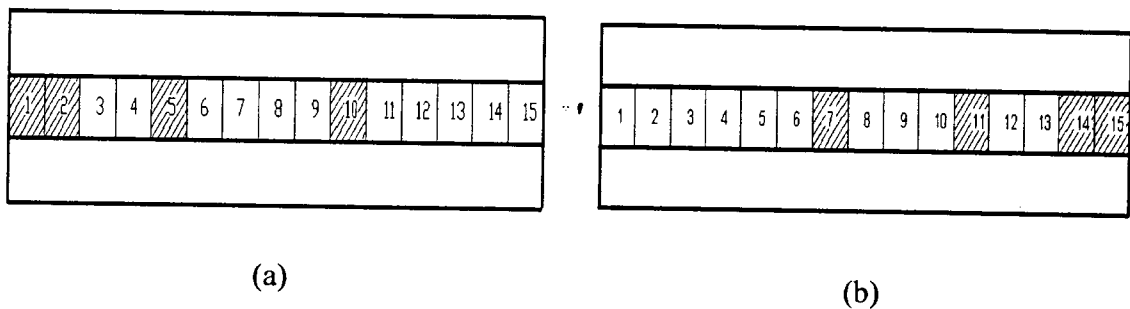


Figure 5.2. Selected configurations of partially treated MR sandwich beams with maximum modal damping factors corresponding to first five modes under a constant magnetic field: (a) configuration A; and (b) configuration B.

### 5.4.1. Full-state observer based LQR control

#### 5.4.1.1 Response to impulse disturbance

The free vibration response of the closed-loop fully-and partially- treated beams were evaluated under an impulse force applied at the free end of the clamped-free beam. The results are presented to illustrate the effectiveness of the LQR controller design described in Eq. (5.21). The weighting matrices  $[Q]$  and  $[R]$  of the controller were identified through minimization of a composite performance function of the peak displacement along the  $z$ -axis and the settling time, such that

$$\text{Minimize } f(x) = \alpha_1 t_s + \alpha_2 d_z(l) \quad (5.27)$$

where  $t_s$  is the settling time,  $d_z(l)$  is the deflection at the tip along the  $z$ -axis (transverse deflection), and  $\alpha_1$  and  $\alpha_2$  are the constant weighting factors. The settling time was identified as the displacement responses of the beam reach the order of  $10^{-6}$  m. The above minimization problem was solved using the sequential quadratic programming (SQP) method available in optimization toolbox [Matlab<sup>®</sup>], where the maximum field intensity was limited,  $B \leq 4000$  Gauss. Limit constraints were also imposed on  $[R]$  and  $[Q]$ , as

$$[R_l] \leq [R] \leq [R_u]; \text{ and } [Q_l] \leq [Q] \leq [Q_u]; \quad (5.28)$$

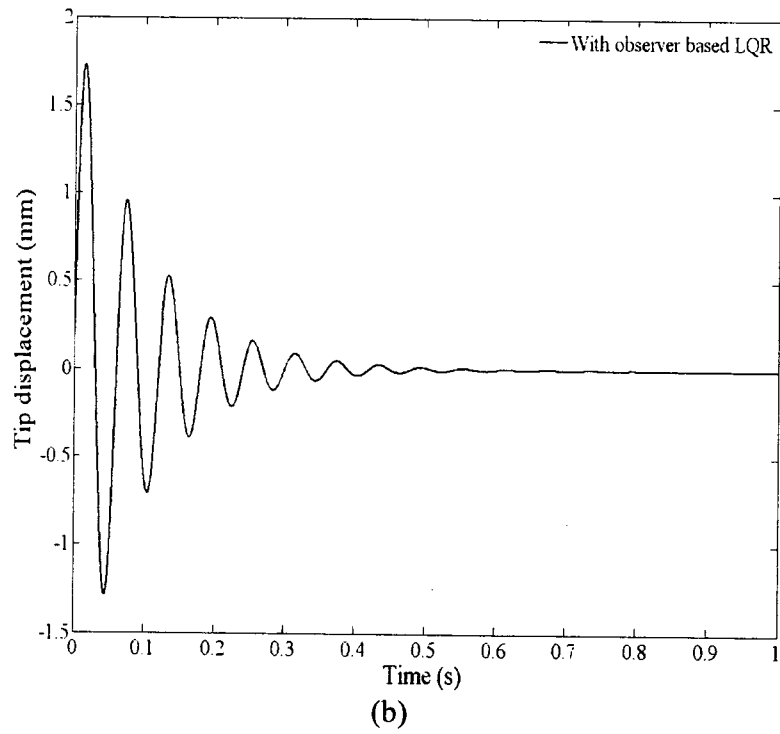
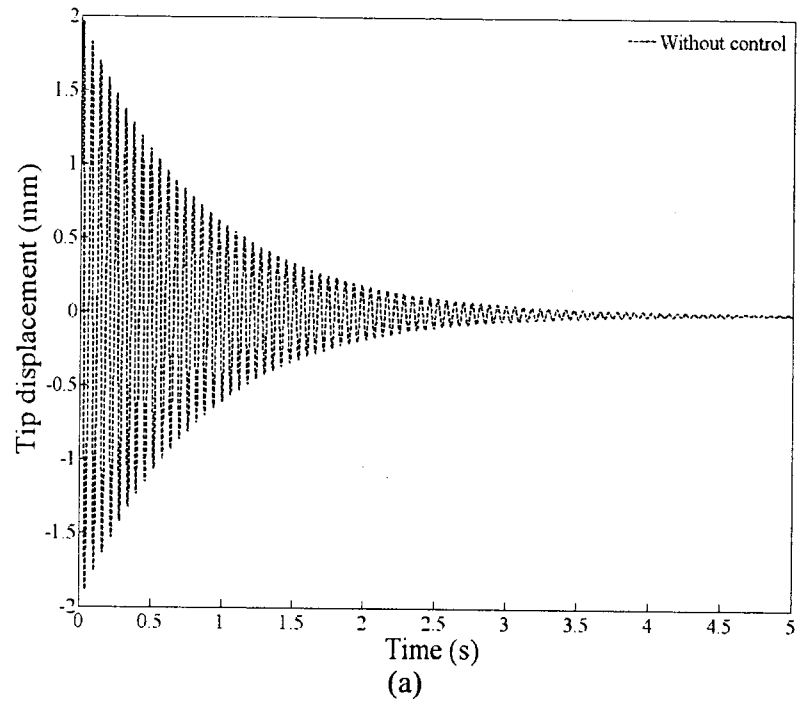
The limiting values,  $[R_l]$ ,  $[R_u]$ ,  $[Q_l]$  and  $[Q_u]$ , were identified through a parametric study involving the effects of variations in  $[R]$  and  $[Q]$  on  $t_s$  and  $d_z(l)$  together with the required field intensity. The lower and upper bounds were identified as the values when the magnetic field,  $B$ , exceeded 4000 Gauss, which are summarized in Table 5.1 together with the optimal values  $[R^*]$  and  $[Q^*]$  for the fully-and partially-treated beams obtained from the solutions of the minimization problem in Eq. (28). It should be noted that the minimization problem was solved assuming different weighting factors ranging from 0 to

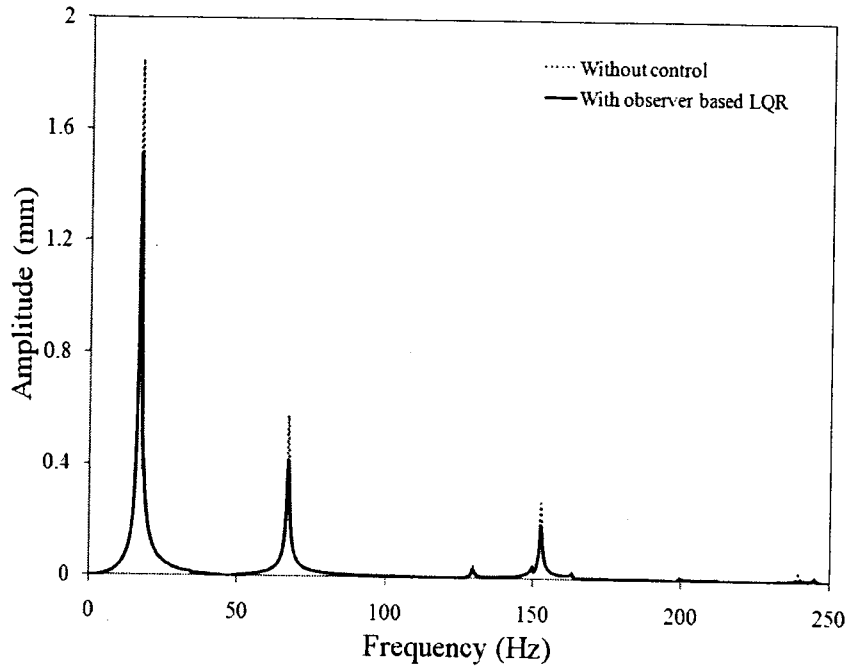
1 ( $\alpha_1 + \alpha_2 = 1$ ) and different values of the starting vectors. All of the solutions converged to very similar values of  $[R]$  and  $[Q]$ .

Table 5.1. The lower and upper bounds of  $[R]$  and  $[Q]$  and the optimal values,  $[R^*]$  and  $[Q^*]$

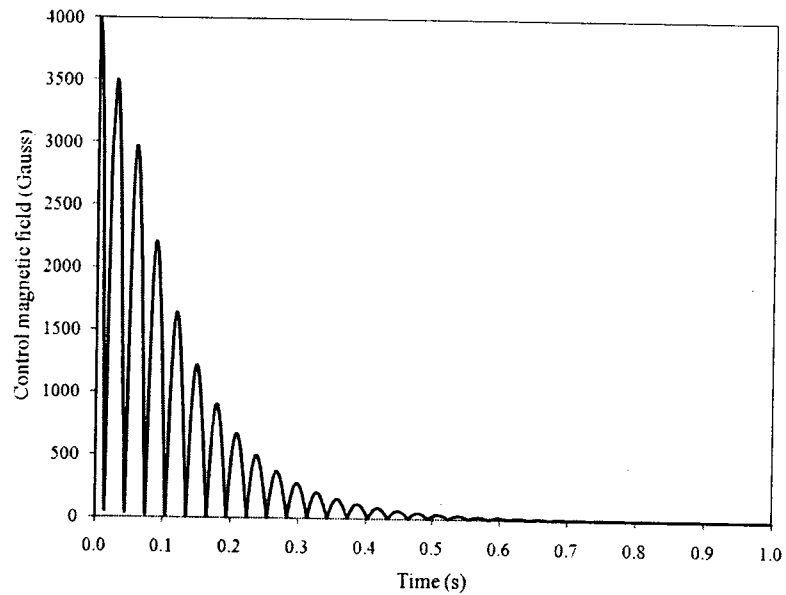
Beam	$[R_l]$	$[R_u]$	$[Q_l]$	$[Q_u]$	$[Q^*]$	$[R^*]$
Fully treated MR sandwich beam	10	100	100	2500	1390	39.45
Configuration A	10	60	100	3000	2690	50.45
Configuration B	10	175	100	2500	2300	151.5

The time-history and the frequency spectra of the tip deflection responses of the controlled fully-treated MR sandwich beam to an impulse excitation are compared with those of the passive beam ( $B=0$ ) in Figures 5.3 (a)-3(c). The time-history of the required control magnetic field is also shown in Figure 5.3(d). From the results, it is evident that the LQR control algorithm can significantly attenuate the tip displacement with the permissible intensity of the control magnetic field. The results show that the settling time of the controlled beam is in the order of 0.59 s, which is significantly lower than 4.325 s of the passive beam. The amplitude spectra of the tip displacement response, illustrated in Figure 5.3(c), also shows substantially lower deflections of the controlled beam corresponding to all of the modes observed upto 250 Hz.





(c)



(d)

Figure 5.3. The tip deflection responses of the fully-treated MR sandwich beam with and without the LQR control and subject to a unit load impulse: (a) time-history: without control; (b) time-history: with observer based control; (c) amplitude spectrum; (d) time-history of control magnetic field.

The results show that the amplitudes corresponding to the first three natural frequencies of the controlled fully-treated beam are 18%, 28% and 32%, respectively, lower than those of the uncontrolled beam. The natural frequencies of the controlled beam, however, are quite close to those of the passive beam. Although it has been shown that the application of a constant magnetic field significantly alters the stiffness property of the MR beam, the results in Figure 3 do not show a notable change in the natural frequencies corresponding to the first three modes. This is mostly attributed to the rapid settling time of the controlled beam, where the control magnetic field vanishes at  $t > 0.5$  s, as seen in Figure 5.3(d).

Figures 5.4 (a) and 5.4 (b) show the time-histories and amplitude spectra, respectively, of free vibration responses of the partially treated sandwich beams (configuration A) with and without the observer-based controller, evaluated at the tip. The figures compare the responses of the controlled and passive ( $B=0$ ) partially-treated beams subject to an impulse unit load. The results show substantially lower settling time of the partially treated beam employing the LQR control algorithm compared to that of the passive beam. The settling time of the controlled partially treated beam is 0.53 s, which is slightly lower than that of the fully treated beam (0.59s). The deflection amplitudes of the partially treated beam corresponding to the first three modes, however, are significantly greater than those of the fully treated beam, but lower than those of the respective passive beam. The deflection amplitudes of the controlled partially-treated beam corresponding to the first three modes are 14%, 15% and 9% lower than those of the uncontrolled beam. A further comparison of Figures 5.3(c) and 5.4(b) suggests

considerable difference in the natural frequencies of the fully- and partially-treated beams. These are attributable to the differences in their structures, particularly the density of the MR fluid and the elastic material ( $\rho_2 > \rho_1$ ).

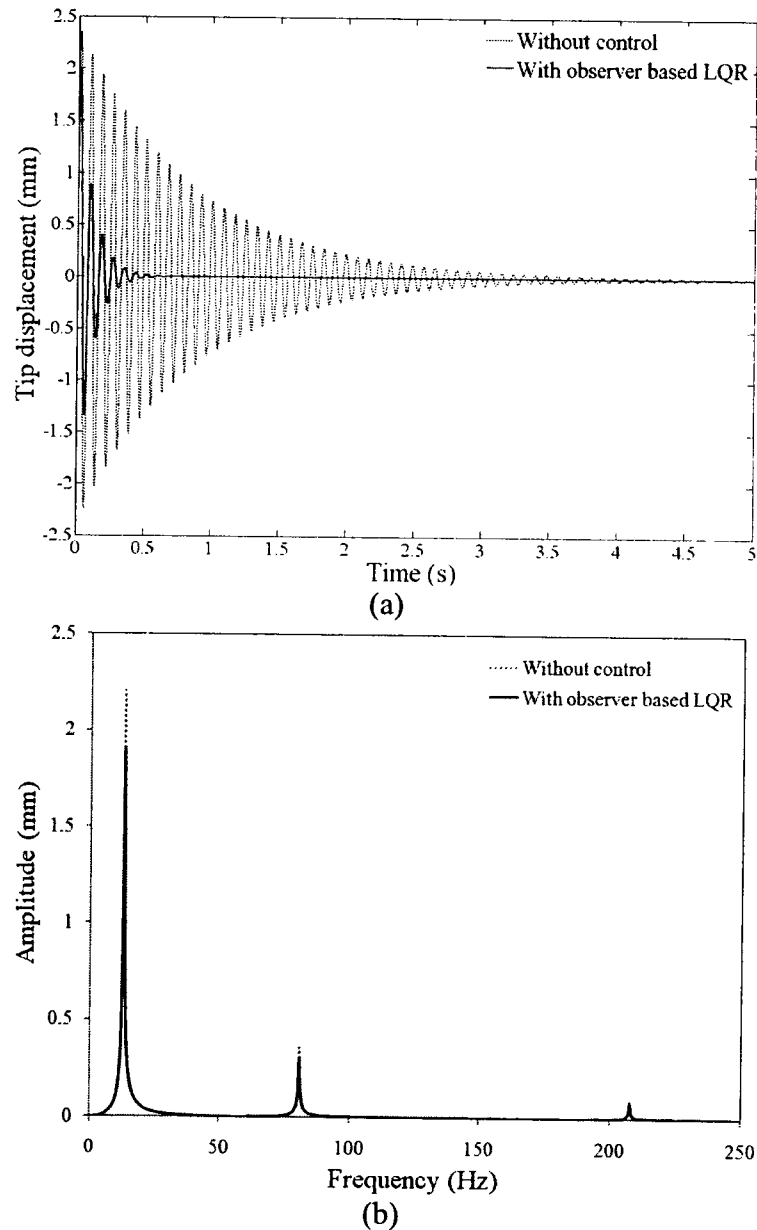


Figure 5.4. The tip deflection responses of the partially-treated MR sandwich beam (configuration A) with and without the observer based LQR control and subject to a unit load impulse: (a) time-history; (b) amplitude spectrum.

The time-histories and amplitude spectra of tip displacement responses of configuration B of the controlled as well as passive partially-treated sandwich beams are illustrated in Figures 5.5(a) and 5.5(b), respectively. The greater treatment near the free end yields larger reduction in the tip displacement, while the settling time tends to be slightly higher for both the controlled as well as passive beams compared to the fully-treated and configuration A of the partially-treated beams. The implementation of the LQR control algorithm yields peak tip displacement of 1.45 mm and settling time of 0.62 s. The corresponding values for the passive beam are 1.77 mm and 4.4 s, respectively. The amplitudes corresponding to the first three natural frequencies of the controlled structure are 15%, 41% and 56%, respectively, lower than those of the passive beam. The deflection amplitudes of the controlled configuration B are substantially lower than those of the controlled configuration A. This is particularly attributable to relative higher modal damping factors of configuration B. Furthermore, the peak displacement response at the tip of the passive partially-treated beam (configuration B) is almost comparable to that of the fully treated passive beam, as observed from the time-history of the responses. Similar trend has also been reported in the transverse response of the fully and various configurations of the partially treated beams (Chapters 3 and 4). The results also show that the implementation of the LQR control to configuration B yields significantly higher reductions in deflection amplitudes corresponding to the first three modes compared to those of observed for the fully treated and configuration A of the partially treated beam.

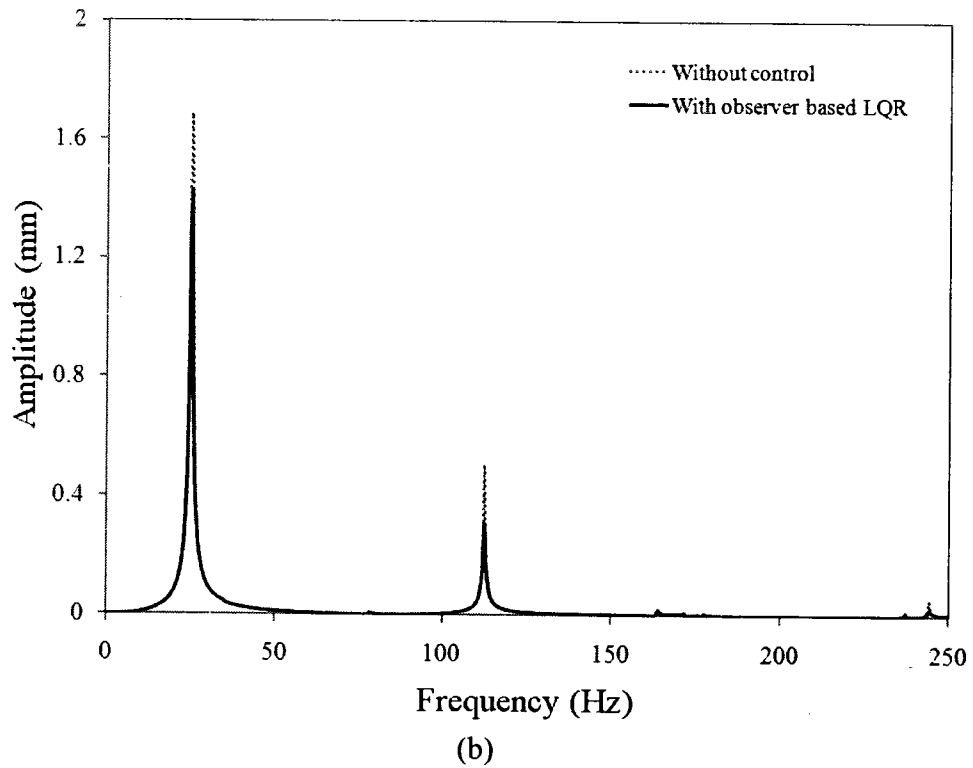
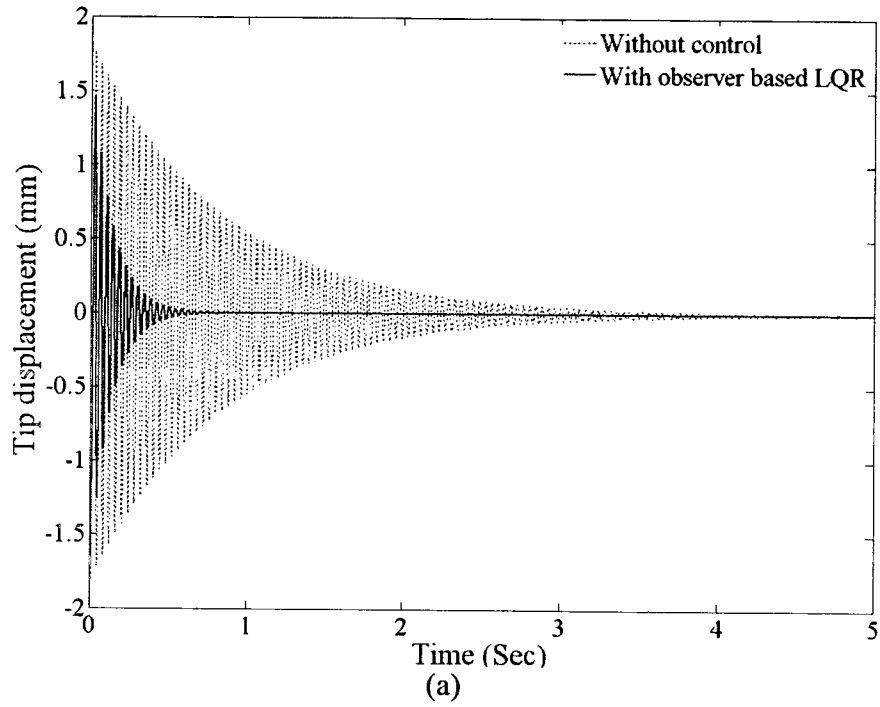


Figure 5.5. The tip deflection responses of the partially-treated MR sandwich beam (configuration B) with and without the observer based LQR control and subject to a unit load impulse: (a) time-history; (b) amplitude spectrum.

#### 5.4.1.2. Response to a white noise disturbance

The effectiveness of the LQR control in suppressing the steady-state vibration is further evaluated under a Gaussian white noise force disturbance applied at the tip along z-axis (variance = 3.15 N<sup>2</sup>; mean ≈ 0). The optimal state weighing matrices,  $[R^*]$  and  $[Q^*]$ , were subsequently evaluated in a similar manner through solution of the following minimization problem:

$$\text{Minimize, } f(x) = \sum_{i=1}^n d_{z_{p_i}}(l) \quad (5.29)$$

The above minimization problem considers the peak transverse deflection,  $d_{z_{p_i}}(l)$ , at the tip corresponding to the first five modes ( $n=5$ ). The peak deflections corresponding to different modes were extracted from the amplitude spectrum of the tip deflection response by defining five distinct frequency ranges around the known natural frequencies of the passive beam ( $B=0$ ). The lower and upper bounds of  $[R]$  and  $[Q]$  were obtained from a parametric study as in the case of impulse excitation, and are summarized in Table 5.2 together with the optimal values,  $[R^*]$  and  $[Q^*]$  for the fully- and partially-treated beams.

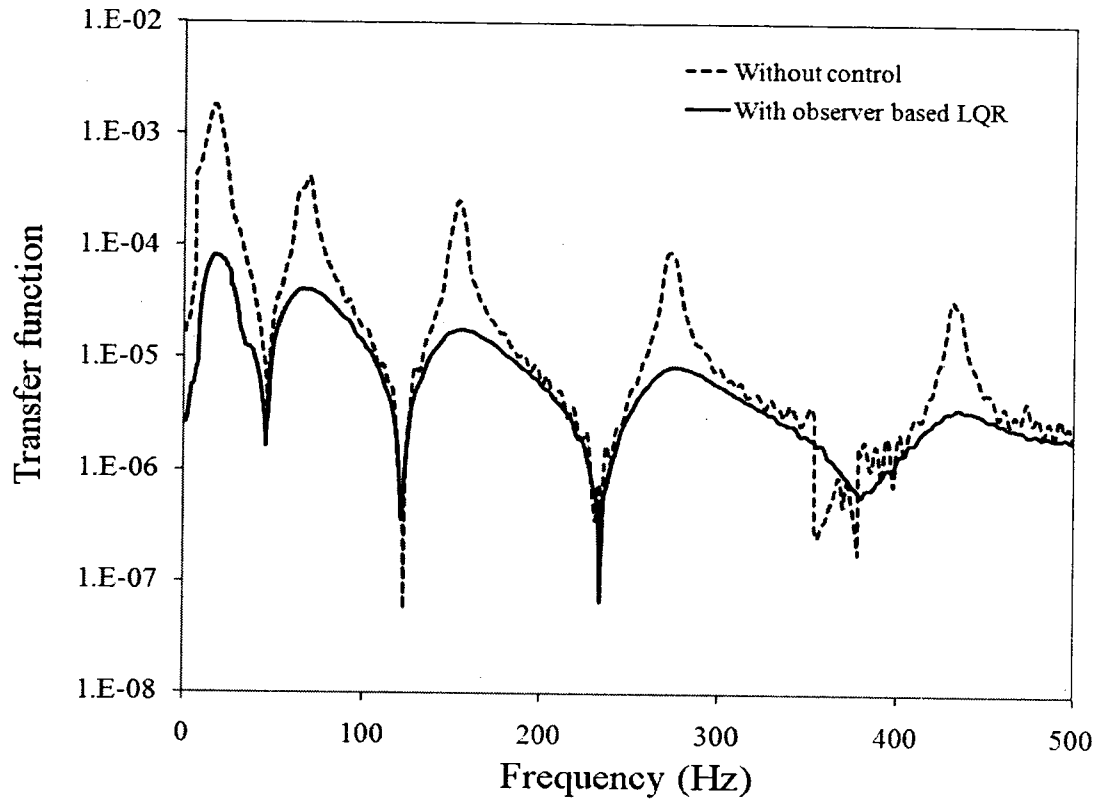
Table 5.2. The lower and upper bounds of  $[R]$  and  $[Q]$  and the optimal values,  $[R^*]$  and  $[Q^*]$

Beam	$[R_l]$	$[R_u]$	$[Q_l]$	$[Q_u]$	$[Q^*]$	$[R^*]$
Fully treated MR sandwich beam	43	45	4000	4300	4125	43.25
Configuration A	25	65	1750	3500	2800	51.5
Configuration B	25	65	1750	3500	2800	51.5

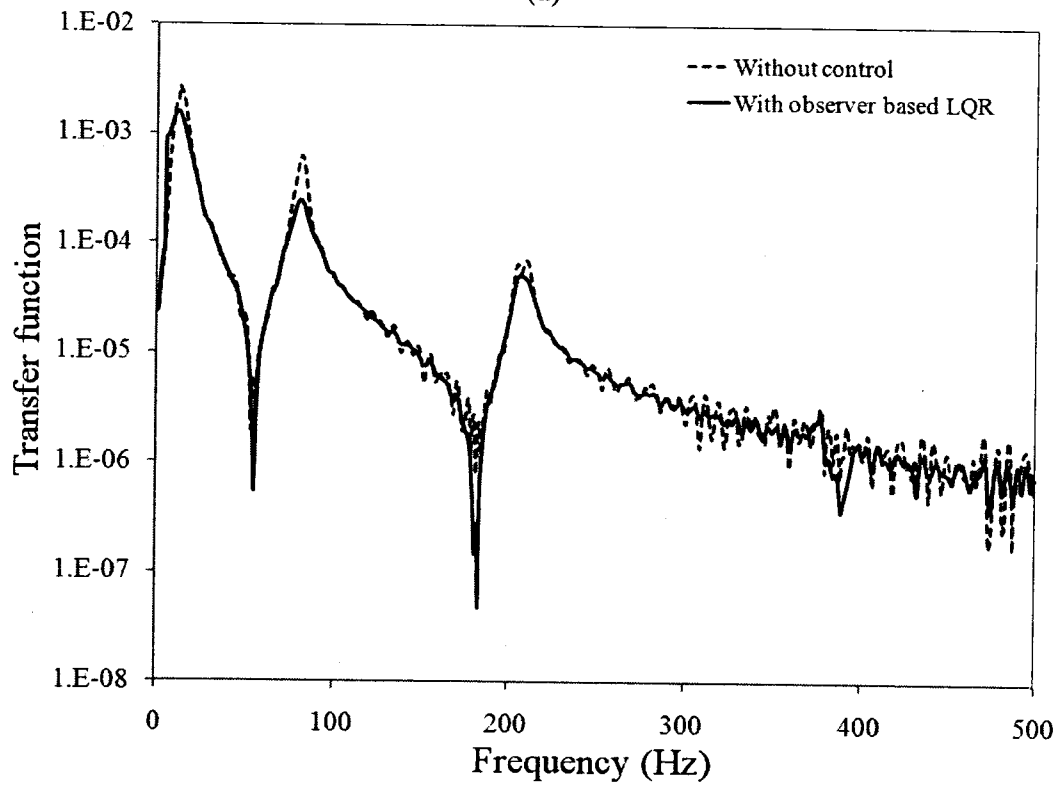
The deflection responses of the fully- and partially-treated beams with and without the controller were evaluated in terms of transfer function (TF) of the tip displacement. Figure 5.6 compares the transfer function of tip displacement responses of the controlled

beams with those of the corresponding passive beams ( $B=0$ ). The results show that the LQR control can reduce the deflection amplitudes corresponding to all the modes considered, irrespective of the MR fluid treatment. It should be noted that the TFs are presented upto only 500 Hz, while the fifth mode of the partially treated beams lies at a frequency above 500 Hz. The fully-and partially-treated beam (configuration B), in particular, yield most significant reductions in the tip deflections compared to those of the passive beams ( $B=0$ ). The configuration A of the partially-treated beam, however, exhibits relatively smaller reduction in the peak responses compared to the respective passive beam.

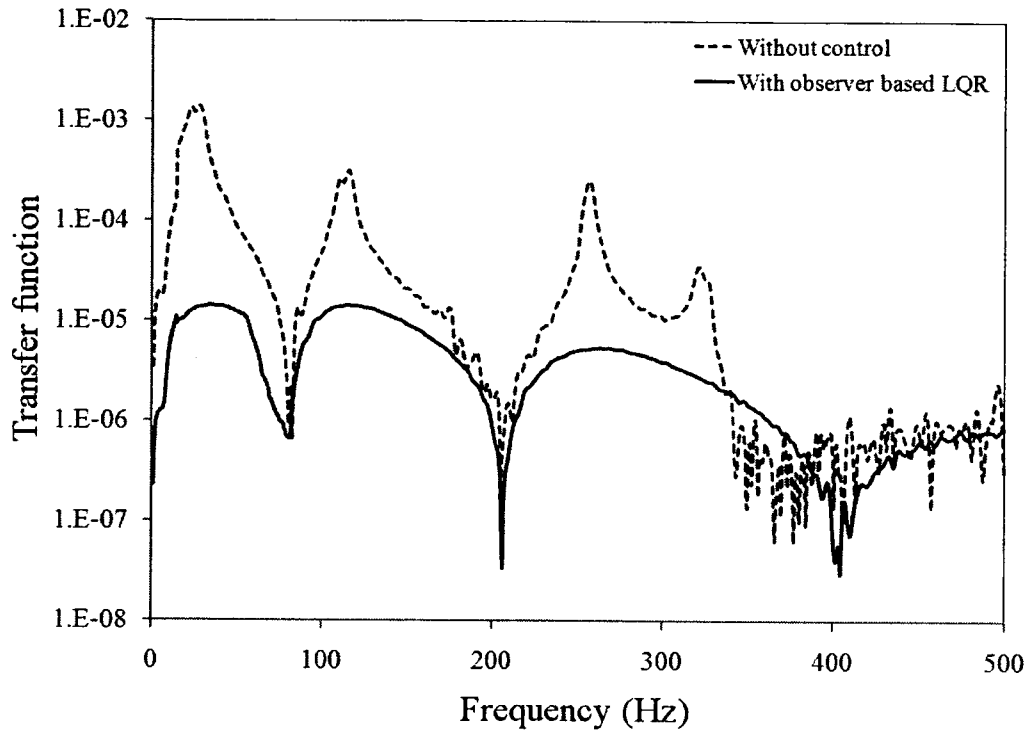
The most significant reductions are evident in deflection corresponding to the first mode for all the beams considered. For the fully-treated beam, the TF reveals that the LQR control yields 96%, 90%, 93% , 91% and 99% reductions in the peaks corresponds to the first five modes, respectively. It can also be seen that the first and fifth modes deflection peaks are entirely attenuated, as seen in Figure 5.6(a). The reductions in the peak deflections of the partially-treated beam (configuration B) corresponding to the first three modes are 99%, 96% and 98%, respectively. The first and fourth modes deflections in this case are also entirely attenuated, as seen in Figure 5.6(c). The reductions in the peak amplitudes of partially-treated beam, configuration A, are relatively much smaller than those observed for configuration B for all the modes, as seen in Figure 5.6 (b). This is mostly caused by the distribution of the MR fluid segments near the support, and is consistent with the free vibration responses presented in Figures 5.4 and 5.5.



(a)



(b)



(c)

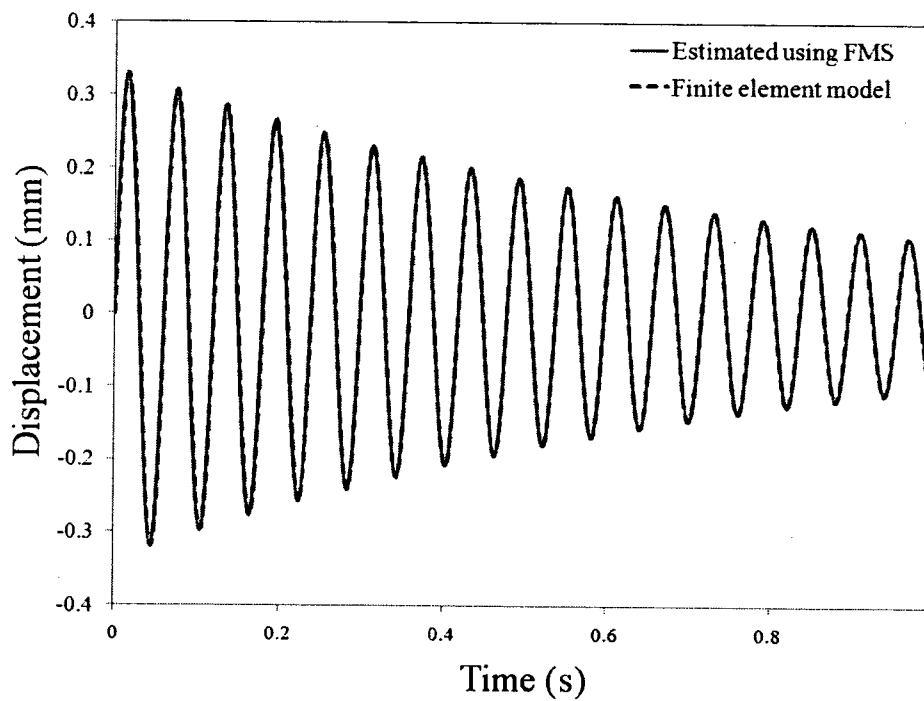
Figure 5.6. Comparisons of the transfer functions of the tip displacement responses of beams with and without observer based LQR control: (a) Fully treated beam; (b) configuration A; and (c) configuration B.

#### 5.4.2. Flexural mode shape (FMS) based LQR control

Simulations are performed to examine the validity of the flexural mode shape (FMS) based optimal controller in estimating the state vector. The effectiveness of the FMS controller is subsequently evaluated in suppressing the free and forced vibration responses under both the impulse and white-noise force excitation at the tip. The effectiveness of the proposed FMS estimator and control method are demonstrated for the fully-treated beam alone, while the simulation parameters are taken as those described in previous section.

The validity of the FMS estimator is initially investigated considering the impulse excitation for the passive and controlled fully-treated beams. For this purpose,

the finite element model was analyzed to yield the transverse deflection amplitudes obtained at  $x = l = 300$  mm and  $x = l/2 = 150$  mm, which were applied to estimate the deflections at different coordinates, using Eq. (5.23). The estimated deflection responses at different locations were then compared with those derived from the FE model to examine the validity of the FMS estimator. The results revealed very good state estimation for both the passive and the controlled fully-treated beams. As an example, Figures 5.7(a) and 5.7(b) compare the estimated deflection responses of the passive beam with those derived from the finite element model at  $x = 100$  mm and  $x = 200$  mm, respectively. For the purpose of clarity, the responses are compared only in the 0 to 1s interval, which invariably show that the estimated and computed responses overlap. Figures 5.8(a) and 5.8(b) present comparison of the computed and estimated deflection responses of the fully-treated beam employing the FMS-based LQR controller at  $x = 100$  mm and  $x = 200$  mm which further validate the FMS based estimator.



(a)

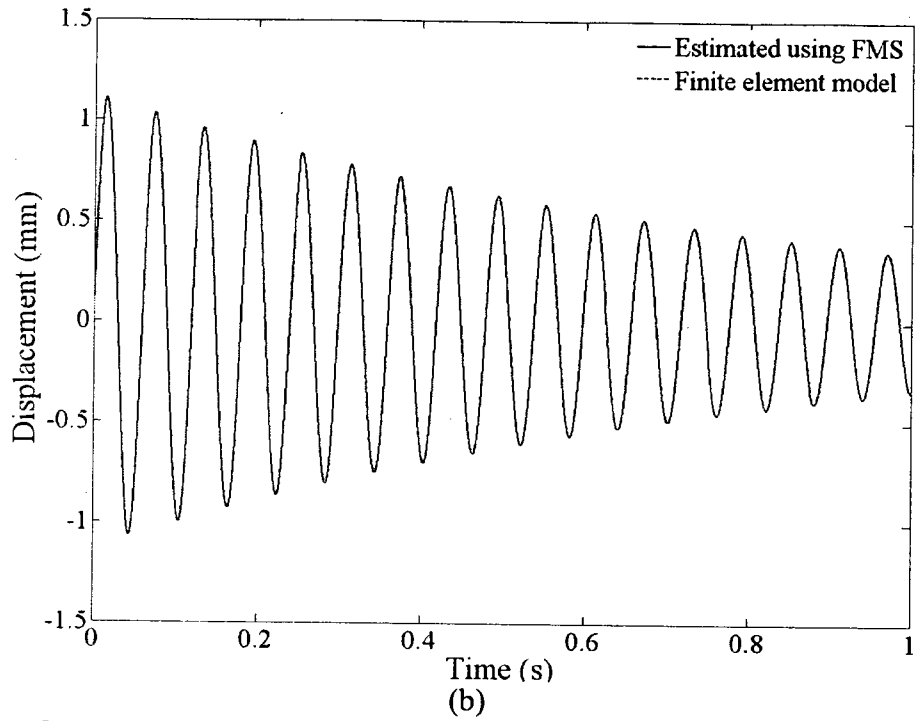
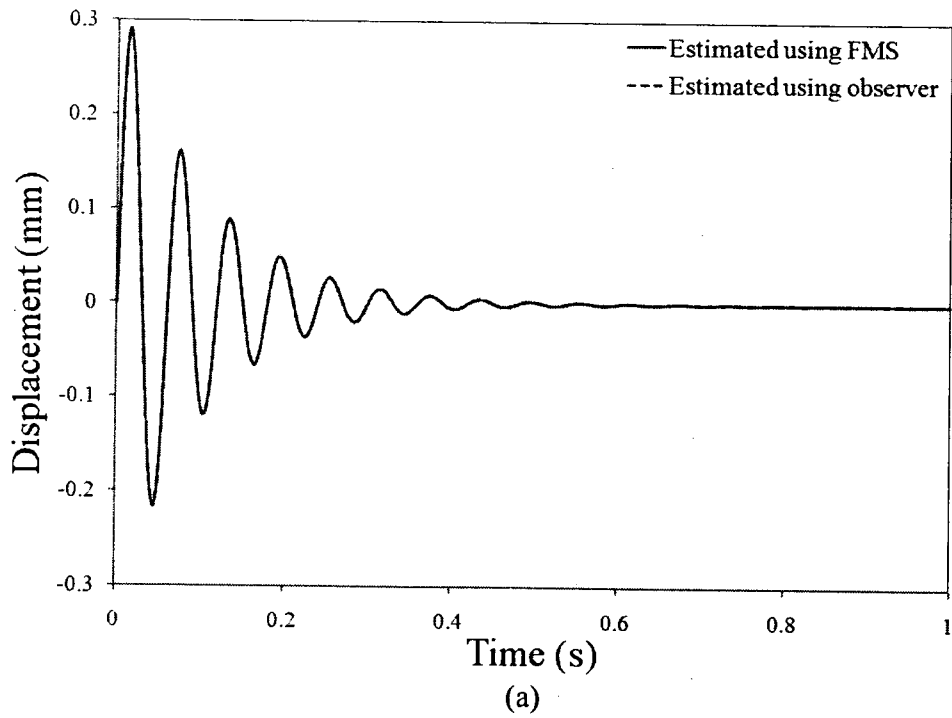


Figure 5.7 Comparisons of deflection responses of the fully treated passive beam estimated using FMS and the finite element model: (a)  $x=100$  mm; and (b)  $x=200$  mm



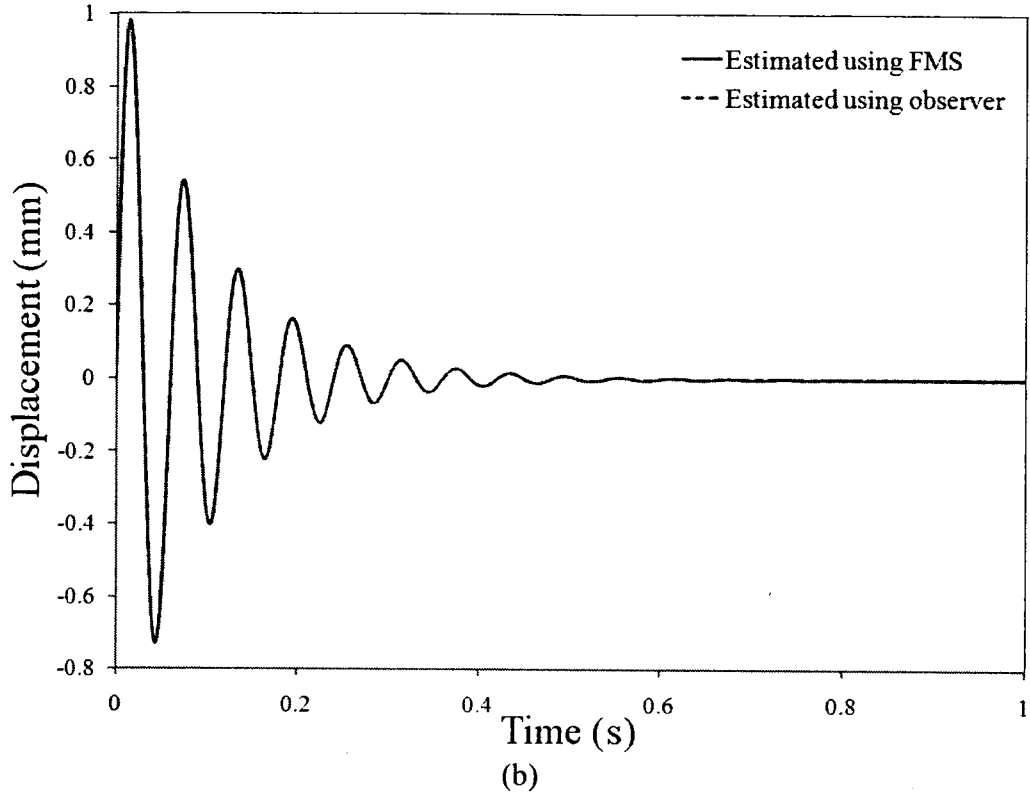


Figure 5.8. Comparisons of deflection responses of the fully treated beam estimated using FMS based and observer based LQR controllers : (a)  $x = 100$  mm; and (b)  $x = 200$  mm

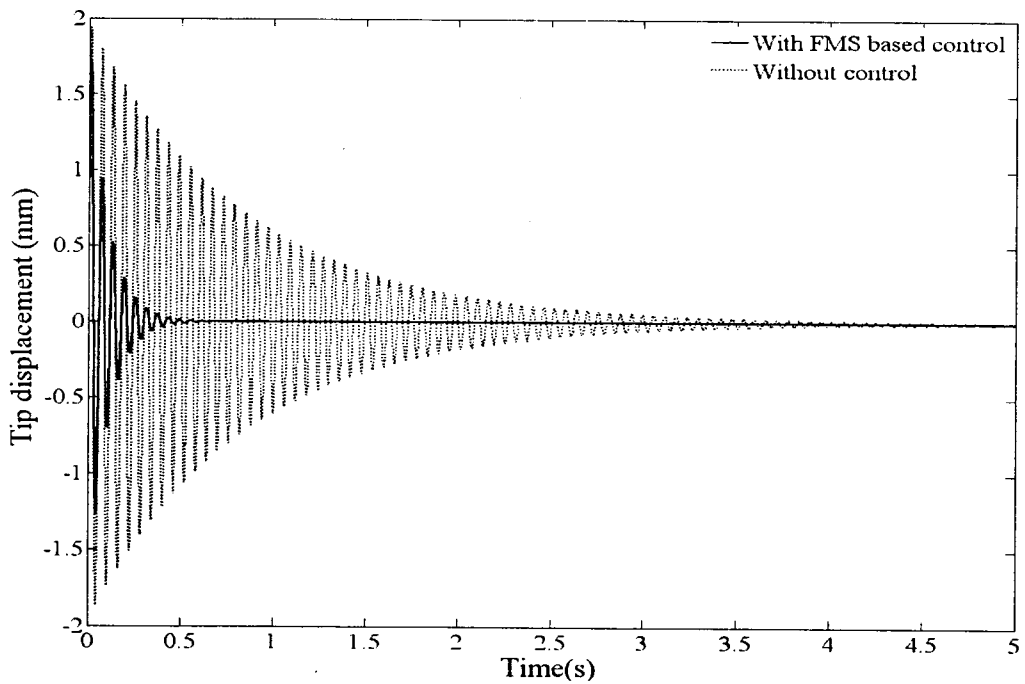


Figure 5.9. Open and closed loops responses at the tip of the fully treated MR sandwich beam under the impulse disturbance at the tip of the beam using FMS based controller.

From Figures 5.7 and 5.8, it is evident that the FMS-based LQR control can effectively adapt to the state of the beam. The proposed limited state control can thus yield vibration attenuation performance similar to the full state observer based control. Furthermore, the tip deflection responses of the fully-treated beam with and without FMS based LQR controller are shown in Figure 9 under the unit impulse excitation. The results show that the settling time and peak displacement has been significantly reduced. The settling time of the controlled beam is in the order of 0.59 s, which is significantly lower than 4.325 s of the passive beam ( $B=0$ ).

The deflection responses of the fully treated beam with and without the FMS based control are further evaluated under a white-noise force excitation applied at the tip. Figure 5.10 compares the transfer function of tip displacement responses of the controlled beam with that of the corresponding passive beam ( $B=0$ ). The results show that the FMS based LQR control can reduce the deflection amplitudes corresponding to all the modes considered in the 0-500 Hz frequency range. The TF reveals that the FMS based LQR control yields the deflection reduction as good as the observer based LQR. The reductions in the peaks corresponds to the first five modes are 96%, 90%, 93%, 91% and 99%, respectively. It can also be observed that the first and fifth modes deflection peaks are entirely attenuated. This confirms the effectiveness of the FMS-based limited state optimal controller.

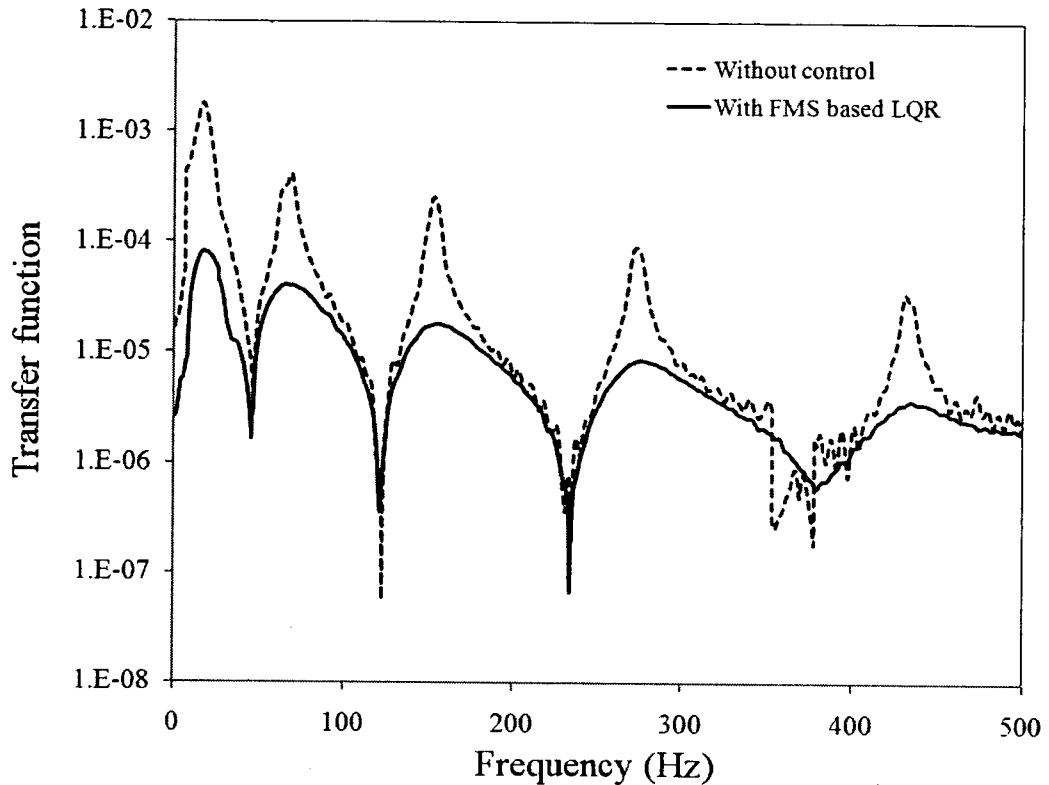


Figure 5.10. Comparisons of the transfer functions of the tip displacement responses of the fully treated beam with and without FMS based LQR control

## 5.5. CONCLUSIONS

In this chapter, the semi-active vibration control of a multilayer beam fully-and partially - treated with MR fluid has been analyzed. The results of the study show that the full-state observer based LQR control can yield substantial reductions in the settling time and free- and forced vibration responses of the beams treated either fully or partially with MR-fluid under an impulse excitation. The observer based LQR control of the fully and partially treated beams resulted nearly 85% reduction in the free-vibration settling time, and 25% reduction in the tip deflection when compared to that of the passive beams. The vibration responses to a white noise force excitation applied at the tip also revealed nearly 90% reductions in the deflections amplitudes corresponding to the higher modes for both the fully and partially-treated beams while the deflection corresponding to the first mode is

entirely attenuated. The limited state control synthesis proposed on basis of the flexural mode shapes of the beam would also resulted in comparable vibration spectra, while reducing the number of feedback variables and the hardware implementation. The approach based on the known flexural mode shapes of the beam and measurements of only a few state variables provided effective estimates of the state vector. The controlled and uncontrolled deflection responses of the beam using FMS based control method evaluated under an impulse and a white-noise force applied at the tip of the beam confirms the effectiveness of the FMS-based limited state controller.

## **CHAPTER 6**

### **CONCLUSIONS AND RECOMMENDATIONS**

#### **6.1 MAJOR CONTRIBUTIONS AND HIGHLIGHTS OF THE STUDY**

This dissertation research explored the vibration suppression potentials of structures treated either fully or partially with the magneto-rheological (MR) fluids. Although a few analytical and experimental studies contributed to the understanding of the vibration suppression capabilities of MR sandwich beams, the effectiveness of the partial treatment of MR fluid in a sandwich structure on vibration control characteristics has not yet been explored theoretically and experimentally. Furthermore, the design and implementation of the semi active control law in the closed loop to control the dynamic characteristics of the fully and partially treated MR sandwich beams were not yet been attempted. The comprehensive studies have thus been carried out to present concepts in a class of smart structures and lead to the development of analytical models that could provide a better understanding of the open and closed dynamic characteristics of a fully and partially treated MR-fluid sandwich beam. The foremost contributions of the dissertation research are summarized below:

- Formulation of an analytical model of a fully treated MR sandwich beam using the Ritz formulation and finite-element method, and theoretical and experimental investigation on the dynamic characteristics of the MR-fluid sandwich beam with different end conditions under the application of different magnetic field.

- Development of the relationship for the complex shear modulus of the MR fluid as a function of applied magnetic field by performing a free oscillation experiment.
- Formulation of analytical models of a partially treated MR sandwich beam with different end conditions and investigation on its dynamic characteristics as functions of magnetic field and MR fluid segments, theoretically and experimentally.
- Formulation of an optimization problem to determine optimal locations of the MR fluid segments to maximize the modal damping factors corresponding to individual and multiple modes for different end conditions.
- Development of an optimal closed loop control strategy based on Linear Quadratic regulator (LQR) using full order observers for suppression of vibration of the fully and partially treated MR sandwich beams.
- Development of the feedback approach based on the flexural mode shapes (FMS) of the beam to obtain the estimates of the state vectors on basis of measurements of only a few state variables.

## **6.2 MAJOR CONCLUSIONS**

The major conclusions drawn from the study are summarized below:

- a) The complex shear modulus of the MR fluid is related to the applied magnetic field in a highly nonlinear manner. The relationship could be conveniently derived from the free-vibration response.

- b) The multi-layered MR fluid treated structure could be described by the complex stiffness property for the finite-element analysis.
- c) The natural frequencies corresponding to all the modes and loss factors for the higher modes of vibration of the MR multilayer beams increased substantially with increase in the magnetic field intensity. The transverse deflection response of MR-treated beams reduced significantly with increase in the magnetic field, suggesting superior potential of the MR-fluid treatments. The fundamental mode could increase by nearly 25% under the application of magnetic field of 500 Gauss.
- d) The variations in the natural frequencies and loss factors strongly depend upon the thickness of the MR fluid layer. The natural frequencies corresponding to all the modes considered decreased with increase in the MR layer thickness, while the loss factors increased for the first two modes. Higher loss factors corresponding to higher modes could be obtained by choosing a greater ratio of the MR layer thickness to that of the elastic layer.
- e) Partial-treatments of structures offer added design flexibility. Apart from the natural frequencies, the deflection, the mode shapes and the modal damping factors of the partially-treated MR sandwich beam could be controlled by locating the MR fluid segments within the span of the beam, irrespective of the boundary conditions. Furthermore, the higher modes frequencies could be increased by decreasing the MR fluid layer length.
- f) Optimal locations of MR-fluid segments in a partially-treated structure corresponding to a particular mode or a combination of modes could be identified

through solution of multi-parameter design optimization with an objective to maximize the modal damping factor(s). The solution obtained using the genetic algorithm has converged towards global optima compared to those derived from sequential quadratic programming (SQP) method.

- g) The optimal solutions for the locations of the MR fluid segments obtained by considering linear combination of the first five modes were identical to those obtained for the first mode alone, irrespective of the end conditions. However considering the optimization function as the logarithmic combination of the modes resulted in uniformly distributed modal damping factors for all the modes.
- h) The resulting optimal MR-fluid segments resulted in substantially lower peak displacements and considerably higher modal damping factors for all the modes, except for the first mode of the clamped-free beam.
- i) The optimal design of partially-treated MR fluid sandwich beam derived upon consideration of logarithmic summation of the modes resulted in a more efficient layout of the MR-fluid segments.
- j) The full-state feedback LQR controller provided most significant reductions in the peak deflection amplitudes corresponding to each mode of the fully-and partially - treated MR sandwich beam.
- k) The responses in terms of settling time and peak deflection amplitude of the closed loop controlled system of a partially-treated beam with MR fluid segments away from the free end of the cantilever beam were lower than those of the fully treated beam.

- l) The responses in terms of settling time and peak deflection amplitude of the closed loop controlled system of a partially-treated beam with MR fluid segments close to the free end of the cantilever beam were almost equal to those of the fully treated beam.
- m) The flexural mode shapes of the beam could be applied to obtain estimates of the state vector on the basis of measurements of only a few state variables. This approach could yield a controller design based on the limited state feedback and thereby simplify the hardware requirements.

### **6.3 RECOMMENDATION FOR THE FUTURE WORKS**

The present dissertation research constitutes a preliminary but significant step towards applications of the MR fluids in realizing fully or partially treated multi-layered smart structures. Owing to the observed potential performance benefits in view of enhanced vibration suppression, additional efforts would be desirable to obtain deep insight into the dynamic characteristics of the MR fluid treated structures. Some of the recommended further works are listed below:

- a) The present analytical model can be extended to fully and partially treated MR-fluid multilayer plates or shells or more practical structures. Furthermore, the investigations on altering the flexural mode shapes of the fully and partially treated plates and shells can be performed under different end conditions.
- b) The structural tuning or boundary conditioning of the partially treated MR fluid sandwich structures can be performed through systematic investigations on the

effects of locations and geometry of the MR fluid segments in order to realize desired vibratory and acoustic performance of the structure.

- c) The dynamic characterization of the MR fluids under high frequency applications can be performed by investigating the wave transmission through MR fluid based sandwich structures.
- d) The analytical model formulated in this study can be further extended to investigate the dynamic characteristics of the MR fluid treated sandwich structures under base excitations which would be important for further understanding of the effectiveness of the MR fluid in suppressing the vibration in different applications.
- e) It is important to explore design of compact electromagnets to provide wide variations in the magnetic field, particularly for the partially-treated structures.
- f) It would also be desirable to explore alternate practically reliable controller synthesis such as adaptive, using the known deflection patterns.

## APPENDIX A

### Coefficients of element stiffness and mass matrices for the MR fluid multilayer beam.

The symmetric (6x6) elemental mass and stiffness matrices derived using Lagrange's energy equation are summarized below.

#### Stiffness matrix

$$k_{11} = \int_0^{l_e} \alpha_1 \dot{N}_1^2 dx + \int_0^{l_e} \alpha_2 N_1^2 dx; k_{12} = \int_0^{l_e} \alpha_3 N_1 \dot{N}_2 dx; k_{13} = \int_0^{l_e} \alpha_3 N_1 \dot{N}_3 dx;$$

$$k_{14} = \int_0^{l_e} \alpha_1 \dot{N}_1 \dot{N}_4 dx + \int_0^{l_e} \alpha_2 N_1 N_4 dx; k_{15} = \int_0^{l_e} \alpha_3 N_1 \dot{N}_5 dx; k_{16} = \int_0^{l_e} \alpha_3 N_1 \dot{N}_6 dx;$$

$$k_{22} = \int_0^{l_e} \alpha_4 \ddot{N}_2^2 dx + \int_0^{l_e} \alpha_5 \dot{N}_2^2 dx; k_{23} = \int_0^{l_e} \alpha_4 \ddot{N}_2 \ddot{N}_3 dx + \int_0^{l_e} \alpha_5 \dot{N}_2 \dot{N}_3 dx; k_{24} = \int_0^{l_e} \alpha_3 \ddot{N}_2 N_4 dx;$$

$$k_{25} = \int_0^{l_e} \alpha_4 \ddot{N}_2 \ddot{N}_5 dx + \int_0^{l_e} \alpha_5 \dot{N}_2 \dot{N}_5 dx; k_{26} = \int_0^{l_e} \alpha_4 \ddot{N}_2 \ddot{N}_6 dx + \int_0^{l_e} \alpha_5 \dot{N}_2 \dot{N}_6 dx;$$

$$k_{33} = \int_0^{l_e} \alpha_4 \ddot{N}_3^2 dx + \int_0^{l_e} \alpha_5 \dot{N}_3^2 dx; k_{34} = \int_0^{l_e} \alpha_3 \ddot{N}_3 N_4 dx; k_{35} = \int_0^{l_e} \alpha_4 \ddot{N}_3 \ddot{N}_5 dx + \int_0^{l_e} \alpha_5 \dot{N}_3 \dot{N}_5 dx;$$

$$k_{36} = \int_0^{l_e} \alpha_4 \ddot{N}_3 \ddot{N}_6 dx + \int_0^{l_e} \alpha_5 \dot{N}_3 \dot{N}_6 dx;$$

$$k_{44} = \int_0^{l_e} \alpha_1 \dot{N}_4^2 dx + \int_0^{l_e} \alpha_2 N_4^2 dx; k_{45} = \int_0^{l_e} \alpha_3 N_4 \dot{N}_5 dx; k_{46} = \int_0^{l_e} \alpha_3 N_4 \dot{N}_6 dx;$$

$$k_{55} = \int_0^{l_e} \alpha_4 \ddot{N}_5^2 dx + \int_0^{l_e} \alpha_5 \dot{N}_5^2 dx; k_{56} = \int_0^{l_e} \alpha_4 \ddot{N}_5 \ddot{N}_6 dx + \int_0^{l_e} \alpha_5 \dot{N}_5 \dot{N}_6 dx; \text{ and}$$

$$k_{66} = \int_0^{l_e} \alpha_4 \ddot{N}_6^2 dx + \int_0^{l_e} \alpha_5 \dot{N}_6^2 dx;$$

where

$$\alpha_1 = (E_1 A_1 + E_3 A_3 e^2); \alpha_2 = \bar{G} b h_2 \left( -\frac{(1+e)}{h_2} \right)^2; \alpha_3 = \bar{G} b h_2 \left( \frac{D}{h_2} \right) \left( -\frac{(1+e)}{h_2} \right);$$

$$\alpha_4 = (E_1 I_1 + E_3 I_3); \text{ and } \alpha_5 = \bar{G} b h_2 \left( \frac{D}{h_2} \right)^2;$$

### Mass matrix

$$m_{11} = \int_0^{l_e} \beta_1 N_1^2 dx + \int_0^{l_e} \beta_2 N_1^2 dx; m_{12} = \int_0^{l_e} \beta_3 N_1 \dot{N}_2 dx; m_{13} = \int_0^{l_e} \beta_3 N_1 \dot{N}_3 dx;$$

$$m_{14} = \int_0^{l_e} \beta_1 N_1 N_4 dx + \int_0^{l_e} \beta_4 N_1 N_4 dx; m_{15} = \int_0^{l_e} \beta_3 N_1 \dot{N}_5 dx; m_{16} = \int_0^{l_e} \beta_3 N_1 \dot{N}_6 dx;$$

$$m_{22} = \int_0^{l_e} \beta_5 N_2^2 dx + \int_0^{l_e} \beta_6 \dot{N}_2^2 dx; m_{23} = \int_0^{l_e} \beta_5 N_2 N_3 dx + \int_0^{l_e} \beta_6 \dot{N}_2 \dot{N}_3 dx;$$

$$m_{24} = \int_0^{l_e} \beta_3 N_4 \dot{N}_2 dx; m_{25} = \int_0^{l_e} \beta_5 N_2 N_5 dx + \int_0^{l_e} \beta_6 \dot{N}_2 \dot{N}_5 dx;$$

$$m_{26} = \int_0^{l_e} \beta_5 N_2 N_6 dx + \int_0^{l_e} \beta_6 \dot{N}_2 \dot{N}_6 dx; m_{33} = \int_0^{l_e} \beta_5 N_3^2 dx + \int_0^{l_e} \beta_6 \dot{N}_3^2 dx;$$

$$m_{34} = \int_0^{l_e} \beta_3 N_4 \dot{N}_3 dx; m_{35} = \int_0^{l_e} \beta_5 N_3 N_5 dx + \int_0^{l_e} \beta_6 \dot{N}_3 \dot{N}_5 dx;$$

$$m_{36} = \int_0^{l_e} \beta_5 N_3 N_6 dx + \int_0^{l_e} \beta_6 \dot{N}_3 \dot{N}_6 dx; m_{44} = \int_0^{l_e} \beta_1 N_4^2 dx + \int_0^{l_e} \beta_4 N_4^2 dx;$$

$$m_{45} = \int_0^{l_e} \beta_3 N_4 \dot{N}_5 dx; m_{46} = \int_0^{l_e} \beta_3 N_4 \dot{N}_6 dx; m_{55} = \int_0^{l_e} \beta_5 N_5^2 dx + \int_0^{l_e} \beta_6 \dot{N}_5^2 dx;$$

$$m_{56} = \int_0^{l_e} \beta_5 N_5 N_6 dx + \int_0^{l_e} \beta_6 \dot{N}_5 \dot{N}_6 dx; m_{66} = \int_0^{l_e} \beta_5 N_6^2 dx + \int_0^{l_e} \beta_6 \dot{N}_6^2 dx;$$

where  $\beta_1 = \rho_1 A_1 + e^2 \rho_3 A_3$ ;  $\beta_2 = \rho_2 I_2 \left( -\frac{(1+e)}{h_2} \right)^2$ ;  $\beta_3 = (\rho_2 I_2 + \rho_r I_r) \left( \frac{D}{h_2} \right) \left( -\frac{(1+e)}{h_2} \right)$ ;

$$\beta_4 = (\rho_2 I_2 + \rho_r I_r) \left( \frac{(1+e)}{h_2} \right)^2; \beta_5 = (\rho_1 A_1 + \rho_2 A_2 + \rho_r A_r + \rho_3 A_3),$$

$$\beta_6 = (\rho_2 I_2 + \rho_r I_r) \left( \frac{D}{h_2} \right)^2;$$

$$\dot{N}_i = \frac{dN_i}{dx} \text{ and } \ddot{N}_i = \frac{d^2 N_i}{dx^2}, i=1,2,\dots,6$$

## APPENDIX B

### Coefficients of element stiffness and mass matrices for the partially treated MR fluid multilayer beam.

The symmetric (6x6) elemental mass and stiffness matrices derived using Lagrange's energy equation are summarized below.

Stiffness matrix of the sandwich beam element comprising MR fluid within the mid-layer

$$k_{11} = \int_0^{l_c} \alpha_1 \dot{N}_1^2 dx + \int_0^{l_e} \alpha_2 N_1^2 dx; \quad k_{12} = \int_0^{l_e} \alpha_3 N_1 \dot{N}_2 dx; \quad k_{13} = \int_0^{l_e} \alpha_3 N_1 \dot{N}_3 dx;$$

$$k_{14} = \int_0^{l_c} \alpha_1 \dot{N}_1 \dot{N}_4 dx + \int_0^{l_e} \alpha_2 N_1 N_4 dx; \quad k_{15} = \int_0^{l_e} \alpha_3 N_1 \dot{N}_5 dx; \quad k_{16} = \int_0^{l_e} \alpha_3 N_1 \dot{N}_6 dx;$$

$$k_{22} = \int_0^{l_c} \alpha_4 \ddot{N}_2^2 dx + \int_0^{l_e} \alpha_5 \dot{N}_2^2 dx; \quad k_{23} = \int_0^{l_c} \alpha_4 \ddot{N}_2 \ddot{N}_3 dx + \int_0^{l_e} \alpha_5 \dot{N}_2 \dot{N}_3 dx; \quad k_{24} = \int_0^{l_e} \alpha_3 \dot{N}_2 N_4 dx;$$

$$k_{25} = \int_0^{l_c} \alpha_4 \ddot{N}_2 \ddot{N}_5 dx + \int_0^{l_e} \alpha_5 \dot{N}_2 \dot{N}_5 dx; \quad k_{26} = \int_0^{l_c} \alpha_4 \ddot{N}_2 \ddot{N}_6 dx + \int_0^{l_e} \alpha_5 \dot{N}_2 \dot{N}_6 dx;$$

$$k_{33} = \int_0^{l_c} \alpha_4 \ddot{N}_3^2 dx + \int_0^{l_e} \alpha_5 \dot{N}_3^2 dx; \quad k_{34} = \int_0^{l_e} \alpha_3 \dot{N}_3 N_4 dx; \quad k_{35} = \int_0^{l_c} \alpha_4 \ddot{N}_3 \ddot{N}_5 dx + \int_0^{l_e} \alpha_5 \dot{N}_3 \dot{N}_5 dx;$$

$$k_{36} = \int_0^{l_c} \alpha_4 \ddot{N}_3 \ddot{N}_6 dx + \int_0^{l_e} \alpha_5 \dot{N}_3 \dot{N}_6 dx; \quad k_{44} = \int_0^{l_c} \alpha_1 \dot{N}_4^2 dx + \int_0^{l_e} \alpha_2 N_4^2 dx; \quad k_{45} = \int_0^{l_e} \alpha_3 N_4 \dot{N}_5 dx;$$

$$k_{46} = \int_0^{l_e} \alpha_3 N_4 \dot{N}_6 dx; \quad k_{55} = \int_0^{l_c} \alpha_4 \ddot{N}_5^2 dx + \int_0^{l_e} \alpha_5 \dot{N}_5^2 dx; \quad k_{56} = \int_0^{l_c} \alpha_4 \ddot{N}_5 \ddot{N}_6 dx + \int_0^{l_e} \alpha_5 \dot{N}_5 \dot{N}_6 dx;$$

$$\text{and } k_{66} = \int_0^{l_c} \alpha_4 \ddot{N}_6^2 dx + \int_0^{l_e} \alpha_5 \dot{N}_6^2 dx;$$

$$\text{where } \alpha_1 = (E_1 A_1 + E_3 A_3 e^2); \quad \alpha_2 = \bar{G} b h_2 \left( -\frac{(1+e)}{h_2} \right)^2; \quad \alpha_3 = \bar{G} b h_2 \left( \frac{D}{h_2} \right) \left( -\frac{(1+e)}{h_2} \right);$$

$$\alpha_4 = (E_1 I_1 + E_3 I_3); \text{ and } \alpha_5 = \bar{G} b h_2 \left( \frac{D}{h_2} \right)^2;$$

Mass matrix of the sandwich beam element comprising MR fluid within the mid-layer

$$m_{11} = \int_0^{l_e} \beta_1 N_1^2 dx + \int_0^{l_e} \beta_2 N_1^2 dx; m_{12} = \int_0^{l_e} \beta_3 N_1 \dot{N}_2 dx; m_{13} = \int_0^{l_e} \beta_3 N_1 \dot{N}_3 dx;$$

$$m_{14} = \int_0^{l_e} \beta_1 N_1 N_4 dx + \int_0^{l_e} \beta_4 N_1 N_4 dx; m_{15} = \int_0^{l_e} \beta_3 N_1 \dot{N}_5 dx; m_{16} = \int_0^{l_e} \beta_3 N_1 \dot{N}_6 dx;$$

$$m_{22} = \int_0^{l_e} \beta_5 N_2^2 dx + \int_0^{l_e} \beta_6 \dot{N}_2^2 dx; m_{23} = \int_0^{l_e} \beta_5 N_2 N_3 dx + \int_0^{l_e} \beta_6 \dot{N}_2 \dot{N}_3 dx; m_{24} = \int_0^{l_e} \beta_3 N_4 \dot{N}_2 dx;$$

$$m_{25} = \int_0^{l_e} \beta_5 N_2 N_5 dx + \int_0^{l_e} \beta_6 \dot{N}_2 \dot{N}_5 dx; m_{26} = \int_0^{l_e} \beta_5 N_2 N_6 dx + \int_0^{l_e} \beta_6 \dot{N}_2 \dot{N}_6 dx;$$

$$m_{33} = \int_0^{l_e} \beta_5 N_3^2 dx + \int_0^{l_e} \beta_6 \dot{N}_3^2 dx; m_{34} = \int_0^{l_e} \beta_3 N_4 \dot{N}_3 dx;$$

$$m_{35} = \int_0^{l_e} \beta_5 N_3 N_5 dx + \int_0^{l_e} \beta_6 \dot{N}_3 \dot{N}_5 dx; m_{36} = \int_0^{l_e} \beta_5 N_3 N_6 dx + \int_0^{l_e} \beta_6 \dot{N}_3 \dot{N}_6 dx;$$

$$m_{44} = \int_0^{l_e} \beta_1 N_4^2 dx + \int_0^{l_e} \beta_4 N_4^2 dx; m_{45} = \int_0^{l_e} \beta_3 N_4 \dot{N}_5 dx; m_{46} = \int_0^{l_e} \beta_3 N_4 \dot{N}_6 dx;$$

$$m_{55} = \int_0^{l_e} \beta_5 N_5^2 dx + \int_0^{l_e} \beta_6 \dot{N}_5^2 dx; m_{56} = \int_0^{l_e} \beta_5 N_5 N_6 dx + \int_0^{l_e} \beta_6 \dot{N}_5 \dot{N}_6 dx;$$

$$m_{66} = \int_0^{l_e} \beta_5 N_6^2 dx + \int_0^{l_e} \beta_6 \dot{N}_6^2 dx;$$

where

$$\beta_1 = \rho_1 A_1 + e^2 \rho_3 A_3; \beta_2 = \rho_2 I_2 \left( -\frac{(1+e)}{h_2} \right)^2; \beta_3 = (\rho_2 I_2 + \rho_r I_r) \left( \frac{D}{h_2} \right) \left( -\frac{(1+e)}{h_2} \right);$$

$$\beta_4 = (\rho_2 I_2 + \rho_r I_r) \left( \frac{(1+e)}{h_2} \right)^2; \beta_5 = (\rho_1 A_1 + \rho_2 A_2 + \rho_r A_r + \rho_3 A_3);$$

$$\beta_6 = (\rho_2 I_2 + \rho_r I_r) \left( \frac{D}{h_2} \right)^2;$$

$$\dot{N}_i = \frac{dN_i}{dx} \text{ and } \ddot{N}_i = \frac{d^2 N_i}{dx^2}, i=1, 2, \dots, 6$$

## REFERENCES

Ahmadkhanlou, F., M.S., 2008, "Design, modeling and control of magnetorheological fluid-based force feedback dampers for telerobotic systems," Ph.D.dissertation, The Ohio State university.

Al-Ajmi, M. A. and Bourisli, R. I., 2008, "Optimum design of segmented passive-constrained layer damping treatment through genetic algorithms," *Mechanics of Advanced Materials and Structures*, Vol. 15, pp. 250-257.

Aldemir, U., 2003, "Optimal control of structures with semi-active tuned mass dampers," *Journal of Sound and Vibration*, Vol. 266, pp.847-874.

Ashour,O., Rogers, A.Craig and Kordonsky, W., 1996, "Magnetorheological fluids: materials, characterization, and devices," *Journal of Intelligent Material Systems and Structures*, Vol. 7, pp. 123-130.

Baillargeon, B.P. and Vel, S.S, 2005, "Active vibration suppression of sandwich beams using piezoelectric shear actuators: experiments and numerical simulation," *Journal of Intelligent Material System and Structures*, Vol. 16, pp. 517-530.

Bashtovoi, V.G., Kabachnikov, D.N. and Bossis, G., 2002, "Damping of an elastic beam using an MR suspension in the squeeze mode," *Journal of Intelligent Material Systems and Structures*, Vol.13, pp. 515-519.

Batterbee, D.C. and Sims, N.D., 2007, "Hardware-in-the-loop simulation of magnetorheological dampers for vehicle suspension systems," *Proceeding of IMech E, Part 1: Journal of Systems and Control Engineering*, Vol. 221, pp. 265-278.

Baz, A. and Ro, J., 1995, "Optimum design and control of active constrained layer damping," *Journal of Vibration and Acoustics*, Vol.117, pp. 135-144.

Bonnans, J. F. and Shapiro, A., 2000, "Perturbation analysis of optimization problems," Springer-Verlag, New York.

Breese, D.G. and Gordaninejad, F., 2003, "Semi-active, fail-safe magneto-rheological fluid dampers for mountain bicycles," *International Journal of Vehicle Design*, Vol. 33, pp.128-138.

Burl, J.B., 1999, "Linear optimal control," Addison-Wesley, California.

Carlson, J. D. and Weiss, K. D., 1994, "A growing attraction to magnetic fluids," *Machine Design*, Vol. 66, pp. 61-64.

Carlson, J.D., Catanzarite, D.M. and Clair St., K.A., 1995, "Commercial magneto-rheological fluid devices," 5<sup>th</sup> International Conference on Electro-Rheological, Magneto-Rheological Suspensions and Associated Technology, Sheffield, U.K., 10-14 July 1995.

Choi, Y., Sprecher, A. F. and Conrad, H., 1990, "Vibration characteristics of a composite beam containing an electrorheological fluid," *Journal of Intelligent Material Systems and Structures*, Vol. 1, pp. 91-104.

Choi, Y., Sprecher, A. F. and Conrad, H., 1992, "Response of electrorheological fluid filled laminate composites to forced vibration," *Journal of Intelligent Material Systems and Structures*, Vol.3, pp.17-29.

Choi, S. B., 1999, "Vibration control of flexible structures using ER dampers," *Journal of Dynamics, Measurement and Control, Transaction of ASME*, Vol. 121, pp.134- 38.

Choi, S.B., Nam, M.H. and Lee, B.K., 2000, "Vibration control of a MR seat damper for commercial vehicles," *Journal of Intelligent Material Systems and Structures*, Vol.11, pp. 936-944.

Choi, S.B, Lee, H.K. and Chang, E.G., 2001, "Field test results of a semi-active ER suspension system associated with skyhook controller," *Mechatronics*, Vol.11, pp.345-353.

Choi, S.B., Lee, S. K. and Park, Y. P., 2001, "A hysteresis model for the field-dependent damping force of a magnetorheological damper," *Journal of Sound and Vibration*, Vol. 245, pp. 375-83.

Choi, S.B., Lee, H.S., Park and Y.P., 2002, " $H_{\infty}$  control performance of a full-vehicle suspension featuring magnetorheological dampers," *Vehicle System Dynamics*, Vol.38, pp.341-360.

Choi, S.B. and Han, Y.M., 2003, "MR seat suspension for vibration control of a commercial vehicle," *International Journal of Vehicle Design*, Vol. 31, pp. 202-215.

Choi, Y.T. and Wereley, N.M., 2003, "Vibration control of landing gear system featuring electrorheological/magnetorheological fluids," *Journal of Aircraft*, Vol.40, pp.432-439.

Choi, Y. T., Cho, J. U., Choi, S. B. and Wereley, N. M., 2005, "Constitutive models of electrorheological and magnetorheological fluids using viscometers," *Smart Materials and Structures*, Vol. 14, pp. 1025-1036.

Choi, Y.T., Wereley, N.M. and Jeon, Y.S., 2005, "Semi-active vibration isolation using magnetorheological isolators," *Journal of Aircraft*, Vol. 42, pp. 1244.

Ciocanel, C., 2006, "A particle based constitutive model for MR fluids," Ph.D. thesis, University of Toledo, August.

DiTaranto, R. A., 1965, "Theory of vibratory bending of elastic and viscoelastic Layered finite-length beams," *Journal of Applied Mechanics, Transaction of ASME Ser. E*, Vol. 87, pp. 881-86.

Dogruer, U., Gordaninejad, F. and Evarensel, C.A., 2008, "A new magneto-rheological fluid damper for high-mobility multi-purpose wheeled vehicle (HMMWV)," *Journal of Intelligent Material Systems and Structures*, Vol. 19, pp. 641-649.

Du, H., Sze, K.Y. and Lam, J., 2005, "Semi-active  $H_{\infty}$  control of vehicle suspension with magnetorheological damper," *Journal of Sound and Vibration*, Vol. 283, pp.981-996.

Dyke, S. J., Spencer, B.F., Sain, M. K. and Carlson, J. D., 1996, "Modeling and control of MR dampers on seismic response reduction," *Smart Materials and Structures*, Vol. 7, pp. 693-703.

Dyke, S. J., Spencer, B.F., Sain, M. K. and Carlson, J. D., 1998, "An experimental study of MR dampers on seismic protection," *Smart Materials and Structures*, Vol. 7, pp. 693-703.

Ericksen, E.O. and Gordaninejad, F., 2003, "A magneto-rheological fluid shock absorber for an off-road motorcycle," *International Journal of Vehicle Design*, Vol. 33, pp.139-152.

Fukuda, T., Takawa, T. and Nakashima, K., 2000, "Optimum vibration control of CFRP sandwich beam using electro-rheological fluids and piezoceramic actuators," *Smart Materials and Structures*, Vol. 9, pp. 121-125.

Gandhi, M. V., Thomson, B. S. and Choi, S. B., 1989, "A new generation of innovative ultra-advanced intelligent composite materials featuring electro-rheological fluids: An experimental investigation," *Journal of Composite Materials*, Vol. 23, pp.1232-55.

Genç, S. and Phulé, P.P., 2002, "Rheological properties of magnetorheological fluids," *Smart Materials and Structures* Vol. 11, pp.140-146.

Giuclea, M., Sireteanu, T., Stancioiu, D. and Stammers, C.W., 2004, "Model parameter identification for vehicle vibration control with magnetorheological dampers using computational intelligence methods," *Proceeding of IMech E, Part 1: Journal of Systems and Control Engineering*, Vol. 218, pp.561-581.

Goncalves, F.D., 2001, "Dynamic analysis of semi-active control techniques for vehicle applications," Ph.D., Thesis dissertation, Virginia Polytechnic Institute and State University.

Goncalves, F. D., Koo, J. H. and Ahmadian, M., 2006, "A Review of the state of the art in magnetorheological fluid technologies – Part I: MR fluid and MR fluid models," *The Shock and Vibration Digest*, Vol.38, pp. 203–219.

Gu, Y, Clark, R.L., Fuller,C.L. and Zander, A.C., 1994, "Experiments on active control of plate vibration using piezoelectric actuators and polyvinylidene fluoride (PWDF) modal sensors," *Journal of Vibration and Acoustics*, Vol. 116, pp. 303-308.

Gu,Z.Q. and Oyadiji, S.O., 2008, " Application of MR damper in structural control using ANFIS method," *Computers and Structures*, Vol. 86, pp.427-436.

Guo, D.L., Hu, H.Y. and Yi, J.Q., 2004, "Neural network control for a semi-active vehicle suspension with a magnetorheological damper," *Journal of Vibration and Control*, Vol. 10, pp. 461-471.

Haiqing, G., King, L.M., and Cher,T.B., 1993, "Influence of a locally applied electrorheological fluid layer on vibration of a simple cantilever beam," *Journal of Intelligent Material Systems and Structures*, Vol. 4, pp. 379-384.

Haiqing, G., King, L.M., 1997, "Vibration characteristics of sandwich beams partially and fully treated with electrorheological fluid," *Journal of Intelligent Material Systems and Structures*, Vol.8, pp. 401-413.

Han, Y.M., Jung, J.Y., Choi, S.B., Choi, Y.T. and Wereley, N.M., 2006, "Ride quality investigation of an electrorheological seat suspension to minimize human body vibration," *Proceedings of the Institution of Mechanical Engineers (IMechE) Part D - Journal of Automobile Engineering*, Vol. 220, pp.139-150.

Harland, N.R., Mace, B.R. and Jones, R.W., 2001, "Wave propagation, reflection and transmission in tunable fluid filled films," *Journal of Sound and Vibration*, Vol. 241, pp.735-754.

Harland, N.R., Mace, B.R. and Jones, R.W., 2001, "Adaptive-passive control of vibration transmission in beams using electro/magnetorheological fluid filled inserts," *IEEE Transactions on Control Systems Technology*, Vol. 9, pp. 209-220.

He, X. Q., Ng, T.Y., Sivashankar, S. and Liew, K.M., 2001, "Active control of FGM plates with integrated piezoelectric sensors and actuators," *International Journal of Solids and Structures*, Vol.38, pp. 1641-1655.

Hiemenz, G.J. and Wereley, N.M., 1999, "Seismic response of civil structures utilizing semi-active MR and ER bracing systems," *Journal of Intelligent Material Systems and Structures*, Vol.10, pp.646-651.

Hiemenz, G.J., Choi, Y.T. and Wereley, N.M., 2003, "Seismic control of civil structures utilizing semi-active MR braces," *Journal of Computer-Aided Civil and Infrastructure Engineering*. Vol. 18, pp. 31-44.

Hiemenz, G.J., Hu, W. and Wereley, N.M., 2008, "Semi-active magnetorheological helicopter crew seat suspension for vibration isolation," *Journal of Aircraft*, Vol.45, pp. 945-953.

Hong, K.S., Sohn, H.C. and Hedrick, J.K., 2002, "Modified Skyhook Control of Semi-Active suspensions: A New Model, Gain Scheduling, and Hardware-in-the-Loop Tuning," *Journal of Dynamic systems, Measurements and Control*, Vol.124, 158-167.

Hu, Q. and Ma, G., 2005, "Variable structure control and active vibration suppression of flexible spacecraft during attitude maneuver," *Aerospace Science and Technology*, Vol.9, pp. 307-317.

Hu, Y.R. and Ng, A., 2005, "Active robust vibration control of flexible structures," *Journal of Sound and Vibration*, Vol. 288, pp.43-56.

Hu, B., Wang, D., Xia, P. and Shi, Q., 2006, "Investigation on the vibration characteristics of a sandwich beam with smart composites-MRF," *World Journal of Modeling and Simulation*, Vol. 2, pp. 201-206.

Hu, W. and Wereley, N.M., 2008, "Hybrid magnetorheological fluid-elastomeric lag dampers for helicopter stability augmentation," *Smart Materials and Structures* Vol. 17, 045021 (16pp).

Jansen, L.M. and Dyke, S.J., 2000, "Semiactive control strategies for MR dampers:Comparative study," *Journal of Engineering Mechanics*, Vol.126, pp.795-803.

Jolly, M.R., Carlson, J.D. and Munoz, B.C., 1996, "A model of the behavior of magnetorheological materials," *Smart Materials and Structures* Vol. 5, pp.607-614.

Jolly, M.R., Bender, J.W. and Carlson, J.D., 1998, "Properties and applications of commercial magnetorheological fluids," SPIE 5th Annual Int. Symposium on Smart Structures and Materials, San Diego, CA, 15 March, 1998.

Jung, W.J., Jeong, W.B., Hong, S.R. and Choi, S.B., 2004, "Vibration control of flexible beam structure using squeeze mode ER damper," *Journal of Sound and Vibration*, Vol. 273, pp. 185-199.

Jung, H.J., Choi, K.M., Spencer Jr., B.F. and Lee, I.W., 2006, "Application of some semi-active control algorithms to a smart base-isolated building employing MR dampers," *Structural Control and Health Monitoring*, Vol. 13, pp. 693-704.

Kamath, G.M., Wereley, N.M. and Jolly, M.R., 1999, "Characterization of magnetorheological helicopter lag dampers," *Journal of the American Helicopter Society*, Vol. 44, pp. 234-248.

Koo, J.H., Goncalves, F.D. and Ahmadian, M., 2006, "A comprehensive analysis of the response time of MR dampers," *Smart Materials and Structures*, Vol. 15, pp. 351-358.

Kordonski, W. and Golini, D. 1999, "Magnetorheological suspension-based high precision finishing technology (MRF)," *Journal of Intelligent Material Systems and Structures*, Vol. 9, pp. 650-654.

Lai, C.Y. and Liao, W.H., 2002, "Vibration control of a suspension system via a magnetorheological fluid damper," *Journal of Vibration and Control*, Vol. 8, pp. 527-247.

Lam, M. J., Inman, D. J. and Saunders, W. R., 1997, "Vibration control through passive constrained layer damping and active control," *Journal of Intelligent Material Systems and Structures*, Vol. 8, pp. 663-677.

Lam, A. H.F. and Liao, W.H., 2003, "Semi-active control of automotive suspension systems with magneto-rheological dampers," *International Journal of Vehicle Design*, Vol. 33, pp.50–75.

Lara-Prieto, V., Parkin, R., Jackson, M., Silberschmidt, V. and Kęsy, Z., 2010, "Vibration characteristics of MR cantilever sandwich beams: experimental study," *Smart Materials and Structures*, Vol. 19, 015005 (9pp).

Lee, D. Y. and Wereley, N. 2000, "Quasi-steady Herschel-Bulkley analysis of electro and magnetorheological dampers," *Journal of Intelligent Material Systems and Structures*, Vol.10, pp. 761–769.

Lee, C.Y. and Jwo, K.L., 2001, "Experimental study on electrorheological material with grooved electrode surfaces," *Materials and Design*, Vol. 22, pp. 277-283.

Leitmann, G. and Reithmeier, E., 1993, "Semi active control of a vibrating system by means of electrorheological fluids," *Dynamics and Control*, Vol.3, pp.7-33.

Leitmann, G., 1994, "Semi active control of vibration attenuation," *Journal of Intelligent Materials, Systems and Structures*, Vol. 5, pp. 841-846.

Leng, J.S., Liu, S.Y., Du, S.Y., Wang, L. and Wang, D.E., 1995, "Active vibration control of smart composites featuring electro-rheological fluids," *Applied Composite Materials*, Vol. 2, pp. 59-65.

Li, W. H., Chen, G. and Yeo, S. H., 1999, "Viscoelastic properties of MR fluids," *Smart Material Systeems and Structures* Vol. 8, pp. 460-468.

Li, W.H., Du, H., Chen, G., Yeo, S.H. and Guo, N.Q., 2002, "Nonlinear rheological behavior of magnetorheological fluids: step-strain experiments," *Smart Materials and Structures* Vol. 11, pp. 209-217.

Li, W.H. and Du, H., 2003, "Design and experimental evaluation of magnetorheological brake," *International Journal of Advanced Manufacturing Technology*, Vol. 21, pp. 508-515.

Liao, W.H. and Wang, D.H., 2003, "Semiactive vibration control of train suspension systems via magnetorheological dampers," *Journal of Intelligent Material Systems and Structures*, Vol.14, pp.161-172.

Lindler, J. E., Choi, Y.T. and Wereley, N. M., 2003, "Double adjustable shock absorbers utilizing electrorheological and magnetorheological fluids," *International Journal of Vehicle Design*, Vol. 33, pp.189–206.

Liu, Q. and Chattopadhyay, A., 2000, "Improved helicopter aeromechanical stability analysis using segmented constrained layer damping and hybrid optimization," *Journal of Intelligent Material Systems and Structures*, Vol. 11, pp.492-500.

Loh, C.H., Lynch, J.P., Lu, K.C., Wang, Y., Chang, C.M., Lin, P.Y. and Yeh, T.H., 2007, "Experimental verification of a wireless sensing and control system for structural control using MR dampers," *Earthquake Engineering and Structural Dynamics*, Vol. 36, pp. 1303-1328.

Makris, N., Burton, S.A. and Taylor, D.,P., 1996, "Electrorheological damper with annular ducts for seismic protection applications," *Smart Materials and Structures*, Vol.5, pp. 551-564.

Marathe, S., Gandhi, F. and Wang, K. W. 1998. "Helicopter blade response aeromechanical stability with a magnetorheological fluid based lag damper," *Journal of Intelligent Material Systems and Structures*, Vol. 9, pp.272–282.

Margolis, D.L., 1983, "Procedure for comparing passive, active and semi-active approaches to vibration isolation," *Journal of Franklin institute*, Vol. 315, pp. 225-238.

Marksmeier, T.M., Wang, E.L., Gordaninejad, F. and Stipanovic, A., 1998, "Theoretical and experimental studies of an electro-rheological grease shock absorber," *Journal of Intelligent Materials Systems and Structures*, Vol.9, pp. 963-703.

Mazlan, S.A., EkreemN.B. and Olabi, A.G., 2007, "The performance of magnetorheological fluid in squeeze mode," *Smart Materials and Structures*, Vol. 16, pp. 1678-1682.

Mead, D. J. and Markus, S., 1969, "The forced vibration of a three-layer damped sandwich beam with arbitrary boundary conditions," *Journal of Sound and Vibration*, Vol. 10, pp.163-75.

Moon, J.S., Bergman, L.A. and Voulgaris, P.G., 2003, "Sliding mode control of cable-stayed bridge subjected to seismic excitation," *Journal Engineering Mechanics*, Vol. 129, pp. 71-78.

Muc, A. and Gurba, W., 2001, "Genetic algorithms and finite element analysis in optimization of composite structures," *Composite Structures*, Vol. 54, pp.275-281.

Mutambara, A.G.O., 1999, "*Design and Analysis of Control Systems*," 1999, CRC press, Florida.

Nakano, M. and Yamamoto, H., 1999, "Dynamic viscoelasticity of a magnetorheological fluid in oscillatory slit flow," *International Journal of Modern Physics B*, Vol. 13, pp.2068-2076.

Nashif A. D. and Jones David I. G. and Henderson J.P., "*Vibration Damping*," John Wiley & Sons, 1985.

- Nguyen, Q.H. and Choi, S.B., 2009, "Optimal design of MR shock absorber and application to vehicle suspension," *Smart Materials and Structures*, 035012, 11 pp.
- Occhiuzzi, A., Spizzuoco, M. and Serino, G., 2003, "Experimental analysis of magnetorheological dampers for structural control," *Smart Materials and Structures*, Vol. 12, pp.703-711.
- Oh, H. U. and Onoda, J., 2002, "An experimental study of a semi-active magnetorheological fluid variable damper for vibration suppression of truss structures," *Smart Materials and Structures*, Vol. 11, pp. 156-62.
- Ogata, K 2008, "*MATLAB for Control Engineers*," Pearson Prentice Hall, New Jersey.
- Pahlavan, L. and Rezaeepazhand, J., 2007, "Dynamic response analysis and vibration control of a cantilever beam with a squeeze-mode electrorheological damper," *Smart Materials and Structures*, Vol.16, pp. 2183-2189.
- Peel, D.J., Stanway R. and Bullough W.A., 1996, "Dynamic modelling of an ER vibration damper for vehicle suspension applications," *Smart Materials and Structures*, Vol. 5, pp.591-606.
- Petersen, I.R. and Pota, H.R., 2003, "Minimax LQG optimal control of a flexible beam," *Control Engineering Practice*, Vol. 11, pp. 1273-1287.
- Phule, P. P., "Magnetorheological Fluid," U.S. Patent 5,985,168, November16, 1999.
- Pranoto, T., Nagaya, K. and Hosoda, A., 2004, "Vibration suppression of plate using linear MR fluid passive damper," *Journal of Sound and Vibration*, Vol. 276, pp.919-32.

Qiu, J. and Kajika, T., 1999, "Damping effect of multi-layer beams with embedded electrorheological fluid," *Journal of Intelligent Material Systems and Structures*, Vol.10, pp. 521-29.

Rahn, C. D. and Joshi, S., 1998, "Modeling and control of an electrorheological sandwich Beam," *Journal of Vibration and Acoustics*, Vol. 120, pp. 221-27.

Rao, S. S., 1995, "*Mechanical Vibrations*," 3rd edition, Massachusetts: Addison – Wesley publishing company Inc.

Rao S S, 1996, "*Engineering Optimization: Theory and Practice*," A Wiley – Interscience publication, New York.

Rao, S.S., 1999, "*The Finite Element Method in Engineering*," Butterworth Heinemann, Boston.

Rao, M.D., 2003, "Recent applications of viscoelastic damping for noise control in automobiles and commercial airplanes," *Journal of Sound and Vibration*, Vol. 262, pp. 457-474.

Ribakov, Y. and Gluck, J., 2002, "Selective controlled base isolation system withmagnetorheological dampers," *Earthquake Engineering and Structural Dynamics*, Vol. 31, pp.1301–1324.

Sadri, A.M., Wright, J.R. and Wynne, R.J., 1999, "Modelling and optimal placement of piezoelectric actuators in isotropic plates using genetic algorithms," *Smart Materials and Structures*, Vol.8, pp.490-498.

Sahasrabudhe, S.S. and Nagarajaiah, S., 2005, "Semi-active control of sliding isolated bridges using MR dampers: an experimental and numerical study," *Earthquake Engineering and Structural Dynamics*, Vol. 34, pp.965-983.

Sammaier, D., Sename, O. and Dugard, L., 2003, Skyhook and  $H_\infty$  control of semi-active suspensions: Some practical aspects,” *Vehicle system dynamics*, Vol. 39, pp. 279-308.

Savaresi, S.M., Bittanti, S. and Montiglio, M., 2005, “Identification of semi-physical and black-box non-linear models: the case of MR-dampers for vehicles control,” *Automatica*, Vol.41, pp. 113-127.

Schurter, K.C. and Roschke, N.P., 2001, “Neuro-Fuzzy control of structures using magnetorheological dampers,” *Proceedings of the American Control Conference*, Arlington, VA June 25-27, 2001.

See, H., 2003, “Field dependence of the response of a magnetorheological suspension under steady shear flow and squeezing flow,” *Rheologica Acta*, Vol. 42, pp.86-92.

See, H., 2004, “Advances in electro-rheological fluids: Materials, modeling and applications,” *Journal of Industrial Engineering Chemistry*. Vol. 10, pp.1132-45.

Sethi, V. and Song, G., 2005, “Optimal vibration control of a model frame structure using piezoelectric sensors and actuators,” *Journal of Vibration and Control*, Vol.11, pp. 671-684.

Shaw, J., 2000, “Hybrid control of a cantilevered ER sandwich beam for vibration suppression,” *Journal of Intelligent Material Systems and Structures*, Vol. 11, pp. 26-31.

Sims, N.D. and Stanway, R., 1999, “Vibration control using smart fluids : A state of the art-Review,” *The Shock and Vibration Digest*, Vol. 31, pp.195-203.

Sodeyama, H., Sunakoda, K., Suzuki, K., Carlson, J. D. and Spencer, B. F., 2001, “Development of large capacity semi-active vibration control device using magneto-

rheological fluid,” American Society of Mechanical Engineers: Pressure Vessels and Piping Division, Vol. 428, pp.109–114.

Spencer Jr. B.F. Dyke, S.J., Sain, M.K. and Carlson, J.D., 1997, “Phenomenological model of a magnetorheological damper,” ASCE Journal of Engineering Mechanics, Vol. 123, pp. 230–238.

Spencer.Jr., B.F., Yang, G., Carlson, J.D. and Sain, M.K., 1998, “ Smart dampers for seismic protection of structures: A full-scale study,” Second World Conference on Structural Control, Kyoto, Japan, June 28 – July 1, 1998.

Spencer Jr., B. F. and Nagarajaiah, S., 2003, “State of the art of structural control,” Journal of Structural Engineering. Vol. 129, pp. 845-56.

Srikantha Phani, A. and Venkatraman, K., 2003, “Vibration control of sandwich beams using electro-rheological fluids,” Mechanical System and Signal Processing, Vol. 17, pp. 1083-95.

Stanway. R., Sproston, J. L. and El Wahed, A. K., 1996, “Applications of Electrorheological fluids in vibration control: A survey,” Smart Materials and Structures, Vol.5, pp. 464-82.

Stanway, R., Rongong, J.A. and Sims, N.D., 2003, “Active constrained-layer damping: a state-of-the-art review,” Proceedings of Institution of Mechanical Engineers, Part I: Systems and Control Engineering, Vol. 217, pp. 437-456.

Stelzer, G.J., Schulz, M.J., and Allemang, R.J., 2003, “A magnetorheological semi-active isolator to reduce noise and vibration transmissibility in automobiles,” Journal of Intelligent Material Systems and Structures, Vol.14, pp. 743-765.

Sun, Q., Zhou, J.X. and Zhang, L., 2003, "An adaptive beam model and dynamic characteristics of magnetorheological materials," *Journal of Sound and Vibration*, Vol. 261, pp. 465–81.

Thomson, W.T. and Dahleh, M.D., 1998, "*Theory of Vibration with Applications*," 5<sup>th</sup> ed., New Jersey: Prentice hall.

Tang, X. and Conrad, H., 2000, "An analytical model for magnetorheological fluid," *Journal of Physics D: Applied Physics*, Vol. 33, pp.3026-3032.

Trindade, M.A., Benjeddou, A. and Ohayon, R., 2001, "Piezoelectric active vibration control of damped sandwich beams," *Journal of Sound and Vibration*, Vol. 246, pp. 653-677.

Tse, T. and Chang, C.C., 2004, "Shear-mode rotary magnetorheological damper for small-scale structural control experiments," *Journal of Structural Engineering*, Vol. 130, pp. 904-911.

Vasques, C.M.A and Dias Rodrigues, J., 2006, "Active vibration control of smart piezoelectric beams: Comparison of classical and optimal feedback control strategies," *Computers and Structures*, Vol. 84, pp. 1402-1414.

Wang, X. and Gordaninejad, F., 1999, "Flow analysis of field-controllable electro and magneto- rheological fluids using Heeschel-Bulkley model," *Journal of Intelligent Material Systems and Structures*, Vol.10, pp. 601-608.

Wang, J. and Meng, G., 2001, "Magnetorheological fluid devices: Principles, characteristics and applications in mechanical engineering," *Proceedings of Institution of Mech. Eng. Part L: Journal of Materials: Design and Application*, Vol. 215 pp.165-74.

Wang, E.R., Ma, X.Q., Rakhela, S. and Su, C.Y., 2003, "Modelling the hysteretic characteristics of a magnetorheological fluid damper," Proc. Instn Mech. Engrs., Part D: Journal of Automobile Engineering, Vol. 217, pp. 537-550.

Wang, J., Meng, G., Feng, N. and Hahn, E.J., 2005, "Dynamic performance and control of squeeze mode MR fluid damper-rotor system," Smart Materials and Structures, Vol. 14, pp. 529-539.

Wang, J. and Li, Y., 2006, "Dynamic Simulation and Test Verification of MR Shock Absorber under Impact Load," Journal of Intelligent Material Systems and Structures, Vol. 17, pp. 309-314.

Wang, L.X. and Kamath, H., 2006, "Modelling hysteretic behaviour in magnetorheological fluids and dampers using phase-transition theory," Smart Materials and Structures, Vol.15, pp. 1725-1733.

Weiss, K.D., Carlson, J. D. and Nixon, D. A., 1994, "Viscoelastic properties of magneto- and electro-rheological fluids," Journal of Intelligent Material Systems and Structures, Vol.5, pp.772-775.

Weiss, K. D., Carlson, J. D., Duclos, T. G., and Abbey, K. J., 1997, "Temperature independent magnetorheological materials," U.S. Patent 5,599,474.

Wereley, N. M., Li, P., and Kamath, G. M., 1998, "Idealized hysteresis modeling of electrorheological and magnetorheological dampers," Journal of Intelligent Material Systems and Structures, Vol. 9, pp. 642-649.

Wereley, N.M. and Pang, Li., 1998, "Non-dimensional analysis of semi-active electrorheological and magnetorheological dampers using approximate parallel plate models," Smart Materials and Structures, Vol.7, pp. 732-743.

Wereley, N. M, Kamath, G. and Madavan, V., 1999. "Characterization of magnetorheological helicopter lag dampers," *Journal of Intelligent Material Systems and Structures*, Vol. 10, 624-633.

Xu, Y. L., Qu, W. L. and Ko, J.M., 2000, "Seismic response control of frame structures using magnetorheological/electrorheological dampers," *Earthquake Engineering and Structural Dynamics*. Vol. 29, pp. 557-75.

Yalcintas, M. and Coulter, J. P., 1995, "Analytical modeling of electrorheological materials based adaptive beams," *Journal of Intelligent Material Systems and Structures*, Vol. 6, pp. 488-97.

Yalcintas, M. and Coulter, J. P., 1995, "Adaptive beam model with electrorheological materials based adaptive beams," *Journal of Intelligent Material Systems and Structures*, Vol. 6, pp. 498-507.

Yalcintas, M. and Coulter, J. P., 1998, "Electrorheological materials based non-homogeneous adaptive beams," *Smart Materials and Structures*, Vol. 7, pp. 128-43.

Yalcintas, M. and Dai, H., 1999, "Magnetorheological and electrorheological materials in adaptive structures and their performance comparison," *Smart Materials and Structures*, Vol. 8, pp. 560-73.

Yalcintas, M. and Dai, H., 2004, "Vibration suppression capabilities of magnetorheological materials based adaptive structures," *Smart Materials and Structures* Vol. 13, pp.1-11.

Yan, G. and Zhou, L.L., 2006, "Integrated fuzzy logic and genetic algorithms for multi-objective control of structures using MR dampers," *Journal of Sound and Vibration*, Vol. 296, pp. 368-382.

Yang, G., Spencer Jr., B.F., Calson, J.D., Sain, M.K., 2002, "Large-scale MR fluid dampers: modeling and dynamic performance considerations," *Engineering Structures*, Vol. 24, pp. 309-323.

Yang, G., Spencer Jr., B.F., Jung, H.J. and Calson, J.D., 2004, "Dynamic modeling of large-scale magnetorheological damper systems for civil engineering applications," *Journal of Engineering Mechanics*, Vol. 130, pp. 1107-1114.

Yao, G. Z., Yap, F. F., Chen, G., Li, W. H. and Yeo, S. H., 2002, "MR damper and its application for semi-active control of vehicle suspension system," *Mechatronics*, Vol. 12, pp. 963-73.

Yeh, Z. F. and Shih, Y. S., 2006, "Dynamic characteristics and dynamic instability of magnetorheological based adaptive beams," *Journal of Composite Materials*, Vol. 40, pp.1333-59.

Yi, F., Dyke, S.J., Caicedo, J.M. and Carlson, J.D., 2001, "Experimental verification of multiinput seismic control strategies for smart dampers," *Journal of Engineering Mechanics*, Vol. 127, pp. 1152-1164.

Ying, Z.G., Zhu, W.Q., 2003, "A stochastic optimal semi-active control strategy for ER/MR dampers," *Journal of Sound and Vibration*, Vol. 259, pp. 45-62.

Yoo, J.H. and Wereley, N.M., 2002, "Design of high efficiency magnetorheological valve," *Journal of Intelligent Material Systems and Structures*, Vol. 13, pp. 679-685.

Yoshoka, H., Ramallao, J.C. and Spencer, Jr., B.F., 2002, "Smart base isolation strategies employing magnetorheological dampers," *Journal of Engineering Mechanics*, Vol. 128, pp. 540-551.

Yoshida, O. and Dyke, J.S., 2004, "Seismic control of a nonlinear benchmark Building using smart dampers," *Journal Engineering Mechanics*, Vol. 130, pp. 386-392.

Yoshida, O. and Dyke, J.S., 2005, "Response control of full-scale irregular buildings using magnetorheological dampers," *Journal of Structural Engineering*, Vol.131, pp.734-742.

Yu, M., Dong, X.M., Choi, S.B. and Liao, C.R., 2009, "Human simulated intelligent control of vehicle suspension system with MR dampers," *Journal of Sound and Vibration*, Vol. 319, pp. 753-767.

Zhang, J. and Roschke, P.N., 1999, "Active control of a tall structure excited by wind," *Journal of Wind Engineering and Industrial Aerodynamics*, Vol. 83, pp.209-223.

Zhao, Y., Choi, Y.T. and Wereley, N.M., 2004, "Semi-active damping of ground resonance in helicopters using magnetorheological dampers," *Journal of American Helicopter Society*, Vol. 49, pp.468-483.

Zhou, Li, Chang, C.C. and Wang, L.X., 2003, "Adaptive Fuzzy control for nonlinear building- magnetorheological damper system," *Journal of Structural Engineering*, Vol. 129, pp. 905-913.

Zeng, H., Pau, G. S. H. and Wang, Y.Y., 2006, "A comparative study on optimization of constrained layer damping treatment for structural vibration control," *Thin-walled Structure*, Vol. 44, pp.886-896.

Zenkert D, " Introduction to Sandwich Construction," 1995, EMAS Publishing, UK.